

# Designs and applications of multi-functional covalent organic frameworks in rechargeable batteries



Yongkang An<sup>a,1</sup>, Shuangshuang Tan<sup>a,1</sup>, Yu Liu<sup>a</sup>, Kai Zhu<sup>b</sup>, Lei Hu<sup>c</sup>, Yaoguang Rong<sup>d,\*</sup>,  
Qinyou An<sup>a,e,\*</sup>

<sup>a</sup> State Key Laboratory of Advanced Technology for Materials Synthesis and Processing, Wuhan University of Technology, Wuhan 430070, Hubei, P. R. China

<sup>b</sup> School of Information Science and Engineering, Nanjing University Jinling College, Nanjing 210089, Jiangsu, P. R. China

<sup>c</sup> Key Laboratory of Thermo-Fluid Science and Engineering, Xi'an Jiaotong University, Xi'an 710049, Shaanxi, P. R. China

<sup>d</sup> Wuhan National Laboratory for Optoelectronics, Huazhong University of Science and Technology Wuhan 430074, Hubei, P. R. China

<sup>e</sup> Foshan Xianhu Laboratory of the Advanced Energy Science and Technology Guangdong Laboratory Xianhu Hydrogen Valley, Foshan 528200, Guangdong, P. R. China

## ARTICLE INFO

### Keywords:

Covalent organic frameworks  
Li-ion batteries  
Sodium-ion batteries  
Li-S batteries  
Solid-state electrolytes

## ABSTRACT

Recently, covalent organic frameworks (COFs) have attracted widespread attention for the research in rechargeable batteries due to their intrinsic porous structure, adjustable porosity and designable framework. The porous structure with adjustable pore size is stacked into a one-dimensional ordered channel through the  $\pi$ - $\pi$  interaction, which provides favorable pathways for rapid charge transport. Terrific structural designability exhibits unique advantages in electrochemical energy storage systems (EESS), such as active site diversity, structural stability, lithium and sulfur affinity, which furnishes a novel perspective for settling various problems of rechargeable batteries. This review introduces the structural features and reaction mechanisms of COF materials, then summarizes the design concepts and latest applications of redox-active (cathode and anode materials) and non-redox active (separators, hosts and solid-state electrolytes) COFs in rechargeable batteries. Finally, challenges and perspectives in these fields are discussed.

## 1. Introduction

Covalent organic frameworks (COFs), assembled by C, H, O, N, and other elements, are connected by covalent bonds to form geometric and periodic two-dimensional (2D) or three-dimensional (3D) topological structure polymers, which belong to a subclass of porous crystalline polymers [1–6]. The interconnected and extended framework exhibits extraordinary stability due to the inherent strength of covalent bonds between atoms [7–9]. The geometric composition, shape, and pore size of the target COF could be specifically designed for meeting different demands, which is attributed to the diversity of covalent bonds and the precise control of the atomic order. COFs have been providing a new platform for many fields, such as catalysis [10–12], gas adsorption [13–15], semiconductors [16–19], electrolyte membranes [20], and pseudo-capacitors [21–24], due to their designability, high porosity, structural diversity, and stability. More importantly, the nano-scale ordered channels and space formed by the  $\pi$ - $\pi$  stacking provide an ideal environment for the storage, release, separation, and transformation of charge carriers. The functionalized organic units and regular porous structures

make COFs a new candidate for the development of the next-generation rechargeable batteries.

When COFs are used as the electrode materials of rechargeable batteries, they possess the advantages of organic electrode materials, such as abundant resources [25–28], high specific capacity [29–33], being environment friendly [34–37], and light-weight [38–45], and at the same time can effectively avoid the solubility problem of traditional organic electrodes attributing to the gigantic skeleton [46–48]. Compared with linear polymers [49–54], porous-structured 2D COFs could make the distribution of active units in the electrode more uniform and form a neat one-dimensional transformation channel through the stack of strong  $\pi$ - $\pi$  interaction between layers, which is more conducive to the accessibility of alkali metal ions. Compared with inorganic materials, since lithium ions are bonded to COFs by simple and effective covalent bonding in charging and discharging process, the framework structure of COFs will not be significantly changed, thus COF-based batteries have the potential to achieve longer cycling stability [55,56]. Designable molecular engineering techniques can also be used to adjust the physical and electrochemical properties of COFs, such as electronic conductivity, kinetics and redox potentials.

\* Corresponding authors.

E-mail addresses: [ygrong@hust.edu.cn](mailto:ygrong@hust.edu.cn) (Y. Rong), [anqinyou86@whut.edu.cn](mailto:anqinyou86@whut.edu.cn) (Q. An).

<sup>1</sup> Y.A. and S.T. contributed equally to this work.

Moreover, when COFs are used in Lithium-sulfur (Li-S) batteries, the shuttle effect of polysulfides (PSs) could be effectively suppressed through the uniformly distributed microporous structure and rich polar groups, and the conductivity of the sulfur cathode will slightly increase [57–60]. Besides, COFs can also be employed to prepare the solid electrolytes for rechargeable batteries [61–63]. The continuous 1D channel with high structural and thermal stability can accommodate abundant lithium salts and provide a great convenience for ion storage and diffusion. Thus, COFs has been considered as an ideal candidate for solid-state electrolytes in batteries [63–65]. In recent years, COFs have been rapidly developed in rechargeable batteries, and some reviews have reported on it. However, these reviews lack a systematic review to summarize the energy storage mechanisms, application scenarios and optimization strategies of COFs as redox active or inactive components in batteries.

To fill this gap, this work systematically discusses the structural features of COFs and the energy storage mechanism. Then, from the perspective of molecular structure design and nanostructure design, we reviewed the latest research progress of redox-active COFs in cathode/anode materials, focused on the association between COF structure and electrochemical performance, emphasized the importance and necessity of structure design in battery optimization strategies. Subsequently, the applications and optimization methods of COFs without redox active in lithium-sulfur batteries and solid electrolytes were summarized. In the last part of this article, a summary is given, and the challenges and future prospects is also discussed. We are committed to summarizing the innovative work of our predecessors and providing inspiration for the further development and research of COFs.

## 2. Structural features of COFs

COFs are usually composed of structural blocks via reversible condensation reactions (such as Schiff base reaction), which, to a certain extent, allows the incorrectly connected network to dissociate, reorganize and arrange [66–70]. The structural blocks can be divided into linear blocks and non-linear corner blocks, as shown in Fig. 1a. The geometry of the COF skeleton is determined by the size, symmetry, and connectivity of the structural blocks. For example, the quadrangular COFs are composed of cross-shaped corner blocks and linear blocks, while the hexagonal COFs are constituted by triangular corner blocks and linear blocks. In 2005, two 2D COFs named COF-1 and COF-5 was first designed and successfully implemented by Yaghi and co-workers [71]. COF-1 uses diboronic acid to react with itself to form boroxine through dehydration and condensation, and COF-5 uses diboronic acid to react with hexahydroxy triphenylene to form boronate ester. Jiang and co-workers created a star-shaped COF with micropores composed of triangles and hexagons by condensing 1,2,4,5-tetrahydroxybenzene (THB) unit, the linear block, with tetraphenylethene-cored boronic acid (TPEBA) unit, the non-linear corner block [72]. In the design of new COFs, boric acid has become one of the most common functional groups. Subsequently, a variety of reversible reactions have been reported for the synthesis of COFs [73–76]. It is worth mentioning that the Schiff base reaction is widely used in the development of electrode materials because the reaction can generate  $-C=N$  active bonds for energy storage. The development of a large number of reversible reaction methods and functional groups provides a strong guarantee for the diversity of COFs. The highly diversified COFs exhibit great potential to meet the various requirements for energy storage.

Compared with polymers, the blocks of COFs are precisely controlled in 2D structure. The special structure of COFs makes them widely applied in rechargeable batteries (Fig. 1b). Designing active groups on COFs can be used as electrode materials. More importantly, the regularly ordered porous structure provides a large specific surface area for COFs, which can effectively relieve the volume expansion of the battery caused by alkali-metal ions insertion/extraction during the charging/discharging processes. The COFs stacked by AA can form a one-

dimensional channel that can serve as charge transport or as a host material. The regularity, connectivity and  $\pi$ - $\pi$  conjugation of COFs are extremely beneficial for the transport of charge carriers [77,78]. The AB-stacked COFs can form a denser network, which is an effective strategy for protecting electrodes or obstructing the shuttle of macromolecules. In general, the functions of COFs are much more than that, and many application scenarios need to be further explored.

## 3. COFs as redox electrode materials

Since the specific capacity and working voltage of the electrodes are the key parameters of energy density, the development of electrode materials is one of the most important and popular research directions in batteries [79–84]. COFs participate in energy storage mainly through the redox reaction of functional groups. In this section, the energy storage mechanisms of COF materials, optimization strategies as cathodes/anodes will be presented separately.

### 3.1. Energy storage fundamentals of COFs

The charge storage procedure of COFs is associated with the reversible redox reaction of the active organic functional groups. The diversity of the active groups of COFs has benefited from the research and development on the structural design, charge storage mechanism, and micro-morphology of organic electrode materials in the past few decades [29,85–87]. According to the type of functional groups participating in the reaction, organic electrode materials are divided into n-type, p-type, and bipolar materials [55,88]. For n-type organic electrodes, which are also the majority of COFs electrode materials, they first proceed with the reduction reaction (discharge). The initial state of COFs combines with electrons to form a negative charge state and then combines with alkali metal ions to form a discharged state. The oxidation process (charge) is opposite to the reduction (discharge) process. Under external voltage, COFs lose electrons and metal ions from the metal-containing discharge state and are oxidized to the initial state of the electrode. In general, p-type materials first lose electrons and combine with anions in the electrolyte with working voltage and reactivity usually higher than that of n-type materials due to the better redox potential and kinetics. However, the development of p-type materials is limited due to the introduction of a large number of inactive groups which reduces the specific capacity. The bipolar material containing both n-type and p-type active functional groups can be either charged or discharged in the initial state.

The voltage window of the COF-based electrodes depends on the actual redox potential, which determines whether they could be used as the cathodes or anodes [70,89–91]. The redox potential is determined by the functional groups of COFs. As shown in Fig. 2, the structures of common active functional groups in COFs include carbonyl ( $-C=O$ ), imine ( $-C=N-$ ), and azo ( $-N=N-$ ) [52–54,92–101].

Ketones, quinones and imides are common carbonyl-containing functional groups in COFs. The carbonyl group with high potential (2–3 V Vs Li/Li<sup>+</sup>) generally appears as a functional group in the cathodes of the batteries. When the COF electrode discharges, the carbonyl O receives electrons, becoming unstable enol oxygen anions, and then combines with the adjacent alkali metal ions to form a stable covalent bond. The charging process is performed in the opposite way. For example, Xu et al. [95] introduced naphthalene diimide (NDI) unit as the active site in the D<sub>TP</sub>-A<sub>NDI</sub>-COF cathode for lithium-ion batteries (Fig. 3a). For the discharge/charge process, the NDINA unit undergoes a reversible two-electron redox reaction through the enolization reaction and induces the lithiation/delithiation process. Yao et al. [94] prepared a 2D COF material called PPTODB with pyrene-4, 5, 9, 10-tetraone (PTO) as the active block (Fig. 3b, c). When the working voltage window is 1.5–3V, the average voltage of batteries using PPTODB as the electrode can reach values of over 2.5 V. It is proposed that PTO could theoretically perform reversible insertion/extraction of four lithium ions. The cyclic voltammetry (CV) results showed that there were two obvious pairs of redox

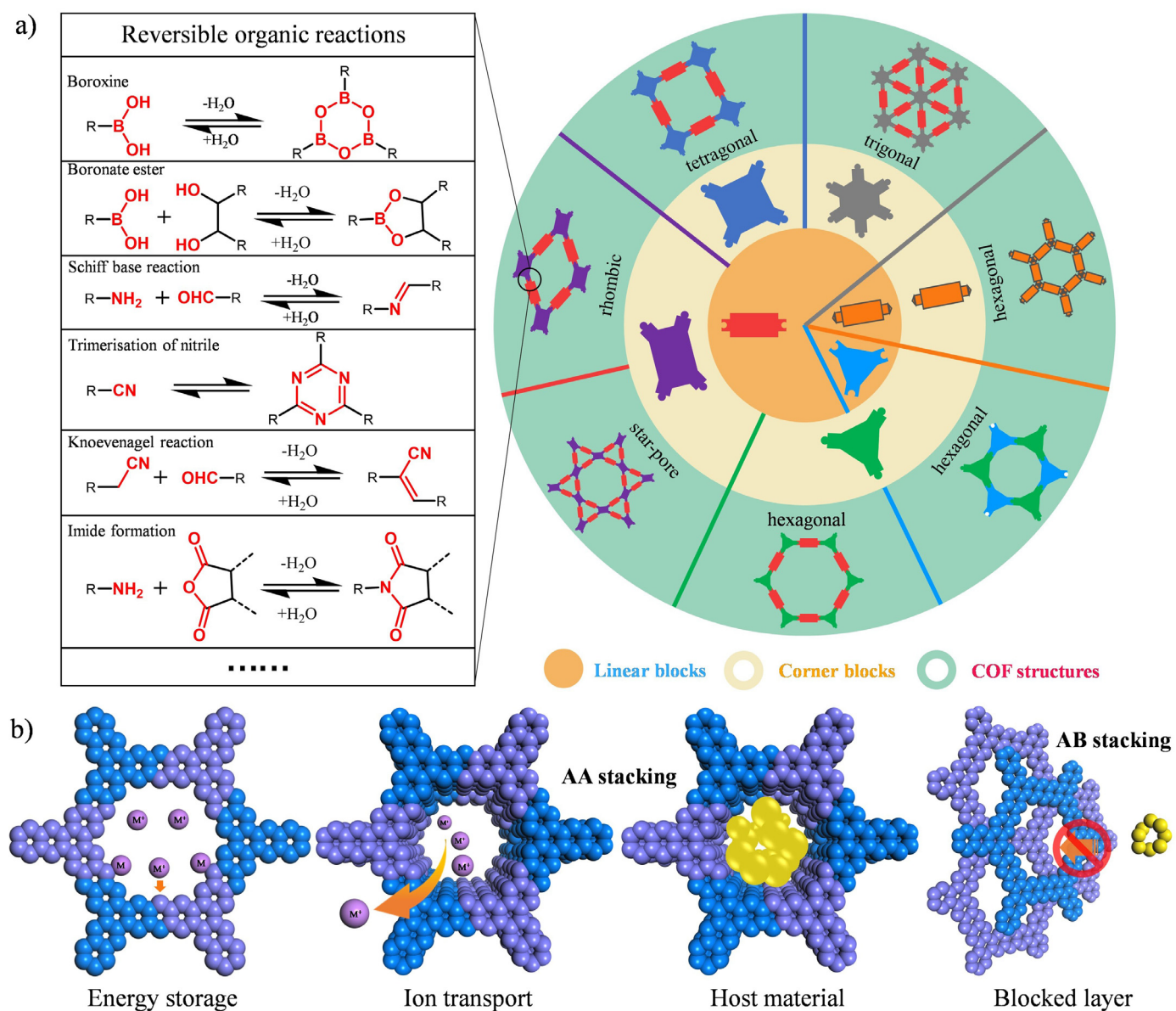


Fig. 1. a) Different types of reversible organic reactions (left) and linear blocks, corner blocks and generated structures (right) in 2D COFs. b) Applications of multifunctional COFs in rechargeable batteries.

peaks between 2–3V (vs. Li/Li<sup>+</sup>), so each pair of peaks should have two electrons to undergo a reversible redox reaction.

Imine (including Schiff and pteridine derivatives) exhibit exceptional design ability, in which planarity and conjugated structure exert a considerable influence in stabilizing their electrochemical activity [35,103–105]. The nitrogen-rich hexaazatrinaphthalene (HATN) monomer owns a higher specific capacity because it could reversibly receive six electrons. Xu et al. [102] introduced HATN into starburst-shaped 2D CCP-HATN and 2D C=N HATN through the Knoevenagel condensation reaction (Fig. 3d, e). The 2D CCP-HATN COFs exhibited two pairs of prominent redox peaks at 1.60/1.58 V and 2.45/2.4 V, respectively, which indicates HATN involves various redox potentials. 2D C=N HATN also showed similar peaks, But the peak area of 2D C=N HATN is smaller than that of CCP-HATN, indicating that the 2D CCP-HATN COFs have higher reactivity.

Azo compounds have been recently discovered as active centers for reversible chemical reactions. By breaking the N=N double bond, it could receive/release two electrons and alkali metal ions reversibly. As displayed in Fig. 3f, Weeraratne et al. [98] synthesized ALP-8 with high

azo-linkage density as a new type of COF electrode material for sodium-ion batteries (SIBs). The reversible redox potential of azo bond measured by CV is between 1.2 and 1.5 V versus Na/Na<sup>+</sup>.

In addition to the above-mentioned acknowledged redox mechanism, there are also some controversial reactions, such as the over-lithiation mechanism of the benzene ring [106]. The mechanism will be discussed in detail in the anode part. Due to the large specific surface area of COFs, a larger contact surface and space is provided for the adsorption of alkali metal ions, which implies that COFs may simultaneously have two energy storage methods (redox active sites and surface adsorption). This behavior may bring additional advantages to the specific capacity of the anode.

The theoretical capacity ( $C_T$ ) is calculated by the equation:

$$C_T = \frac{nF}{3600(M_w/1000)}$$

where  $n$  and  $M_w$  are the number of charge carrier and the molecular weight of the repetitive unit in COF, respectively.  $F$  is the Faraday constant (96485 C mol<sup>-1</sup>). Significantly, the key to the accurateness of the

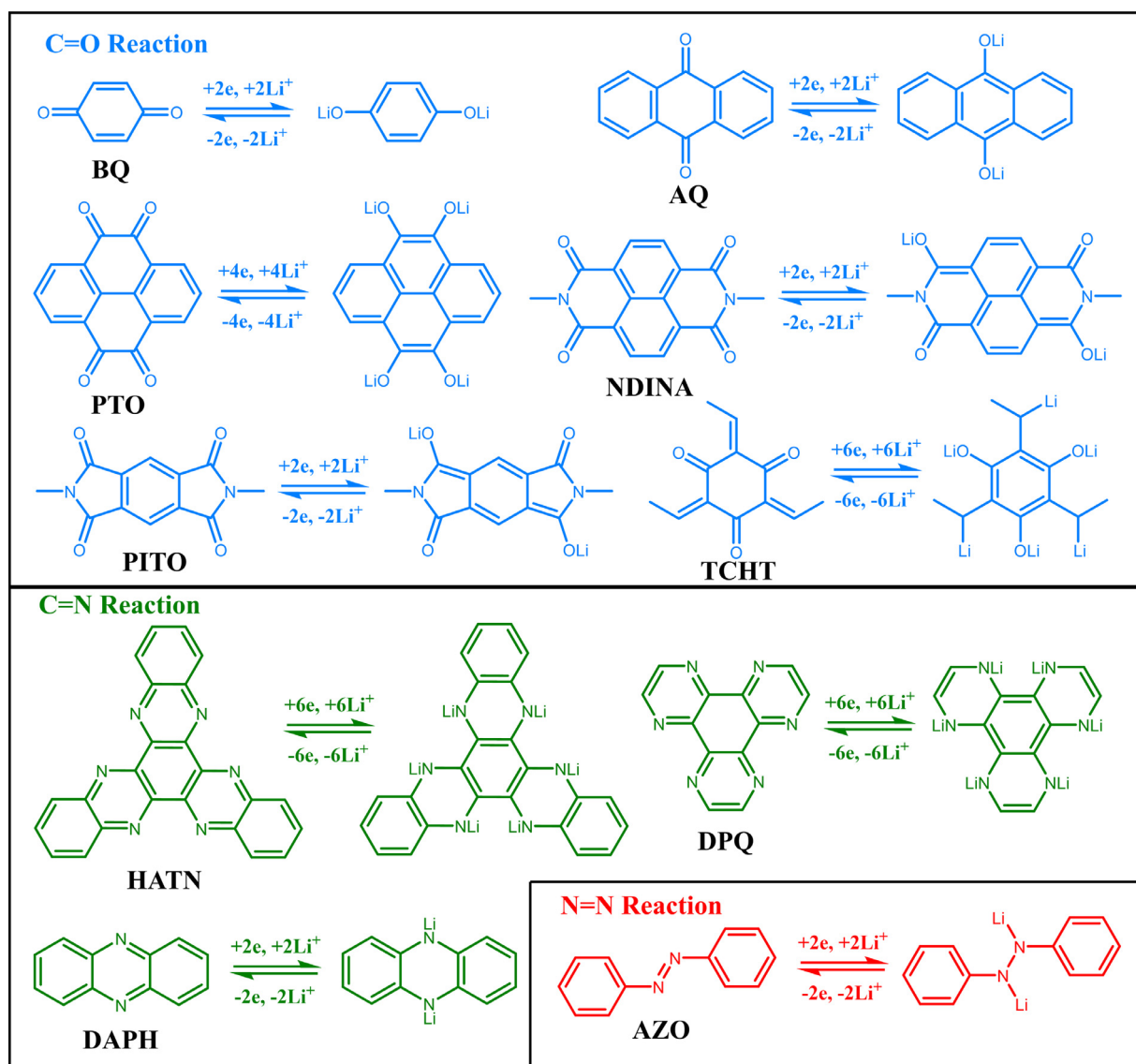


Fig. 2. Common active units and electron transfer numbers in COFs.

oretical capacity lies in the correct division of repeating units. For example, COF PPTODB could be divided into three different repeating units, but only 2 and 3 can be used for calculating the theoretical capacity (Fig. 3b). Additionally, due to the uncertainty of the functional groups, it is difficult to calculate the theoretical capacity of some COFs, which are mainly used as anodes.

### 3.2. Optimization strategies in the cathodes

#### 3.2.1. Increasing redox-active sites

The mass-specific capacity of the electrode materials is critical to the overall performance of the battery, which represents the capacity limit per unit mass of a battery. Improving the specific capacity of COFs materials has always been the main purpose and focus of researchers. Designability of the framework gives COFs the potential for high capacity. Introducing active groups in the framework while reducing the load of inactive groups is considered as an effective way to increase the specific capacity of COF materials. For example, the repeating unit of BQ1-COF contained 6 C=O and 12 C=N redox-active sites, which theoretically could receive/release 18  $\text{Li}^+$  reversibly [107]. Therefore, an ultra-high theoretical capacity of  $773 \text{ mAh g}^{-1}$  could be provided. At a

current density of 0.05 C ( $1\text{C}=773 \text{ mA g}^{-1}$ ), batteries based on BQ1-COF electrode can achieve an extra high specific capacity of  $502.2 \text{ mAh g}^{-1}$  in the second cycle (Fig. 4a). In the voltage of 1.2 V–3.5 V, the BQ1-COF-based electrode exhibited an average discharge voltage of 2.06 V. Compared with the traditional commercial cathode materials of  $\text{LiCoO}_2$  and  $\text{LiMn}_2\text{O}_4$  (energy density is about  $180 \text{ Wh kg}^{-1}$ ), its high energy density ( $1033 \text{ Wh kg}^{-1}$ ) has attracted intensive attention. More importantly, even at an ultra-high rate of  $7.73 \text{ A g}^{-1}$  (10 C), a reversible capacity of  $170.7 \text{ mAh g}^{-1}$  was obtained (Fig. 4b), and the energy and power densities still remained about  $350 \text{ Wh kg}^{-1}$  and  $12.6 \text{ kW kg}^{-1}$ , respectively. The density functional theory (DFT) calculation results showed that the position between the C=O group and the C=N group was adjacent in the extended  $\pi$  conjugated system thus the N and O atoms could generate a synergistic effect and constituted a stable five-membered chelate ring (C–N–Li–O–C) with lithium ions during lithiation process (Fig. 4c). However, after receiving 12 lithium ions, the combination of BQ1-COF and lithium ions became more difficult due to the steric effect and stability, resulting in a significant enhancement in the binding energy of BQ1-COF with  $\text{Li}^+$ . Significantly, the higher average potential of BQ1-COF was attributed to the lower lowest unoccupied molecular orbital (LUMO) level ( $-4.20 \text{ eV}$ ).

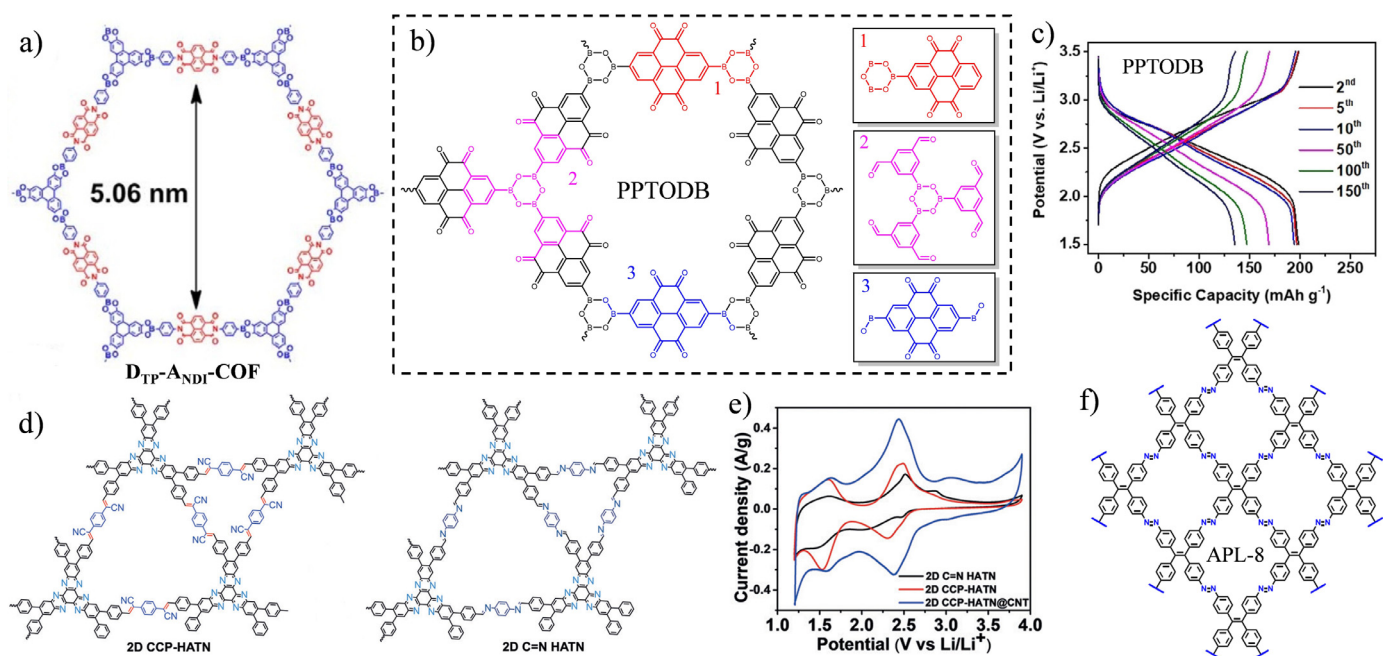


**Fig. 3.** (a) Construction of the  $D_{TP}\text{-A}_{NDI}\text{-COF}$ . Reproduced with permission [95]. Copyright 2015, Nature Publishing Group. (b) Construction of PPTODB. (c) Charge/discharge profiles of PPTODB. Reproduced with permission [94]. Copyright 2019, Wiley-VCH. (d) Constructions of 2D CCP-HATN and 2D C=N HATN. (e) CV curves at a scan rate of  $1\text{ mV s}^{-1}$ . Reproduced with permission [102]. Copyright 2019, Wiley-VCH. (f) The structure of APL-8. Reproduced with permission [98]. Copyright 2019, American Chemical Society.

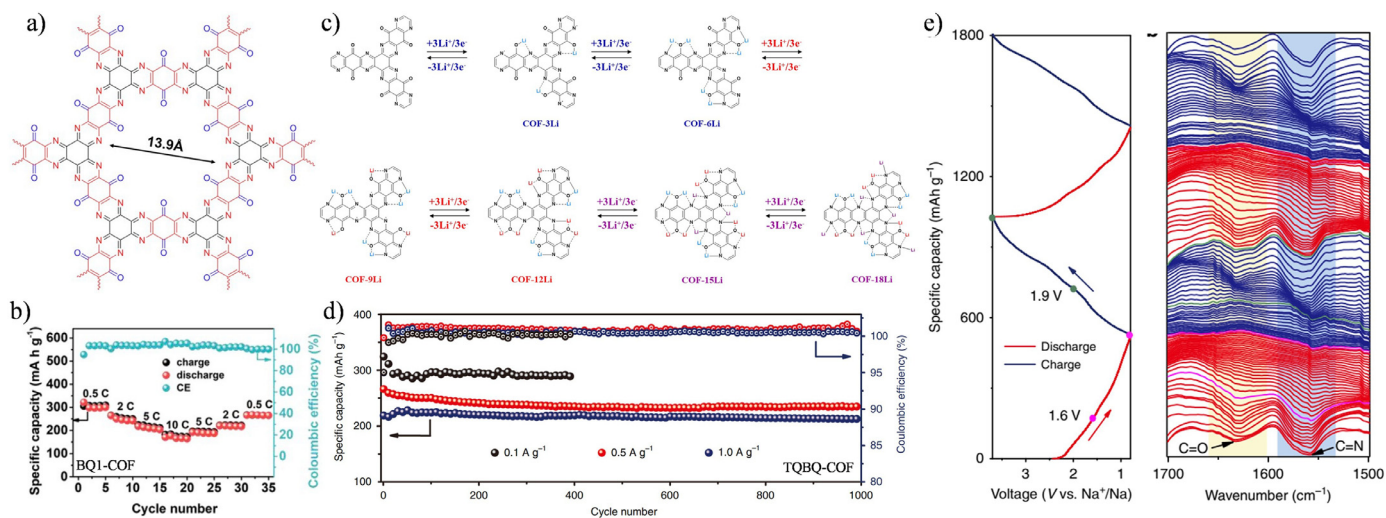


**Fig. 4.** (a) The structure of BQ1-COF or TQBQ-COF materials. (b) Rate performance of BQ1-COF. (c) 18  $\text{Li}^+$  insertion/extraction reactions with a BQ1-COF repeating unit. Reproduced with permission [107]. Copyright 2020, Elsevier Inc. (d) Long-term cycle performance of TQBQ-COF electrode. (e) In-situ FTIR spectra (right) collected corresponding to left. Reproduced with permission [108]. Copyright 2020, Nature Publishing Group.

At the same time, Shi et al. [108] also synthesized TQBQ-COF with the same structure as BQ1-COF and applied it to SIBs. In 1–3.6 V and at  $0.02\text{ A g}^{-1}$ , the TQBQ-COF electrode exhibited an initial discharge capacity of  $452.0\text{ mAh g}^{-1}$ . After 1000 cycles at  $0.5$  and  $1.0\text{ A g}^{-1}$ , the reversible capacities of the TQBQ-COF based batteries still maintained 91.3% and 96.4% (Fig. 4d), which delivered  $236.5$  and  $213.6\text{ mAh g}^{-1}$ , respectively. The compacted density of TQBQ-COF was calculated to be above  $1.63\text{ g cm}^{-3}$  by powder compaction, indicating that the volume energy density of the TQBQCOF electrode reached about  $1252\text{ Wh L}^{-1}$ . In-situ Fourier transform infrared (FTIR) spectra were carried out to explain the sodium storage mechanism of TQBQ-COF (Fig. 4e). The characteristic peaks at about  $1627$  and  $1545\text{ cm}^{-1}$ , respectively, were assigned to the carbonyl and pyrazine of the TQBQ-COF electrode.

During the sodiation process, these two characteristic peaks gradually decreased. Until discharging to  $0.8\text{ V}$ , the characteristic peak of the carbonyl group almost disappeared, while the characteristic peak of C=N was slightly reserved. During the desodiation process, the characteristic peaks of  $1627$  and  $1545\text{ cm}^{-1}$  reappeared and gradually increased, and finally returned to the initial state. The reversible insertion/extraction process of Na ions was proven by the same phenomenon in the first two cycles.

### 3.2.2. Increasing the exposure of the active sites

Although the functional groups of COFs are accurately distributed through the long-range ordered frame and regular pores. However, the active sites of COFs are excessively stacked and buried deep in the

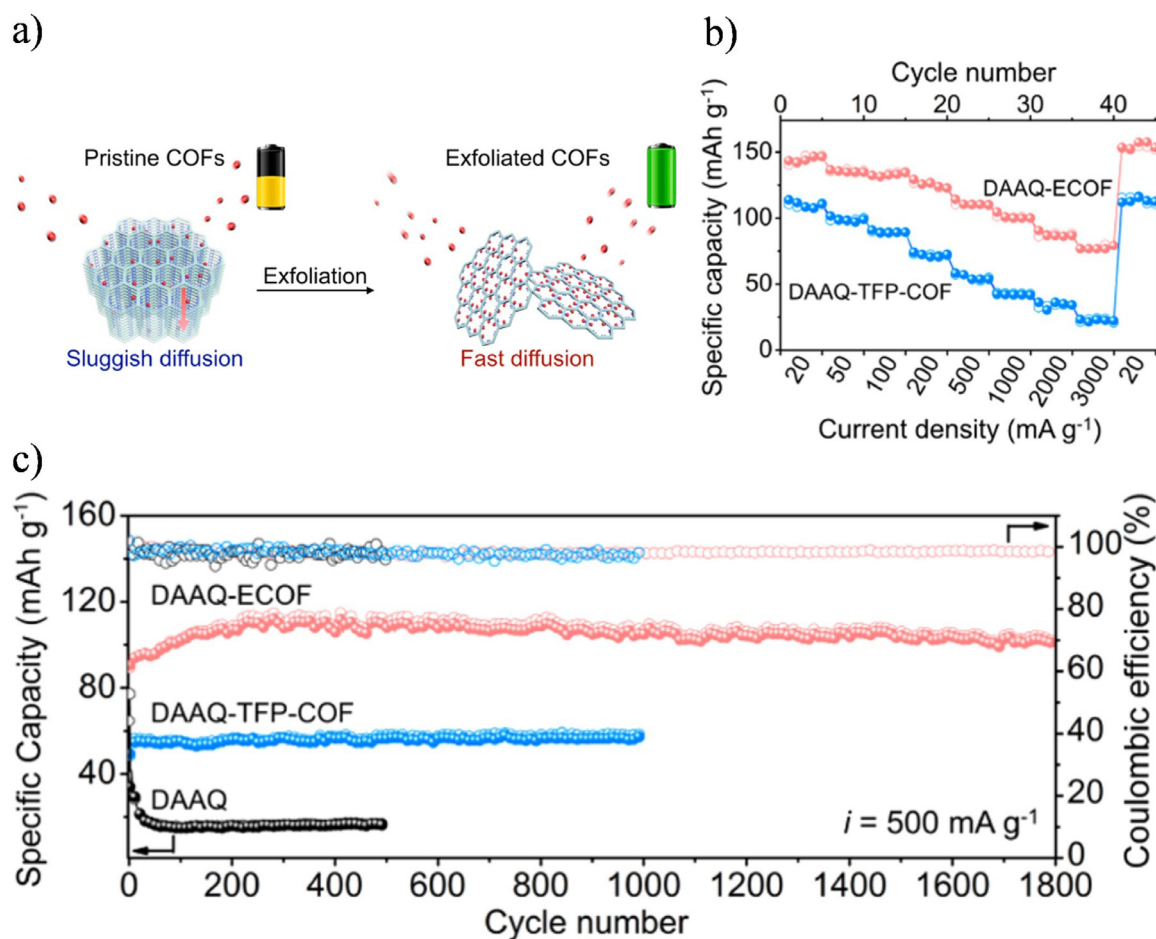


Fig. 5. (a) Schematic illustration for the exfoliation of 2D stacked COFs into exfoliated COFs. (b) Rate cyclability of DAAQ-ECOF and DAAQ-TFP-COF. (c) Long-term cyclability and Coulombic efficiencies. Reproduced with permission [110]. Copyright 2017, American Chemical Society.

center of 1D pore due to the excessive  $\pi$ - $\pi$  interaction force between molecules. The functional groups in the center are difficult to contact and react with alkali metal ions, resulting in insufficient utilization of active sites, thereby reducing the actual specific capacity and rate performance. Molecular structural design is difficult to solve the above problems, while nanostructure designs could make up for this deficiency. Increasing the accessible exposure of active sites by nanostructure designs such as mechanical ball-milling is one of the available means to improve its performance [109]. Wang et al. [110] prepared DAAQ-ECOF with a thickness of about 5 nm by mechanical ball-milling (Fig. 5a). The excessive accumulation of DAAQ-COF was effectively decreased. The  $\text{Li}^+$  diffusion coefficients of the original COF and exfoliated DAAQ-ECOF were  $2.48 \times 10^{-11}$  and  $6.94 \times 10^{-11} \text{ cm}^2 \text{ s}^{-1}$ , respectively, indicating that the ionic conductivity of DAAQ-ECOF has been slightly improved. There was a large amount of  $\text{Li}^+$  on the surface/near-surface of the exfoliated COF, which was beneficial to the full utilization of active sites and the rapid transfer of ions. At a current density of  $20 \text{ mA g}^{-1}$ , DAAQ-ECOF exhibited a 96% theoretical capacity (Fig. 5b) and no significant attenuation after 1800 cycles, and still provided a capacity of  $104 \text{ mAh g}^{-1}$  at a rate of  $0.5 \text{ A g}^{-1}$  (Fig. 5c). Under the same conditions, the performance of the DAAQ-ECOF electrode was almost twice of that of the pristine sample. Besides, the PI-COF-1 material composed of PMDA and tris(4-aminophenyl) amine (TAPA) was also stripped into several layers by ball-milling, and the battery performance was improved due to the shortened electron/ion migration length. At  $0.1 \text{ C}$  ( $1 \text{ C} = 14.2 \text{ mA g}^{-1}$ ), the initial  $85 \text{ mAh g}^{-1}$  increased to  $112 \text{ mAh g}^{-1}$  after stripping.

### 3.2.3. Optimizing electrode conductivity

Organic electrodes usually have the problem of low conductivity, so how to solve this problem is an urgent matter in the organic electrode materials [111–113]. The mainstream methods mainly include two directions: (1) Improve the overall electronic conductivity of the electrode by adding highly conductive additives into the electrode. (2) Reduce the bandgap of COF materials through molecular design and synthesize continuous conjugated large  $\pi$  bonds to improve the inherent conductivity of the material.

Due to the low electrochemical accessibility of active functional groups, the thickness of COF-based device films grown on conductive substrates is limited to less than 250 nm. Fortunately, electrode materials based on COF microcrystalline powders do not need to form a thin film, which will contribute to obtain higher conductivity and simplify manufacturing processes. Therefore, the composites of highly conductive additives with COFs through nanostructure design can improve the electrochemical performances of the cathodes. Wang et al. [114] coated 2D-PAI on carbon nanotubes (2D-PAI@CNT) using the  $\pi$ - $\pi$  stacking interaction as a driving force by condensation reaction for LIBs cathode (Fig. 6a). Compared with the original 2D-PAI electrode ( $28.5 \text{ mAh g}^{-1}$  at  $0.1 \text{ A g}^{-1}$ ), the 2D-PAI@CNT cathode provided a largely enhanced capacity of  $104.4 \text{ mAh g}^{-1}$  (Fig. 6b). Interestingly, even the 2D-PAI/CNT cathode with a mass ratio of 1:1 of 2D-PAI and CNTs still showed a capacity of  $65.6 \text{ mAh g}^{-1}$  under the same conditions, which adequately indicates the great advantage of in-situ CNTs recombination. At  $0.5 \text{ A g}^{-1}$ , no significant capacity degradation was observed in the 2D-PAI@CNT cathode after 8000 cycles, and the capacity was maintained at

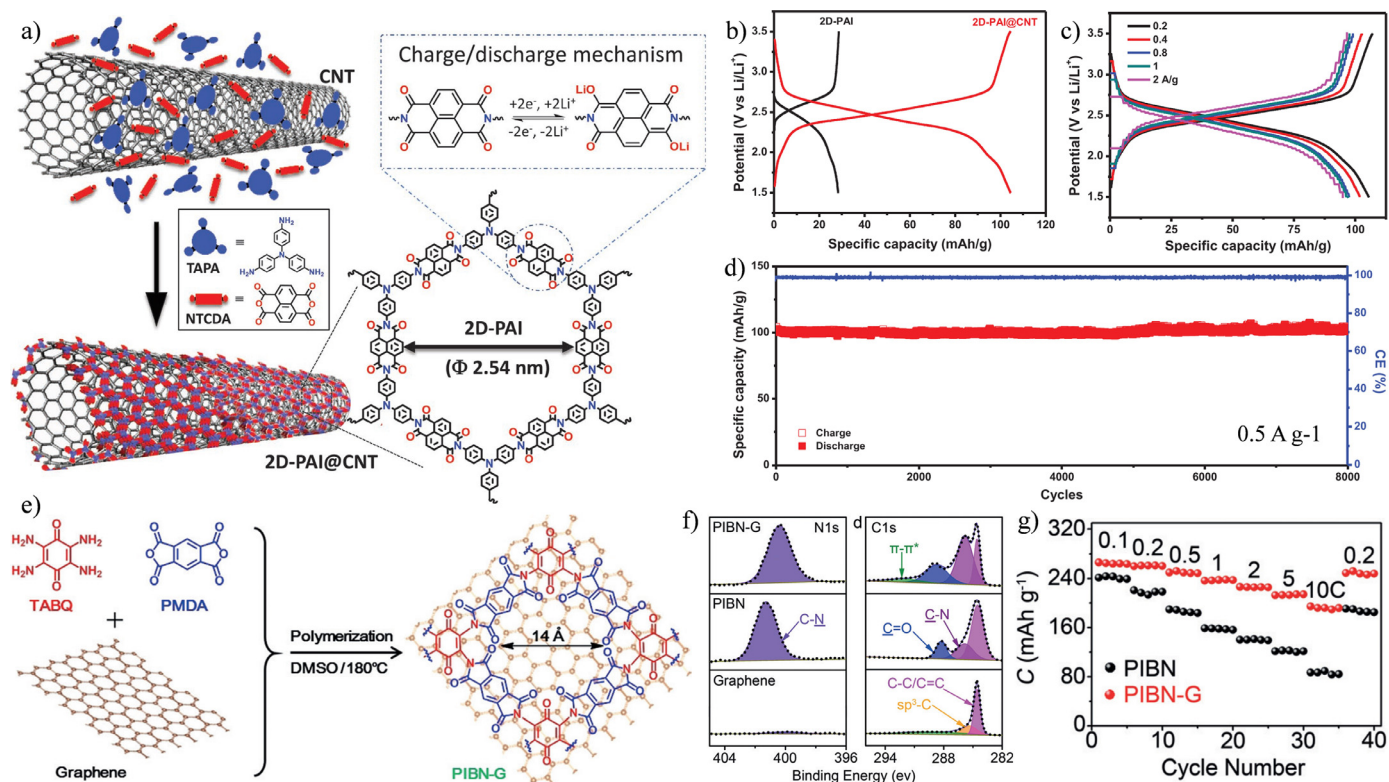


**Fig. 6.** (a) Synthesis of 2D-PAI@CNT and depiction of redox activity. (b) Charge-discharge curves of 2D PAI and 2D PAI@CNT at 0.1 A g<sup>-1</sup>. (c) Charge-discharge curves of 2D PAI@CNT at various current rates. (d) Long-term cyclability of 2D-PAI@CNT. Reproduced with permission [114]. Copyright 2019, Wiley-VCH. (e) Synthesis of PIBN and PIBN-G. (f) XPS spectra of N1s and C1s. (g) Rate performances of PIBN-G and PIBN. Reproduced with permission [93]. Copyright 2018, Wiley-VCH.

100 mAh g<sup>-1</sup> (Fig. 6d). Besides, the reversible capacity only slightly decreased along with the increased rate from 0.2 to 2 A g<sup>-1</sup>, and no increased polarization was observed at different rates (Fig. 6c), indicating that 2D-PAI@CNT possesses a prominent ion/electron migration ability. The introduction of CNTs in COF composites facilitates the electron conductivity. However, the excessive use of CNTs will reduce the overall energy density of the electrode and increase the cost of cell in large-scale applications.

2D graphene is widely used as conductive additives due to its remarkable conductivity. The atoms or molecules could be adsorbed/desorbed on the surface due to the abundant oxygen-containing groups, which facilitates the growth of specific COFs. 20 wt% graphene was introduced during the synthesis of PIBN COF to synthesize PIBN-G by Luo et al (Fig. 6e) [93]. The DFT calculated results of differential charge density showed that the charge was transferred from graphene to PIBN through the intermolecular  $\pi$  electron interaction, which not only enhanced the stability of PIBN but also improved the electron transport of PIBN-G. In the N1s spectrum of Fig. 6f, the binding energy of PIBN-G was significantly lower than that of PIBN, which indicates that there is electron transfer and  $\pi$ - $\pi$  stacking between the phenyl group of the COF and the carbon ring of sp<sup>2</sup> hybrid graphene. In rate tests (Fig. 6g), PIBN-G exhibited twice the capacity of PIBN at 5 C, which is attributed to the external influence of graphene on the conductivity of the COF cathode material.

In addition to inorganic conductive materials, conductive polymers can also be used as additives to improve the conductivity of electrodes. Vitaku et al. [115,116] synthesized DAAQ-TFP COF and employed it for energy storage (Fig. 7a), but it was found that its rate performance was not desirable. After adding conductive poly(3,4-ethylenedioxythiophene) (PEDOT), its conductivity has been increased from the original  $4.8 \times 10^{-5}$  to  $7.2 \times 10^{-5}$  S cm<sup>-1</sup>. The rate performance of DAAQ-TFP COF is significantly improved, especially at high

rates (Fig. 7b). Then 2,7-diaminophenazine (DAHP) instead of DAAQ was utilized to prepare DAHP-TFP COF. In contrast, although the conductivity of the DAHP-TFP COF electrode had been further enhanced by introducing PEDOT, the effect on the rate performances were not prominent. The change of Li<sup>+</sup> diffusion coefficients indicated that PEDOT had little effect on the DAHP-TFP COF electrode diffusion coefficient. It is not the electron transport but the ion transport playing a limiting role in this electrode material, which means that increasing the ion diffusion rate may be another way to improve battery performance. Although conductive additives (such as PEDOT, CNTs, RGO, etc.) can effectively improve the conductivity of the electrode, the introduction of a large number of additives may hinder the commercialization of high energy density batteries. From a long-term perspective, the problems related to poor conductivity could be eradicated by both improving intrinsic conductivity and introducing conductive additives.

In COF materials, there are no free electrons or ions, which makes their charge transfer rate sluggish in general. It limited the development of COFs as battery cathode materials. Fortunately, the chemical and physical properties of the framework could be finely tuned through the excellent designability. The LUMO energy level could be effectively fine-tuned by introducing the acceptor unit to form an electronic push-pull effect, thereby improving the operating voltage and conductivity. Shi et al. calculated the density of state (DOS) and found that the energy bandgap between highest occupied molecular orbital (HOMO) and LUMO energy levels could be reduced by introducing N atoms, and the bandgap of TQBQ-COF can reach below 1.0 eV, implying that the TQBQ-COF possesses a characteristic of semiconductors [108]. The experimentally measured electronic and ionic conductivity (for discharge products) were about 10<sup>-9</sup> S cm<sup>-1</sup> and 10<sup>-4</sup> S cm<sup>-1</sup>, respectively, which shows that the conductivity has been effectively improved. In addition, the synthesis method and crystallinity of COFs also have a signif-

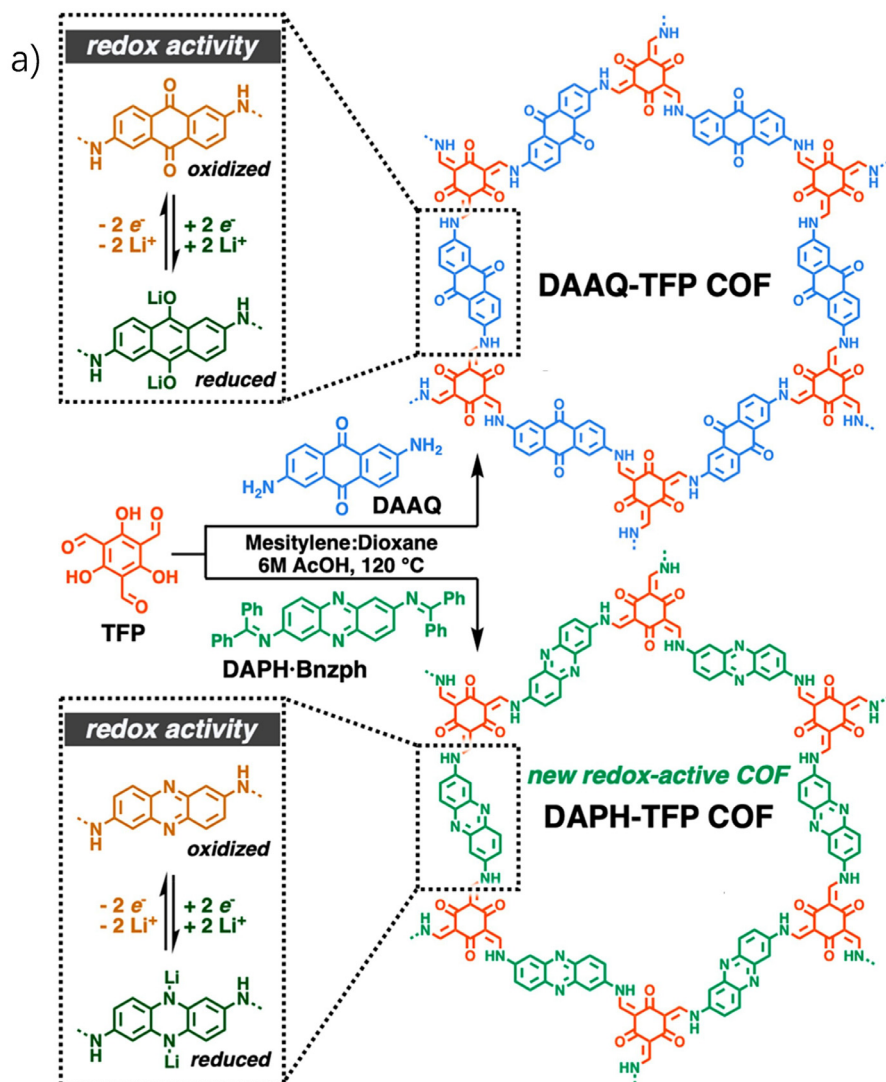
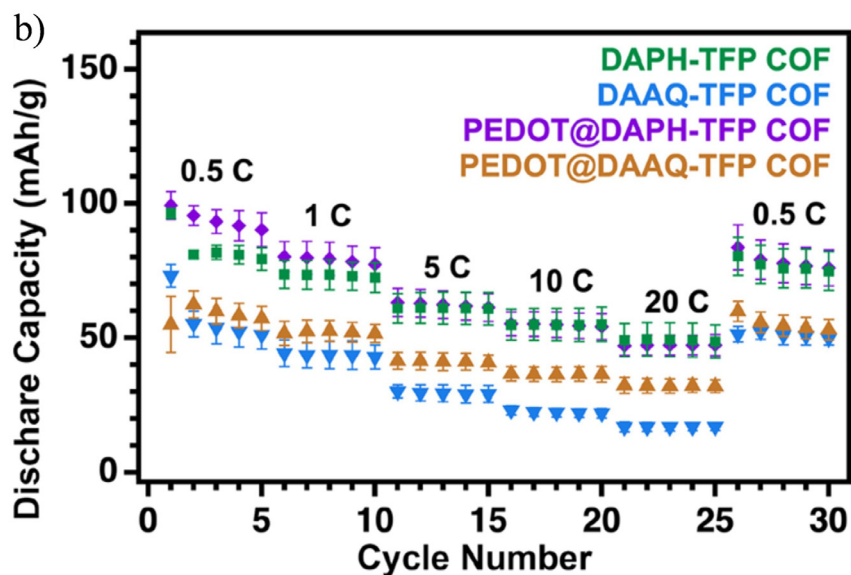


Fig. 7. (a) Synthesis of DAAQ-TFP and DAPH-TFP COFs and energy storage process. (b) Rate capabilities. Reproduced with permission [116]. Copyright 2019, American Chemical Society.



**Table 1**  
COFs as the cathodes

Batteries	Materials	Active unit	Rate performance		Cycling performance	Voltage range (V)	Specific surface (m <sup>2</sup> g <sup>-1</sup> )	Ref.
			CD	SC				
LIBs	BQ1-COF	-C=N-, -C=O	386.5	~300	1540/1000/198.4	1.2-3.5	94.73	[107]
			1546	~250				
			3865	~210				
LIBs	PI-ECOF-1	-C=O	7730	170.7	142/300/72	1.5-3.5	576	[109]
			1420	60				
	PI-ECOF-1/rGO50	-C=O	14.2	167	142/300/~106	1.5-3.5	223	
			142	132				
			1420	90				
LIBs	PI-COF-2	-C=O	12.8	103	128/300/~59	1.5-3.5	720	
			640	10				
	PI-COF-2/rGO30	-C=O	12.8	124	128/300/~88	1.5-3.5	173	
			640	37				
LIBs	PIBN	-C=O	28	244.8	-/-/-	1.5-3.5	-	[93]
			1400	~120				
LIBs	PIBN-G	-C=O	28	271	1400/300/208.1	1.5-3.5	-	[118]
			1400	206.7				
LIBs	2D-PAI@CNT	-C=O	100	104.4	500/8000/100	1.5-3.5	768	[110]
			2000	95				
LIBs	2D-PAI	-C=O	100	28.5	-/-/-	1.5-3.5	1248	[110]
			20	145				
LIBs	DAAQ-ECOF	-C=O	500/1800/104	154	500/1800/104	1.5-4.0	316	
			100	129.1				
			1000	98.6				
			3000	76				
LIBs	DAAQ-TFP-COF	-C=O	20	110	500/1000/~59	1.5-4.0	-	
			3000	~24				
			200	69				
LIBs	D <sub>TP</sub> -A <sub>NDI</sub> -COF	-C=O	1000	58	200/700/74	1.5-3.5	1933	[95]
			50	104.3				
LIBs	Tp-DANT-COF	-C=O	200	92.3	1000/600/71.7	1.5-4.0	511	[54]
			1986.7	66.3				
			50	118.1				
LIBs	Tb-DANT-COF	-C=O, -C=N	2014.7	66.6	-/-/-	1.5-4.0	376	
			100	842				
			500	480				
LIBs	PGF-1	-C=N	72.5	~140	2900/1000/~75	1.25-2.5	649	[117]
			580	~100				
LIBs	AZO-1	-N=N	2900	~75	4000/5000/~126	1.2-3.0	317.4	[120]
			100	205				
			1000	173				
LIBs	Azo-CTF	-N=N-	4000	141	500/1200/165	1.5-4.0	384	[121]
			100	309				
			2000	174				
LIBs	HATNPF1	-C=N	100	205	500/1200/102	1.5-4.0	288	
			2000	112				
LIBs	HATNPF2	-C=N	100	116	500/1000/~91	1.2-3.9	-	[102]
			1000	94				
LIBs	2D CCP-HATN@CNT	-C=N	20	198	20/150/135.2	1.5-3.5	-	[94]
			1500	98				
LIBs	DAAQ-TFP	-C=O	157	53.5	314/500/~14	1.4-3.6	1140	[115]
			3140	~22				
	PEDOT@DAAQ-TFP	-C=O	157	59.8	314/500/~28	1.4-3.6	347	
			3140	~36				
LIBs	DAPH-TFP	-C=O, -C=N	171	81.7	342/500/~35	1.4-3.6	1155	
			3420	~55				
LIBs	PEDOT@DAPH-TFP	-C=O, -C=N	171	93.2	342/500/~35	1.4-3.6	230	
			3420	~55				
SIBs	TQBQ-COF	-C=O, -C=N	20	452	1000/1000/213.6	1-3.6	-	[108]
			1000	234				
			5000	180.6				
RMBs	COF	-C=N	10000	134.3	770/3000/37	0.8-2.5	428	[122]
			77	102				
			770	72				

icant influence on electronic conductivity. Liu et al. synthesized PGF-1 with better crystallinity under alkaline conditions as cathode for LIBs, which electronic conductivity can reach 0.3 S cm<sup>-1</sup> [117]. These examples indicate that the conductivity of COFs can be adjusted as desired. However, few reports are focusing on improving the intrinsic elec-

tronic conductivity of molecule units, although it may be a promising way to meet the requirements of electrodes. Apart from that, Table 1 summarizes the electrochemical properties of redox-active COFs as the cathodes.

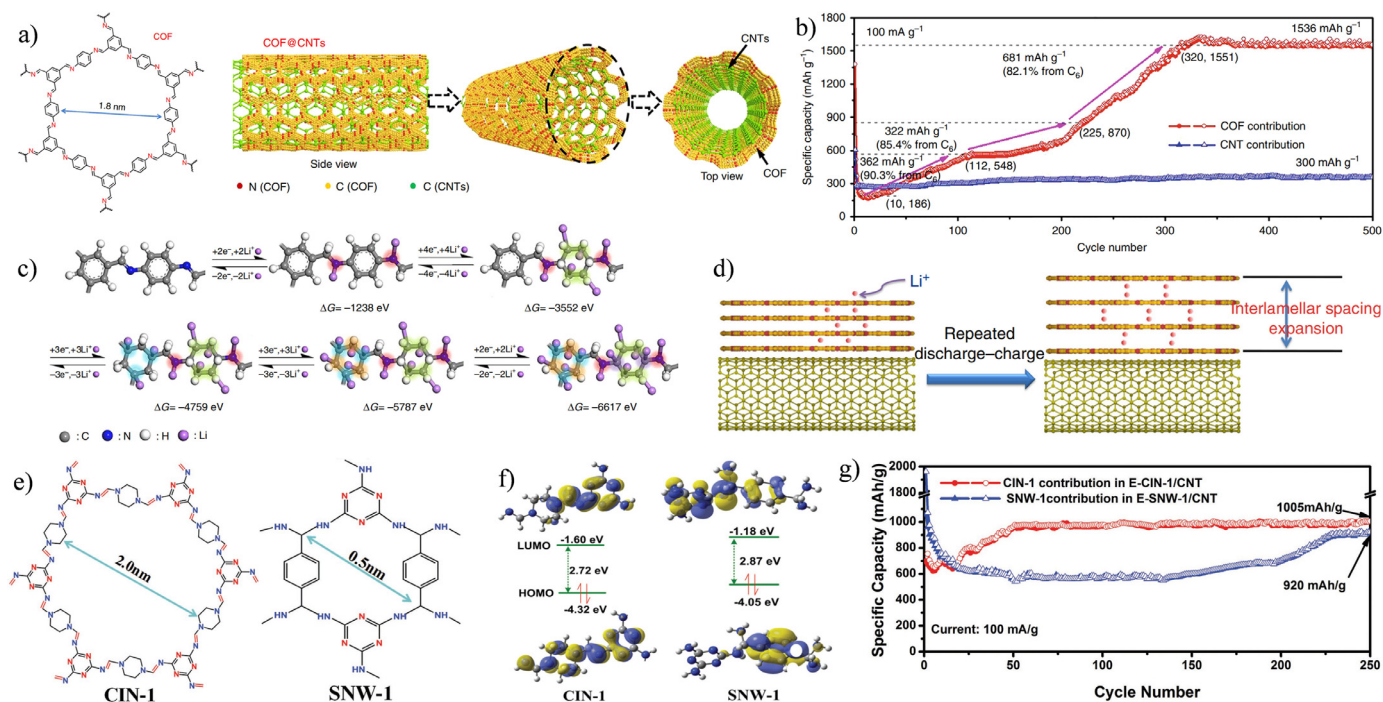


**Fig. 8.** (a) The structure of COF and COF@CNTs with few COF layers covered on the exterior surface of CNTs. (b) Cycle performance of COF (based on the mass of COF) in COF@CNTs. (c) The structure evolution of COF@CNTs during the lithiation process. (d) Facilitated Li<sup>+</sup> transport and storage into expanded COF layers during the repeated charge and discharge process. Reproduced with permission [124]. Copyright 2018, Nature Publishing Group. (e) The structures of CIN-1 and SNW-1. (f) HOMO/LUMO energy diagrams of the CIN-1 and SNW-1 monomers. (g) Capacity contribution of CIN-1 in E-CIN-1/CNT and SNW-1 in E-SNW-1/CNT. Reproduced with permission [125]. Copyright 2018, Wiley-VCH.

### 3.3. Optimization strategies in the anode

#### 3.3.1. Low potential active sites increasing the specific capacity

The redox potential of the active site in COFs determines whether the material acts as a cathode or anode. Even the same active site (such as -C=N-) has different redox potentials in different COF structures [107,123]. The redox activity of the material depends on the intrinsic reaction kinetics and the battery system. To design the COF anodes, the active functional groups with lower redox potential should be selected. Also, functional groups with large  $\pi$ - $\pi$  conjugates (such as benzene and naphthalene) usually exhibit exceptional lithium storage capacity (overlithiation) at low potentials. Han et al. suggested that each C<sub>6</sub> ring could theoretically accept/release 6 Li<sup>+</sup> reversibly to form a 1:1 Li/C complex. Lei et al. [124] synthesized COF@CNTs composite material with a few layers of COF (about 5 nm) wrapped around CNTs (Fig. 8a). The capacity contribution from the COF in the electrode increased from 186 mAh g<sup>-1</sup> to 1536 mAh g<sup>-1</sup> after 320 charge and discharge activations (Fig. 8b). This is attributed to the gradual lithiation of the C=N group and the benzene ring through a five-step lithiation/delithiation process, which makes COF@CNTs have a 14-lithium super storage capacity (Fig. 8c). During the activation process, the interlayer distance gradually expands as more Li<sup>+</sup> enters into the COF layer, thereby increasing the opportunity of the lithiation/delithiation of the benzene ring (Fig. 8d). The reversible changes of the C=N bond and C=C bond of the benzene ring were clearly detected by the FTIR and Raman technologies. Also, DFT was performed to theoretically calculate the two possible lithiation sites in each repeating unit. First, electron-rich N atoms were preferentially reacted with lithium ions, and then sp<sup>2</sup> hybridized carbon atoms on the two benzene rings could provide up to 12 lithiation sites through the formation of Li<sub>6</sub>/C<sub>6</sub>. It is worth noting that the reversible capacity of the COF is even higher than the theoretical capacity of inorganic anode materials such as Fe<sub>2</sub>O<sub>3</sub>, Co<sub>3</sub>O<sub>4</sub> and CuO (700-1000 mAh g<sup>-1</sup>). Subsequently, Lei et al. [125] prepared two stripped E-CIN-1/CNT and

E-SNW-1/CNT COF composite materials by the ball-milling method, and the reversible capacity could reach 1005 and 920 mAh g<sup>-1</sup> (based on the mass of COF), respectively, after 250 cycles at a current density of 0.1 A g<sup>-1</sup> (Fig. 8e-g). They guessed that the superior properties of these two composite materials might be related to the benzene ring, piperazine ring and triazine ring in addition to the C=N and -NH- groups participating in the redox reaction.

1,3,5-triformylphloroglucinol and amino groups frequently form low redox potential active sites and appear in COF materials as triangular corner blocks. Zhao et al. [123] designed a Tp-Azo-COF material with dual carbonyl and azo active sites for LIBs (Fig. 9a). The Tp-Azo-COF anode delivered a current density of 305.97 mAh g<sup>-1</sup> after 3000 cycles at 1 A g<sup>-1</sup> (Fig. 9b) and demonstrated exceptional stability. During the discharging process, the lithium storage first appeared at the C=O-based active site (the three C=O units of  $\beta$ -ketoenamine could receive 3 Li<sup>+</sup>), because the electronegativity of O atoms was stronger than that of N atoms (Fig. 9c). Then the N=N bond was reacted with two Li<sup>+</sup>. During charging, the active sites of Tp-Azo-COF were reduced to C=O bond and N=N bond, and Li<sup>+</sup> was released, completing the reversible reaction. Also, Gu et al. synthesized DAAQ-COF containing  $\beta$ -ketoenamine for SIBs. They proposed that each  $\beta$ -ketoenamine could reversibly receive/release 6 Na<sup>+</sup> ions, that is, in addition to the carbonyl group,  $\alpha$ -C radical intermediates could also receive 3 Na<sup>+</sup>.

#### 3.3.2. Introducing heteroatoms to improve conductivity

The introduction of heteroatoms plays a vital role in the regulations of COFs HOMO/LUMO energy levels as the energy levels and bandgap are significantly influenced by heteroatoms. Reducing the bandgap is beneficial to improve the intrinsic electronic conductivity of COFs. Heteroatoms or functional groups with strong electron-withdrawing properties (such as -F, -Cl, and -CN) can effectively reduce the energy bandgap of the material. Recently, a fluorine-containing COF material (E-FCTF) was reported by Zhang et al. [126] DFT calculation results showed

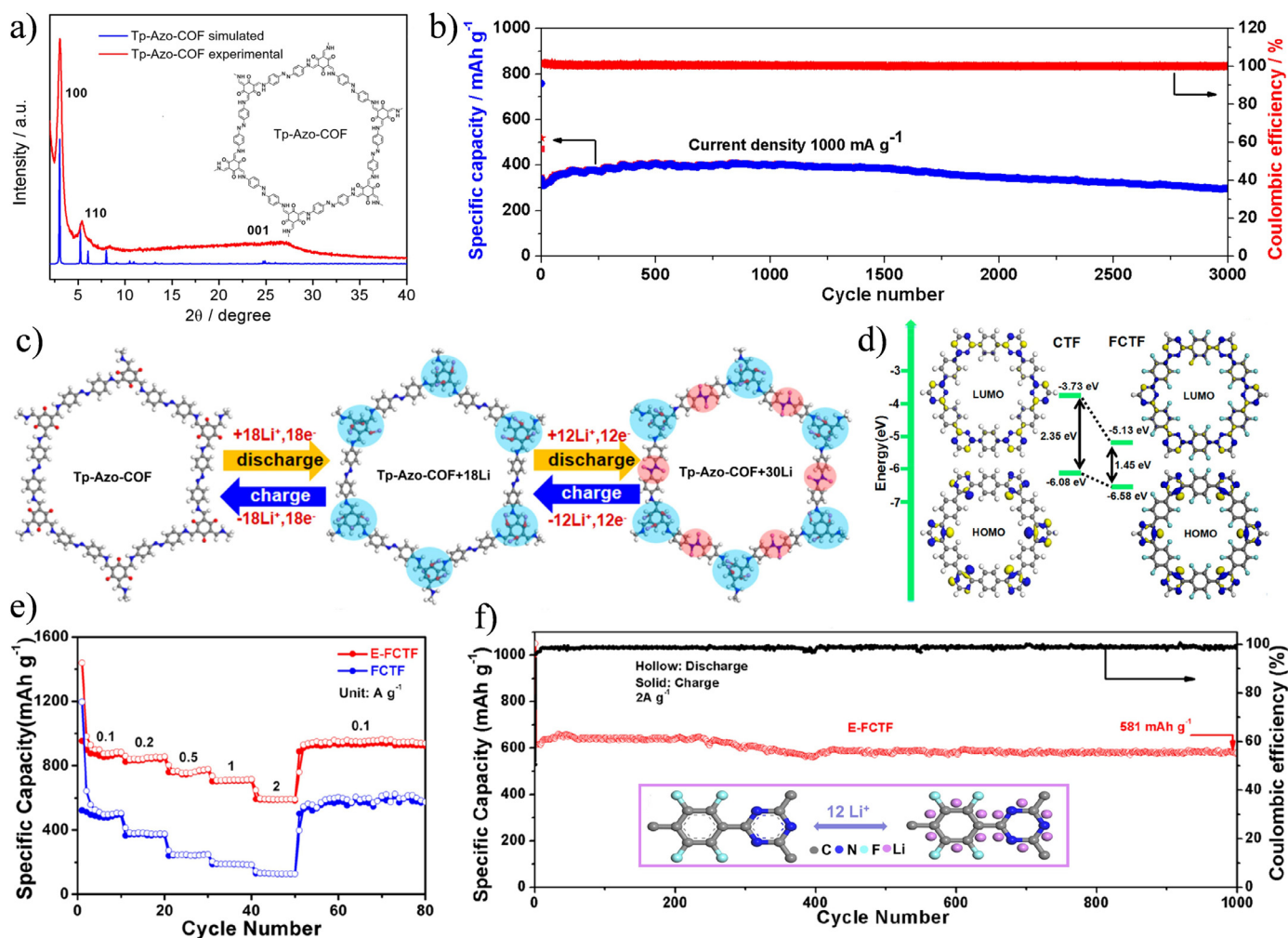


Fig. 9. (a) PXRD and structure patterns of Tp-Azo-COF. (b) Long-term cyclability of Tp-Azo-COF. (c) Structural evolution during the lithiation/delithiation procedure. Reproduced with permission [123]. Copyright 2020, American Chemical Society. (d) HOMO and LUMO diagrams of CTF and FCTF. (e) Rate capabilities of E-FCTF and FCTF. (f) Long-term cyclability of E-FCTF. Reproduced with permission [126]. Copyright 2019, American Chemical Society.

that the HOMO/LUMO energy level and bandgap of FCTF were significantly lower than those of fluorine-free CTF ( $-6.58/-5.13$  eV Vs  $-6.08$  eV/ $-3.73$  eV), resulting in the improvement of the conductivity and electrochemical performance of the FCTF electrode (Fig. 9d). The Galvanostatic intermittent titration techniques (GITT) results showed that the Li<sup>+</sup> diffusion coefficient ( $D_{Li^+}$ ) of the E-FCTF electrode stripped by ball-milling was higher than that of the fluorine-free E-CTF electrode, attributed to the shortened transport path and the introduction of F atoms. The E-FCTF-based electrode obtained reversible capacities of 886, 845, 771, 709, and 593 mAh g<sup>-1</sup> at 0.1, 0.2, 0.5, 1, and 2 A g<sup>-1</sup> (Fig. 9e), respectively. More importantly, excellent long-cycle performance (Fig. 9f) was achieved at 2 A g<sup>-1</sup> current density (581 mAh g<sup>-1</sup> retained after 1000 cycles).

### 3.3.3. Increasing the exposure of the active sites

Besides the designs and optimizations of anodes by molecular engineering, nanostructure designs have attracted intensive attention in recent years to improve battery storage performance. By changing the contact environment between the active sites and the electrolytes, the electrochemical performances of COFs can be improved. Apart from the common ball-milling method, a variety of methods have been developed to improve the electrochemical performance of COF-based anode by increasing the exposure of the active sites, including chemical exfoliated [127], acid-base driven method [128], self-exfoliated [129] and methanesulfonic acid stripping [130]. For instance, the TFPB-COF bulk

was stripped into E-TFPB-COF by Chen et al. [127] through the strong oxidant intercalation method (Fig. 10a), then E-TFPB-COF/MnO<sub>2</sub> retaining MnO<sub>2</sub> nanoparticles was prepared to prevent COFs from agglomerating again. After 300 cycles at 0.1 A g<sup>-1</sup> (Fig. 10b), the electrodes based on E-TFPB-COF/MnO<sub>2</sub> and E-TFPB-COF showed ultra-high reversible capacities of 1359 and 968 mAh g<sup>-1</sup>, respectively. As to the lithium storage mechanism, they presumed that the reversible lithiation process between E-TFPB-COF and lithium ions located on the frame wall (or the interlayers) was assigned to the redox reaction of the imine bonds and the benzene rings of the C=C bonds, which ultimately constituted N-Li and C-Li bonds (Fig. 10c). The excellent capacity and rate performances of the E-TFPB-COF/MnO<sub>2</sub> electrode were attributed to the stripping two-dimensional layered structure, which shortens the ion diffusion distance, improves the reaction kinetics of Li<sup>+</sup>, and the synergies effect between the COF and the MnO<sub>2</sub> nanoparticles.

The organic radical reaction is applied as an active site for charge storage in rechargeable batteries because of its higher reactivity and fast kinetics. However, the instability of most radical reactions and the irreversible dimer reactions between nearby free radicals result in the loss of electrode redox activity. Therefore, preventing side reactions is essential to maintain the reversible capacity and cycle life of the battery. Gu et al. [130] prepared four kinds of 2D DAAQ-COF materials with a thickness of 4–250 nm with NIB anode by ball milling and methanesulfonic acid stripping methods to explore the relationship between the stability

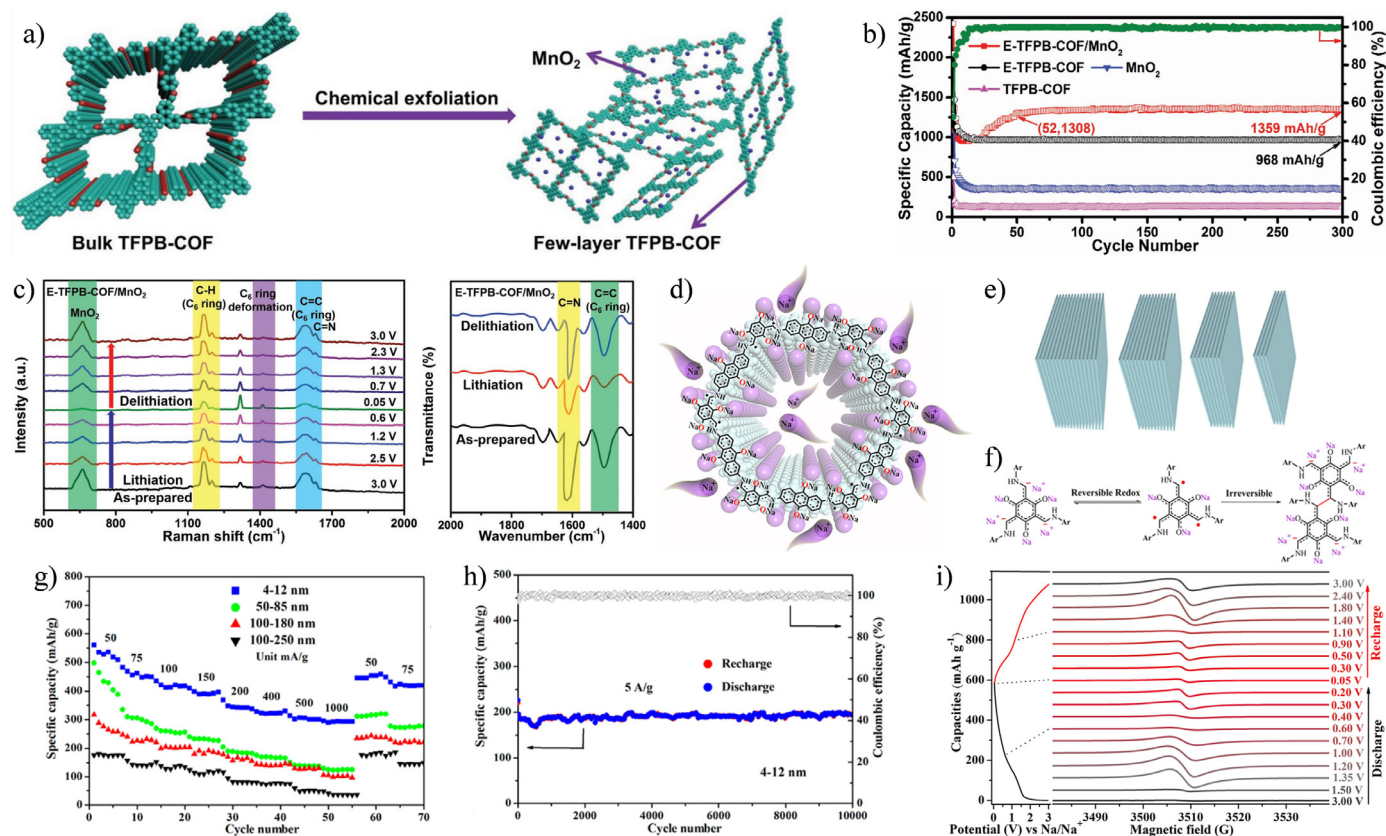


**Fig. 10.** (a) Schematic illustration of the chemical exfoliation of the TFPB-COF. (b) Cycle performances at 0.1 A g<sup>-1</sup>. (c) In-situ Raman (left) and ex-situ FTIR spectra (right) of the E-TFPB-COF/MnO<sub>2</sub> anode. Reproduced with permission [127]. Copyright 2019, Wiley-VCH. (d) The structure of DAAQ-COF. (e) Illustration of the 2D-COF with different stacked thickness. (f) Redox and deactivation mechanism of the radical intermediates. (g) Rate performances of the samples with different stacked thickness. (h) Long-term cyclability of the 4-12 nm thick sample. (i) EPR spectra upon discharging. Reproduced with permission [130]. Copyright 2019, American Chemical Society.

of radical intermediates and the thickness of COFs (Fig. 10d, e). At a current density of 50–1000 mA g<sup>-1</sup>, the COF treated with methanesulfonic acid and methanol (with a thickness of 4–12 nm) exhibited better rate performance than that under other conditions (Fig. 10g). More importantly, the capacity of the thinnest sample remained at 198 mAh g<sup>-1</sup> after 10,000 cycles at a rate as high as 5 A g<sup>-1</sup> (Fig. 10h). In the electron paramagnetic resonance (EPR) spectrum (Fig. 10i), strong fluctuations were detected at the 1.2 V and 0.3 V discharge sites, corresponding to the formation of two CO• radical intermediates, respectively. At the 0.6 and 0.05 V, the above two fluctuations were weakened, indicating the reduction of carbonyl radicals. The same fluctuations were found during the charging process, demonstrating the superior stability and reversibility of the C-O• radical intermediate (Fig. 10f). The experimental results showed that the self-discharge behavior could be effectively suppressed by reducing the thickness of the COF layers and adjusting the reactivity and stability of the free radical intermediate. A larger specific surface area is more conducive to the contact between the active site and the electrolyte. The factors that affect the surface area mainly include particle size, particle shape, and pore content. One of the main purposes of the exfoliated method is to increase the specific surface area of the material. However, COFs with a large specific surface area exhibits a large number of pores, therefore the tap density of the prepared electrode sheet is low, which may affect its commercial application in the future.

### 3.3.4. Carbonization

Carbon materials, especially the carbon materials doped with heteroatoms, are widely utilized as anode materials ascribing to their abundant reserves, high conductivity, and low cost [131–133]. However, the

uneven distribution of the doped atoms seriously impedes the doping effect. The ultra-customizable COFs and uniformly distributed pore sizes offer a satisfactory solution to this issue by providing atomically ordered heteroatoms and fast-transmitting ion channels after carbonization, which highly improves the utilization of heteroatoms and alleviates volume expansion. Zhang et al. [133] prepared three batches of N-doped NPCs by carbonizing TPPA-COFs at high temperatures of 500, 600 and 700°C, respectively, and utilized the as-prepared materials as the anode materials in LIBs and SIBs (Fig. 11a). At a current density of 100 mA g<sup>-1</sup>, NPC-2 provided a reversible capacity of 488 mAh g<sup>-1</sup> and 237.7 mAh g<sup>-1</sup> in LIBs and SIBs (Fig. 11b), respectively. In addition, Ni et al. [134] also reported their work about COF carbonization (Fig. 11c). Due to the high reactivity and conductivity provided by the N, B doped atoms, LIBs based on NBC-900 electrodes still maintained a high reversible capacity of 205.5 mAh g<sup>-1</sup> at 5.0 A g<sup>-1</sup> (Fig. 11d). It should be noted that although the conductivity of the COF material is increased by carbonization, the functional groups on the COF are also destroyed due to high temperature [135], which means that the advantages of COFs are lost, including redox activity and the inherent high specific capacity. As shown in Table 2, we summarized the electrochemical performances of the recently published redox active COFs as anodes.

## 4. Applications of non-redox active COFs

In Li-S batteries, COFs can effectively suppress the shuttle effect of lithium polysulfide due to the regular and ordered porous structure, and enhance the conductivity of sulfur cathodes [139–141]. Besides, the diffusion of PSS may also be prevented from interacting with PSS through the heteroatoms inherent in COFs (such as N, O, F). For solid-

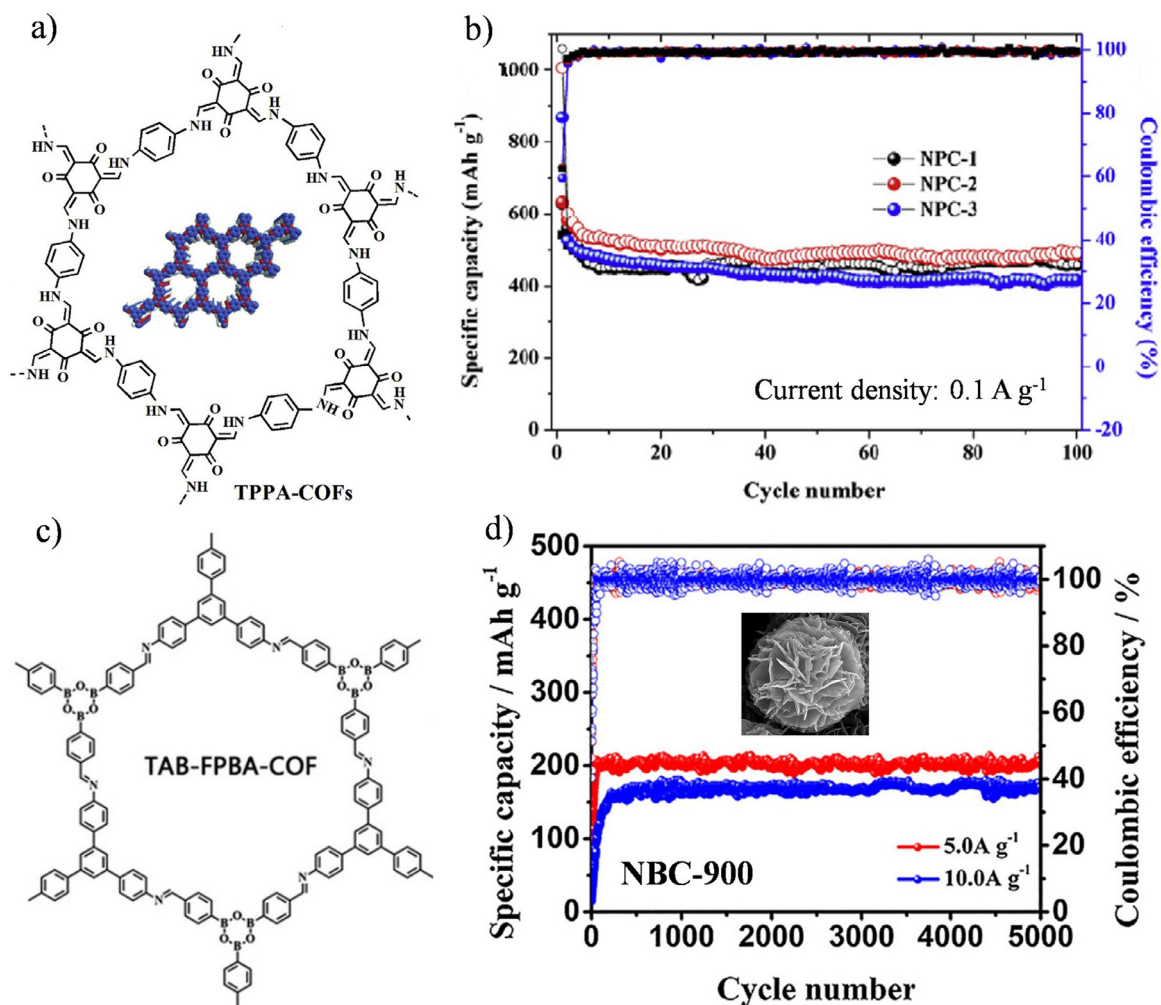


**Fig. 11.** (a) The structure of TPPA-COFs. (b) Cycling performances of NPCs. Reproduced with permission [133]. Copyright 2017, Elsevier Inc. (c) The structure of TAB-FPBA-COF. (d) Long-life cycling performances of NBC-900. Reproduced with permission [134]. Copyright 2019, Elsevier Inc.

state electrolytes, high thermal stability and ionic conductivity are the main advantages for assembling batteries. By using nanopores to provide a migration channel for lithium salts, COF-based solid-state electrolytes could introduce anion/cation or solvent molecules into COFs itself through exceptional design ability to promote ionic conductivity [63]. In this section, the application of COFs in Li-S batteries and solid electrolytes will be introduced respectively.

#### 4.1. Li-S batteries

Lithium-sulfur (Li-S) batteries have been one of the research hotspots contributed by their abundant resources, low cost, high theoretical energy density ( $2600 \text{ Wh kg}^{-1}$ ) and desirable theoretical specific capacity ( $1675 \text{ mAh g}^{-1}$ ) [142-148]. However, challenges still exist. First, the shuttle effect seriously impedes the further development of Li-S batteries [82,149-151]. During the charge-discharge process, insoluble  $\text{Li}_2\text{S}$  and  $\text{Li}_2\text{S}_2$ , and soluble polysulfide (PSs) intermediates ( $\text{Li}_2\text{S}_n$ ,  $n = 4, 6, 8$ ) can be formed. Those intermediates will diffuse from the cathode to the anode through the organic electrolyte and then deposit on the anode surface, resulting in the reduction of battery capacity, inadequacy of coulombic efficiency, and the rapid decline of cycle life. Second, it is difficult to achieve the theoretical capacity of the Li-S batteries without any improvements due to that the poor conductivity of sulfur and PSs lead to low utilization [152-154]. Finally, the volume expansion of the sulfur cathode after discharge can reach 80% [155-159], resulting

in mechanical damage to the lithium battery, which is also a serious obstacle to the commercialization of Li-S batteries.

Fortunately, the COFs composed of a robust covalent bond skeleton possess a large specific surface area, long-term stability and precise controllability. Through highly flexible molecular design, multifarious pore shapes, sizes and volumes can be realized to meet the customization requirements of Li-S batteries, such as the capture of lithium polysulfides, fast ions diffusion, and the provision of a host for sulfur. In this section, the applications of COFs are elaborated in both the host materials and the modified membranes.

##### 4.1.1. COFs as host materials for the sulfur cathodes

We summarized the design ideas of the host materials in the sulfur cathodes by reviewing previous research work on Li-S batteries [30,81,132,143,150,153,160,161]. The following characteristics are required for an ideal host material. (1) High conductivity for improving sulfur insulation and rate performances. (2) An excellent mesoporous structure for meeting the rapid transformation of ions. (3) The microporous structure for anchoring polysulfide. Apart from the traditional physical obstruction method, the mainstream interception methods are divided into two types. One is the introduction of lithium-philic heteroatoms or functional groups to interact with  $\text{Li}^+$ , leading to the capture of lithium polysulfide. The other is the introduction of sulfur-philic atoms or functional groups to interact directly with S. (4) Appropriate holes to accommodate the volume change of the sulfur cathode during charging and discharging process. (5) The regular and ordered porous

**Table 2**  
The electrochemical performances of COF-based anodes.

Batteries	Materials	Rate performance		Cycling performance	Voltage range (V)	BET surface area (m <sup>2</sup> g <sup>-1</sup> )	Ref.
		CD	SC				
LIBs	COF@CNTs <sup>1</sup>	100	1020	100/500/1021	0.005-3.0	52.7	[124]
		1000	470				
		5000	217				
LIBs	E-CIN-1/CNT <sup>1</sup>	100	538	100/250/744	0.001-3.0	525.1	[125]
		1000	210				
		5000	97				
LIBs	E-SNW-1/CNT <sup>1</sup>	100	542	100/250/687	0.001-3.0	380.1	[123]
		1000	367				
		5000	212				
LIBs	Tp-Azo-COF	240	494.5	1000/3000/306	0.01-3.0	632	[126]
		1600	145.8				
		2400	90.8				
LIBs	E-FCTF	100	871	2000/1000/581	0.005-3.0	583	[129]
		500	762				
		2000	586				
LIBs	IISERP-CON1	50	835	500/1000/~595	0.01-3.0	507	[127]
LIBs	E-TFPB-COF/MnO <sub>2</sub>	100	~1000	100/300/1359	~0-3.0	345	[128]
		1000	~750				
		100	816				
LIBs	f-CTF-1	100	816	1000/500/560	0.05-3.0	-	[128]
		1000	573				
		10000	186				
LIBs	N <sub>2</sub> -COF	200	~806	1000/500/~610	0.05-3.0	1496	[51]
		5000	497				
		200	~860				
LIBs	N <sub>3</sub> -COF	200	~860	1000/500/~600	0.05-3.0	1142	[101]
		5000	~555				
		200	535.3				
LIBs	PA-COF	200	535.3	1000/2000/240.9	0.01-3.5	43.0	[101]
		5000	141.8				
		200	442.2				
LIBs	TB-COF	200	442.2	1000/2000/226.2	0.01-3.5	21.7	[52]
		5000	144.0				
		666	200				
LIBs	TThP	666	200	1000/200/381	0.005-3.0	-	[133]
LIBs	NPC-2 (Carbonization)	100	505.7	5000/5000/143	~0-3.0	482.06	[130]
		5000	102.7				
		50	239.5				
SIBs	NPC-2 (Carbonization)	50	239.5	2500/5000/88.8	0.005-3.0	-	[130]
SIBs	DAAQ-COF (4-12 nm)	2500	127	5000/10000/198	0.05-3.0	-	[99]
		50	500				
		1000	300				
SIBs	TFPB-TAPT	200	145	-	0.05-1.6	120	[136]
SIBs	Aza-COF	60	523	3000/500/241	0.01-3.0	240	[137]
		6000	161				
		100	90				
SIBs	IISERP-CON16	100	90	-	0.05-3.0	920	[137]
		100	195	-	0.05-3.0	1452	
		100	400	1000/1400/312.8	0.05-3.0	1745	
SIBs	ALP-8	1000	~320	83.4/150/~168	0.01-3.0	550	[98]
		278	108				
		2780	70				
SIBs	PID	15	100	15/120/81	1.5-3.5	1430	[138]

structure is uniformly distributed on the host material to ensure sufficient contact between the active sites and the electrolyte.

**4.1.1.1. Heteroatom adsorption.** To enhance the adsorption ability of COF materials for lithium PSs (LiPSs), the introduction of functional groups on the COFs is considered to be a valid strategy [162-167]. The soluble LiPSs could be anchored through the interaction of the secondary bond between electron-rich polar groups on COFs and Li<sup>+</sup>. For example, an unpaired electron is possessed by the P orbital of every nitrogen atom in triazine, which could be used as an electron donor, and a strong interaction could be formed with polysulfide terminal Li.

Besides, due to the large  $\pi$  conjugated area and the presence of four nitrogen atoms, the porphyrin unit has a stronger nucleophilic ability. Hu et al. [166] synthesized a 3D layered porous COF microflower (COF-MF) structure through a dissolution-reconstruction mechanism (Fig. 12a). The active sites were fully exposed by the unique chemical composition and morphology. The combination of the theoretical and experimental analysis showed that the porphyrin unit in COF-MF acts as a unique anchoring site for the first time and possesses a strong polysulfides adsorption capacity, thereby the shuttle effect is inhibited

effectively. The COF-MF@S-60%-based cathode showed discharge capacities of 1083, 1004, 895 and 743 mAh g<sup>-1</sup> at the rates of 0.2, 0.5, 1 and 2 C (1.0 C = 1675 mA g<sup>-1</sup>, Fig. 12b), respectively. More importantly, the sample retained 53% of the initial value (862 mAh g<sup>-1</sup>) after 1000 cycles (Fig. 12c). A large number of anchor points were exposed by the nitrogen-containing groups in COF-MF, which is beneficial to inhibit the shuttle of LiPSs. At present, COFs with regular micro morphology are rarely reported in Li-S batteries, except for the COF-MF. In addition, strong interactions can be generated with lithium atoms of lithium polysulfide through nitrogen-containing groups such as imines, secondary amines, imides, and hydrazones to improve the cycle performance of Li-S batteries.

Utilizing the interaction between the electron acceptor groups on COFs and the sulfur atoms (electron donor group) of lithium PSs is another way to suppress the shuttle effect. The COF-1 as the framework of the sulfur was synthesized with six-membered boroxine (B<sub>3</sub>O<sub>3</sub>) as the corner block by Ghazi et al (Fig. 12d) [167]. At a current density of 0.2 C, based on the mass of sulfur, the initial specific capacity of the electrode was as high as 1628 mAh g<sup>-1</sup>, and the actual capacity of 929 mAh g<sup>-1</sup> was obtained after 100 cycles (Fig. 12e). In addition, they also pre-

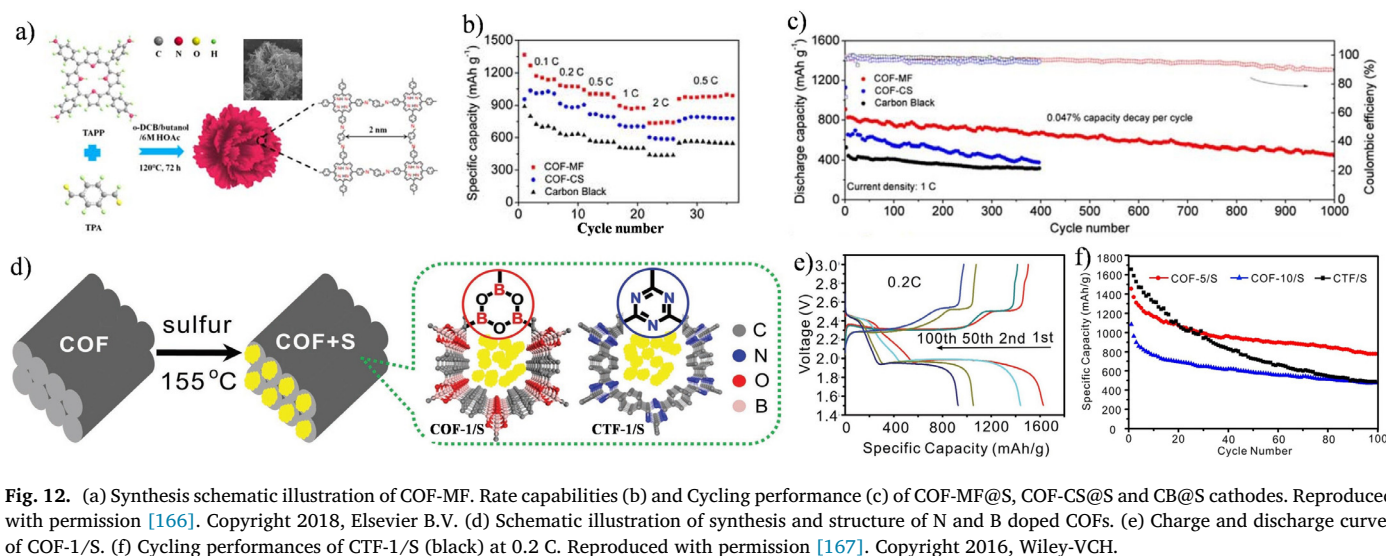


**Fig. 12.** (a) Synthesis schematic illustration of COF-MF. Rate capabilities (b) and Cycling performance (c) of COF-MF@S, COF-CS@S and CB@S cathodes. Reproduced with permission [166]. Copyright 2018, Elsevier B.V. (d) Schematic illustration of synthesis and structure of N and B doped COFs. (e) Charge and discharge curves of COF-1/S. (f) Cycling performances of CTF-1/S (black) at 0.2 C. Reproduced with permission [167]. Copyright 2016, Wiley-VCH.

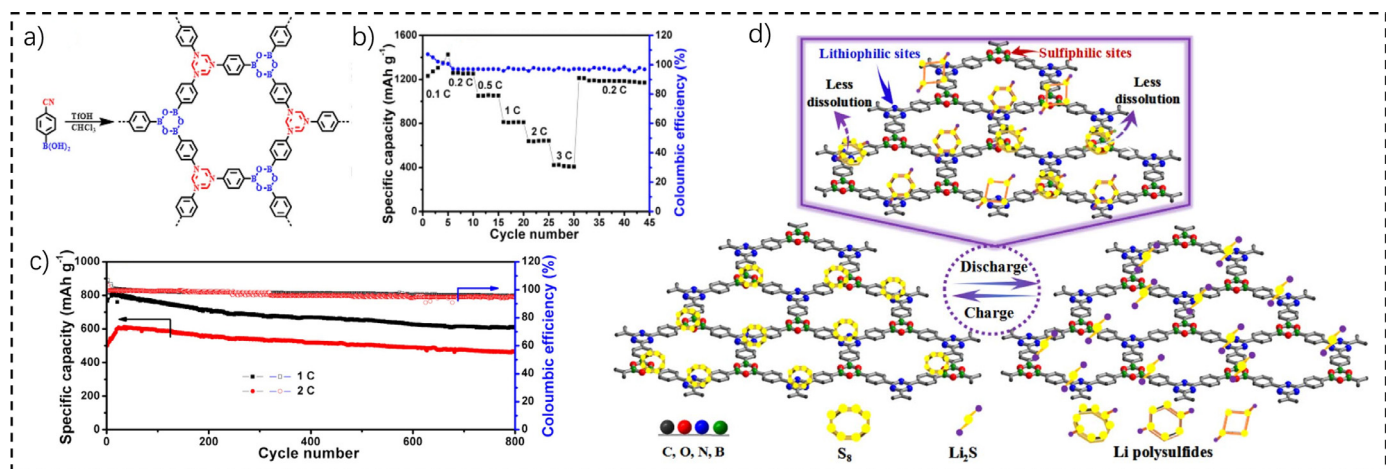


**Fig. 13.** (a) Schematic diagram for TB-COF synthesis. Discharge capacities (b) and Cycling performances (c) of TB-COF. (d) Schematic illustration for the lithiophilic and sulfurphilic interactions between TB-COF and lithium PSs. Reproduced with permission [165]. Copyright 2018, Elsevier B.V.

pared CTF-1 containing triazine-rings and compared the performance with COF-1 (Fig. 12f). The results showed that although both have similar pore sizes, COF-1 exhibits significantly higher cycling performance than that of CTF-1, as the efficiency of CTF-1-captured PSs through indirect interaction is not as high as that of COF-1-captured PSs through indirect interaction. Although the diffusion of PSs was inhibited by single adsorption interaction, it could not be entirely prevented.

The TB-COF containing lithium- and sulfur-philic bifunctional groups was designed and synthesized by Xiao et al (Fig. 13a) [165]. After two cycles at 0.1C, the cathode based on TB-COF/S can provide a discharge capacity of 1417 mAh g<sup>-1</sup> (Fig. 13b). The reversible capacity of 663 mAh g<sup>-1</sup> was retained after 800 cycles at 1 C (Fig. 13c). The higher density and periodic distribution of triazine and oxyboronyl in TB-COF provide sufficient electrochemical active centers for the interaction of the COF with Li<sup>+</sup> and polysulfide anions, thus efficaciously reducing the shuttle effect of LiPSs (Fig. 13d). In addition, boron-containing groups such as borazine and borate ester could also have strong interaction with sulfur atoms of LiPSs, which provides more choices for the design of COFs.

**4.1.1.2. Bonding sulfur with COFs through the covalent bond.** To anchor the PSs chain on the wall of the COF channel, Jiang et al. [168] synthesized a TFPPy-ETTA-COF material through the imine bond (C=N) and sulfur to form a C-S covalent bond at high temperature (Fig. 14a).

The electrochemically inert skeleton was converted into energy storage COF by the immobilized polysulfide chain and provided a brand-new interface for the redox reaction. A high capacity of 1069 mAh g<sup>-1</sup> was produced at 0.1 C, but as the current density increased from 0.2 to 0.5, 0.8, and 1 C, the reversible capacity rapidly decayed from 698 to 524, 414, and 347 mAh g<sup>-1</sup> (Fig. 14b), respectively. Compared with the physical isolation in the COF channel, the covalent bonding method may be easier to inhibit the shuttle of polysulfides. But this may also change its electrochemical activity and charge conduction, making the rate performance unsatisfactory. Related works on combining polysulfide chains with COFs through covalent bonds were also reported by Sang et al (Fig. 14c, d) [57,169-172]. Remarkably, there is a lack of relevant evidence to prove that this C-S covalent bond still be restored after repeated charging/discharging cycles.

**4.1.1.3. Carbonization.** It is a good way to obtain the doped carbon material with uniform molecular size distribution by introducing the active sites into the frameworks in the form of covalent bonds and then carbonizing at high temperatures [173-175]. Chen et al. coated COF-10 on the surface of CNTs by condensation reaction to form COF-10@CNT. Then COF-10@CNT was carbonized at high temperature to prepare BOC@CNT with boron/oxygen co-doping and used as a host material for the sulfur cathode (Fig. 15a) [174]. Boron/oxygen co-doping could increase the electronic conductivity and anchor the PSs, which

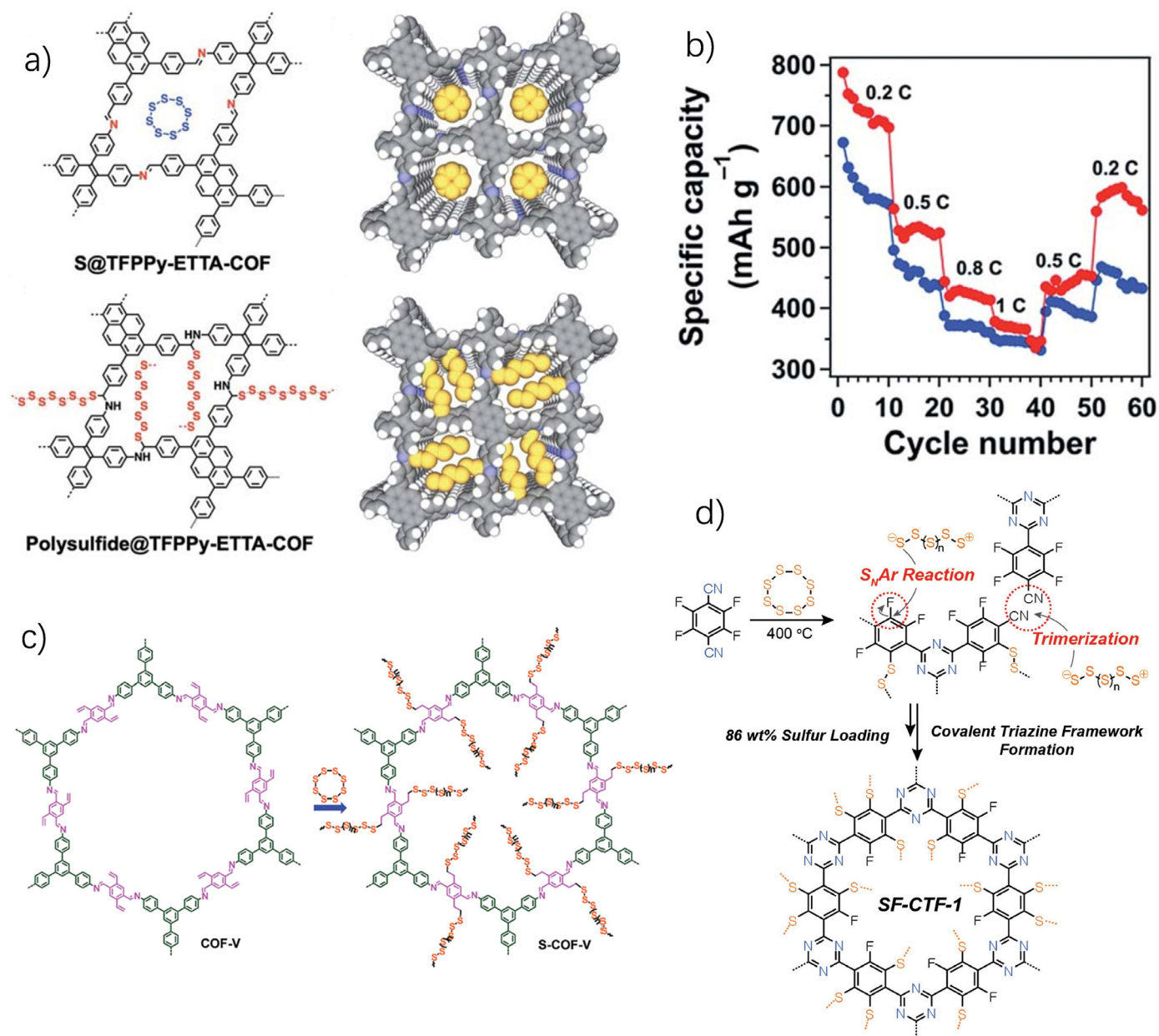


**Fig. 14.** (a) Schematic diagram of physical isolation and covalent bonding of sulfur. (b) Rate performances of polysulfide@TFPPy-ETTA-COF (red) and S@TFPPy-ETTA-COF (blue). Reproduced with permission [168]. Copyright 2019, Royal Society of Chemistry. (c) Schematic illustration of S-COF-V vulcanization. Reproduced with permission. Copyright 2018, Royal Society of Chemistry. (d) Schematic diagram of SF-CTF-1 synthesis. Reproduced with permission [169]. Copyright 2017, Wiley-VCH.

is conducive to improving the electrochemical properties of Li-S batteries. At rates of 0.1, 0.2, 0.5, 1, 2 and 5 C (1 C=1672 mAh g<sup>-1</sup>), the BOC@CNT/S cathode exhibited the superior specific capacities of 1359, 1251, 1057, 959, 768 and 636 mAh g<sup>-1</sup>, respectively. Compared with the BOC@CNT/S cathode, the BOC/CNT/S (made by COF-10 and CNTs through physical mixing and then carbonization) delivered a poor cycle performance, and the discharge capacity dropped quickly from 1362 to 1100 mAh g<sup>-1</sup> after 10 cycles at 0.1 C. The overpotentials of BOC@CNT/S and BOC/CNT/S were 170 mV and 330 mV, respectively, which confirmed that the uniform coating of the COF on the surface of carbon nanotubes improved the redox reaction kinetics during charge/discharge processes (Fig. 15b).

In addition to introducing doping atoms into the backbone of COFs, one-dimensional holes of COFs could also be utilized. Recently, Yang et al. [175] prepared HCPT/COF composite materials by uniformly em-

bedding hybrid anatase/rutile TiO<sub>2</sub> nanodots (10 nm) into the porous COF interlayers (Fig. 15c). At a rate of 0.5 C, the initial discharge capacity of the HCPT@COF/S electrode obtained 1036 mAh g<sup>-1</sup> and still retained 875 mAh g<sup>-1</sup> after 800 cycles. In contrast, the COF/S cathode showed rapid capacity decay after 500 cycles, and the final discharge capacity was only 487.6 mAh g<sup>-1</sup>. The discharge capacities based on HCPT@COF/S electrodes were 1061, 1031, 928, and 740 mAh g<sup>-1</sup> at current densities of 0.2, 0.5, 1.0, and 2.0 C (Fig. 15d), respectively. DFT calculations showed that the interaction between Ti and S atoms was stronger than that between N and Li atoms in the COF (Fig. 15e). The mixed phases of rutile and anatase produced synergistic adsorption of lithium polysulfide at different discharge stages, which could effectively prevent the shuttle effect. Table 3 summarizes the electrochemical properties of inactive COFs in lithium-sulfur batteries.

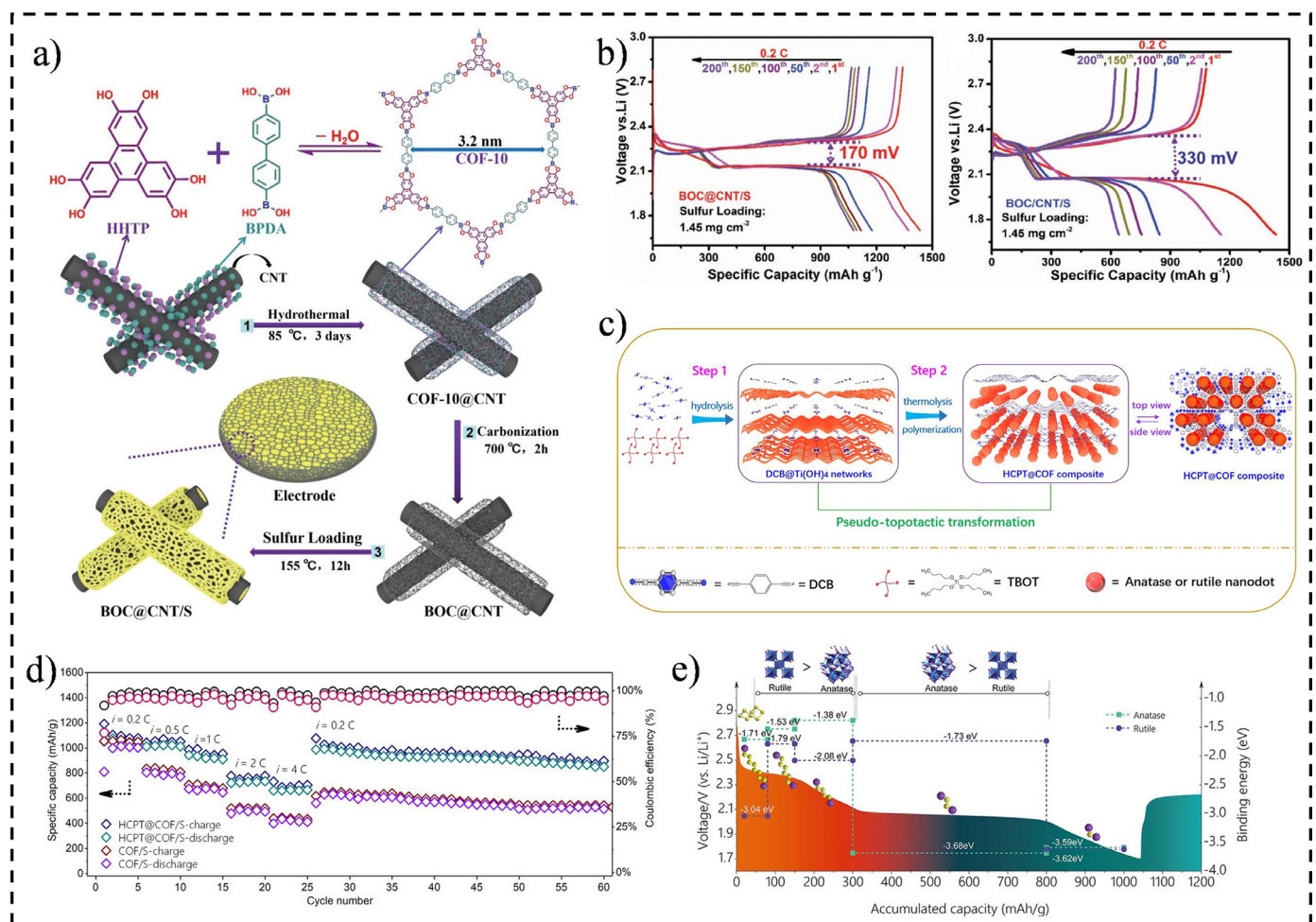


**Fig. 15.** (a) Synthesis schematic illustration of the BOC@CNT/S. (b) Galvanostatic charge/discharge profiles of BOC@CNT/S (left) and BOC/CNT/S (right) cathodes. Reproduced with permission [174]. Copyright 2019, Wiley-VCH. (c) Synthesis schematic illustration of the HCPT@COF/S composites. (d) Rate performances of the HCPT@COF/S and COF/S electrodes. (e) The binding energy of rutile and anatase TiO<sub>2</sub> with Li-PSs at different reaction stages. Reproduced with permission [175]. Copyright 2019, American Chemical Society.

#### 4.1.2. COFs as membrane modification layers

In addition to the polar matrix and porous material technologies, the use of COFs for simple and economically feasible separator projects is also of infinite value in overcoming the shuttle effect [177–181]. Teng et al. prepared a CNT@DMTA-COF nanocomposite material and applied it as a separator material for Li-S batteries (Fig. 16a) [178]. The Li-S batteries based on COF-CNT separator at the current density of 1 A g<sup>-1</sup>, the battery capacity displayed a high capacity of 1068 mAh g<sup>-1</sup> (Fig. 16b). Even at 2 A g<sup>-1</sup>, it could still obtain an excellent capacity of 600 mAh g<sup>-1</sup> after 700 cycles. When the temperature dropped below -10 °C, the capacity was 1200 mAh g<sup>-1</sup> at 0.5 A g<sup>-1</sup>, and maintained at about 300 mAh g<sup>-1</sup> after 200 cycles at a higher rate of 2 A g<sup>-1</sup>. When tested in a high-temperature environment at 50 °C, a capacity of 400 mAh g<sup>-1</sup> could also be delivered after 300 cycles at 2 A g<sup>-1</sup> (Fig. 16c). The excellent performance of Li-S batteries in a wide temperature range benefits from superior conductivity and ion diffusion. The COF-CNT layer in the battery served as a secondary collector and adsorption of soluble polysulfide. The COF-CNT-based composite membrane has a significant effect on blocking the shuttle of polysulfides, which is attributed to the synergy between CNTs and COFs.

Depositing a modified layer on the separator is widely regarded as one of the effective strategies for inhibiting PSs shuttle in Li-S batteries. However, the diffusion path of lithium ions may be sacrificed by the dense coating on the separator, resulting in reduced conductivity of lithium ions. To prepare a separator modification layer with

a rapid conversion channel for lithium ions, Sun et al. [179] treated the COF nanosheets with lithium acetate at 60 °C for 24 hours to synthesize lithiated Li-CON (Fig. 16d, e). Li-CON as a separator modification layer can not only capture lithium polysulfide through pyridine N on Li-CON but also acts as a lithium-ion migration medium to adjust the diffusion behavior of lithium ions through lithiation sites. Compared with the CON@GN/Celgard and the Celgard separators, the Li-CON@GN/Celgard separator has the highest diffusion coefficient among the three batteries, indicating their excellent lithium-ion conductivity. The Li-CON@GN/Celgard separator-based batteries exhibit a higher lithium-ion conductivity (0.609 mS cm<sup>-1</sup>) than that of the CON@GN/Celgard separator-based batteries, which may be attributed to the lithium conductive nano-channels in the Li-CON. The batteries with Li-CON@GN/Celgard separator have an initial capacity of up to 982 mAh g<sup>-1</sup> at 1 C and still retains 645 mAh g<sup>-1</sup> after 600 cycles (Fig. 16g). In addition, the relatively low activation energy of the lithiation site in Li-CON greatly promoted the dissociation of Li<sub>2</sub>S (Fig. 16h).

#### 4.2. COFs for solid-state electrolytes

To achieve large-scale applications, solid-state electrolytes must possess an ionic conductivity close to liquid electrolytes and superior thermal stability [182,183]. Generally, ionic conductivity is closely related to ion concentration and mobility. COFs connected by covalent bonds and arranged periodically have attracted tremendous attention in solid-

**Table 3**  
COFs in Li-S batteries.

Application	Materials	COF/S Mass ratio	Rate performance		Cycling performance CD/CN/Retained SC (mA h g <sup>-1</sup> )	Voltage range (V)	Ref.
			CD	SC (mA h g <sup>-1</sup> )			
HM	CTF-1	66:34	168 1680	920 541	168/50/762	1.1-3.0	[162]
HM	S/Azo-COF	61:39	3344	770	1672/100/602	1.5-2.8	[163]
HM	Por-COF/S	45:55	168 1680	1000 670	840/200/633	1.8-2.7	[164]
HM	COF-MF@S	40:60	335 1675 3350	1083 895 743	1672/1000/456	1.7-2.8	[166]
HM	TB-COF/S	60:40	~335 ~1675 ~5025	1314 670 434	~1680/800/663	1.5-3.0	[165]
HM	COF-1/S	60:40	167.2 1672	1411 620	836/200/770	1.5-3.0	[167]
HM	SF-CTF-1 (1:3)	14:86	100 1000	878.7 603.2	1000/300/520.1 5000/300/330.3	1.8-2.7	[169]
HM	S-COF-V	33:67	335 1675 10050	1324 967 431	1675/1000/416	1.7-2.8	[57]
HM	COF-F-S	39:61	1675	480	1675/1000/257	1.7-2.8	[170]
HM	POP-F-S	38:62	1675	~315	1675/1000/156	1.7-2.8	[168]
HM	polysulfide @TFPPy-ETTA-COF	62:38	~1675	347	167.5/130/585	1.7-2.8	[168]
HM	cPpy-S-CTF 2.5%	19:81	167.5 1675	900 660	837.5/500/610	1.8-2.7	[172]
HM	N-GC-TpPa/S (Carbonization)	25:75	50 1675	1387 869	1675/200/670	1.5-3.0	[173]
HM	BOC@CNT/S (Carbonization)	31.5:68.5	167.2 1672 836	1359 959 636	1672/500/794	1.7-2.8	[174]
HM	HCPT@COF/S (Carbonization)	30.7:69.3	334 1670 3340	1061 928 740	835/800/875	1.7-2.8	[175]
HM	Py-COF/S	30:70	840 3360 8400	1145 944 659	8400/550/481.2	1.8-2.7	[176]
MM	TP-BPY-COF@LSBs	-	167.5 1675 8375	1315 877 572	1675/250/826	1.7-2.8	[177]
MM	COF-CNT-separator	-	1071	1000	2000/700/568	1.8-2.7	[178]
MM	Li-CON@GN/Celgard	-	~1675	885	~1675/600/645	1.7-2.8	[179]

state electrolytes because of their high structural stability, beneficial 1D ion transport channels, and splendid adjustability. Zhang et al. [184] regarded the electrolyte composed of stacked and ordered COF-5, LiClO<sub>4</sub> and THF as a solid, and calculated the microscopic dynamics and structural evolution of the lithium-ion diffusion process in the 1D channel of COF with first-principles (Fig. 17a, b). The results show that although the migration of ClO<sub>4</sub><sup>-</sup> and THF in the electrolyte is limited over a long distance, due to the rotation and short-range translation of solvent molecules and coordination anions, the diffusion trajectory of Li<sup>+</sup> ions exhibits liquid-like behavior, and the calculated diffusion coefficient is about 10<sup>-5</sup> cm<sup>2</sup> s<sup>-1</sup>. Unfortunately, they did not conduct further experiment to prove this phenomenon. More interestingly, their calculation results show that the ionic conductivity can be improved by increasing the pore size of COFs and reducing the volume of anionic groups.

It is well known that solid-state electrolytes need low electronic conductivity, which can avoid the formation of lithium dendrites and internal short [185-187]. Therefore, reducing electronic conductivity is one of the keys to the success of all-solid-state batteries. In the COFs, the electronic conductivity can be reduced by increasing the bandgap of the HOMO/LUMO energy levels, which is contrary to the design concept of the COFs electrode. To designing the wide bandgap molecules, the well-accepted methods [188-193] are summarized as follows: (1) Reducing the length of continuous conjugation of  $\pi$  bond; (2) Introducing alkane chains in the molecule. The length of the alkane chain is positively correlated with electronic conductivity; (3) Expanding the interlayer spacing between molecules; (4) Increasing the twist angle of

adjacent conjugated groups. The requirements of electronic conductivity at the solid electrolyte are easily met by the above methods. Except for ion and electronic conductivities, adverse side reactions may be caused at the interface between the metal anode and COFs, when unmodified COFs are used as solid electrolytes. It would result in the decreased cycle stability. Therefore, effective strategies are needed to solve the above issues.

#### 4.2.1. Introducing the cations into COFs

In a solid conductor, Li<sup>+</sup> and the corresponding anion are closely combined in the form of ion pairs or ion aggregates due to the strong Coulomb interaction. These ion pairs or aggregates cannot release ions, resulting in lower ion concentration and slow ion diffusion kinetics. Therefore, promoting the dissociation of ion pairs in solid conductors has become an important way to improve the ionic conductivity of COFs. Introducing dissociable cations into COFs is a great way to improve the ionic conductivity, ascribing to the weak interaction between the cations and the anions, resulting in more release of free Li<sup>+</sup>. Chen et al. [194] prepared Li-CON-TFSI containing cations without any solvent, and the conductivity measured at 70°C reached 2.09 × 10<sup>-4</sup> S cm<sup>-1</sup>. Since the cationic polarizability on the COF was higher than that of neutral COF materials, the Coulomb interaction could be efficaciously shielded (Fig. 17c, d). Under the action of electrostatic force, the cations on the skeleton interacted with TFSI<sup>-</sup>, which was conducive to increasing the concentration of free lithium ions and thus accelerating ionic conduction. Apart from the above examples, the carbonyl

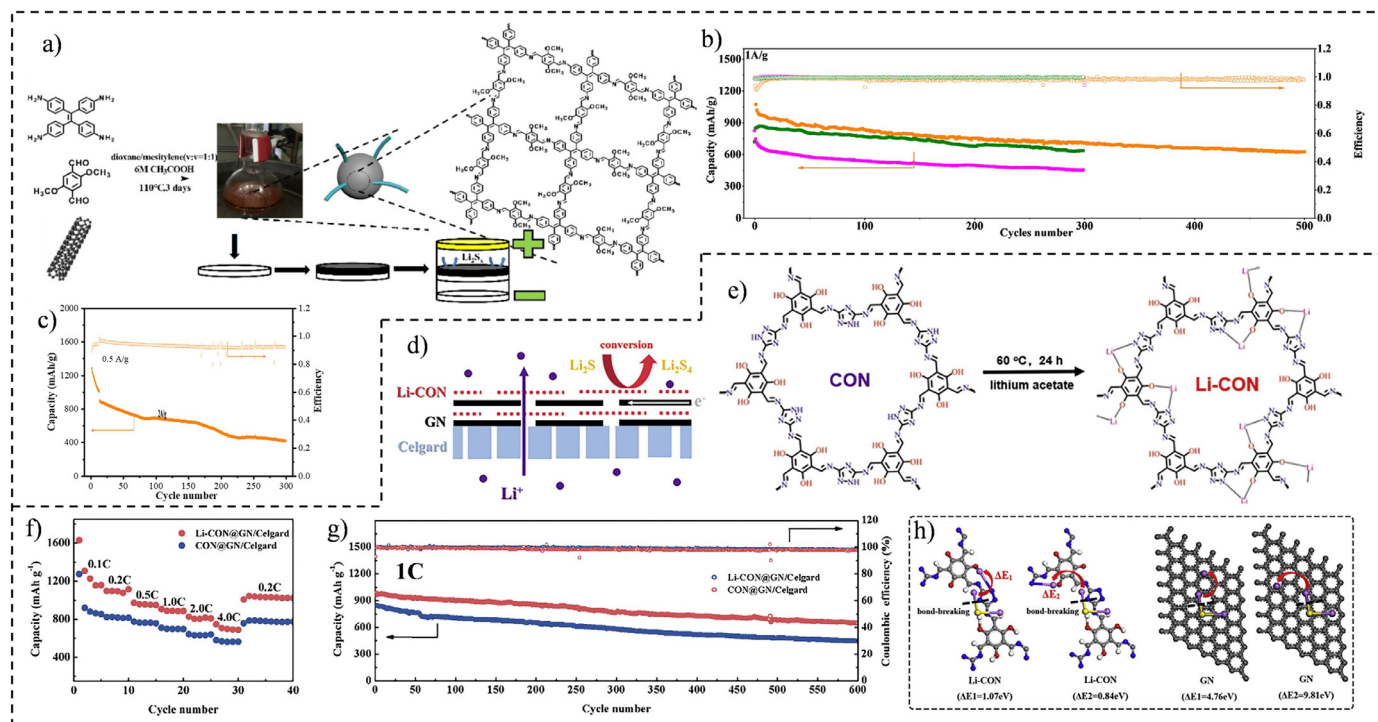


**Fig. 16.** (a) Synthesis schematic illustration of the CNT@DMTA-COF and COF-CNT-separator. (b) Cycling performances of the COF-CNT-separator (orange), CNT-separator (light green) and COF-separator (pink) at 1 A g<sup>-1</sup>. (c) Cycling performance of the COF-CNT-separator at 50°C. Reproduced with permission [178]. Copyright 2020, Elsevier B.V. (d) Schematic of Li-CON@GN/Celgard separator and functions. (e) Synthetic scheme of the Li-CON. Rate performances (f) and long-term cycling performances (g) of the Li-CON@GN and CON@GN cells. (h) The activation energy of reaction process on the surface of the Li-CON and GN, respectively. Reproduced with permission [179]. Copyright 2020, Elsevier B.V.

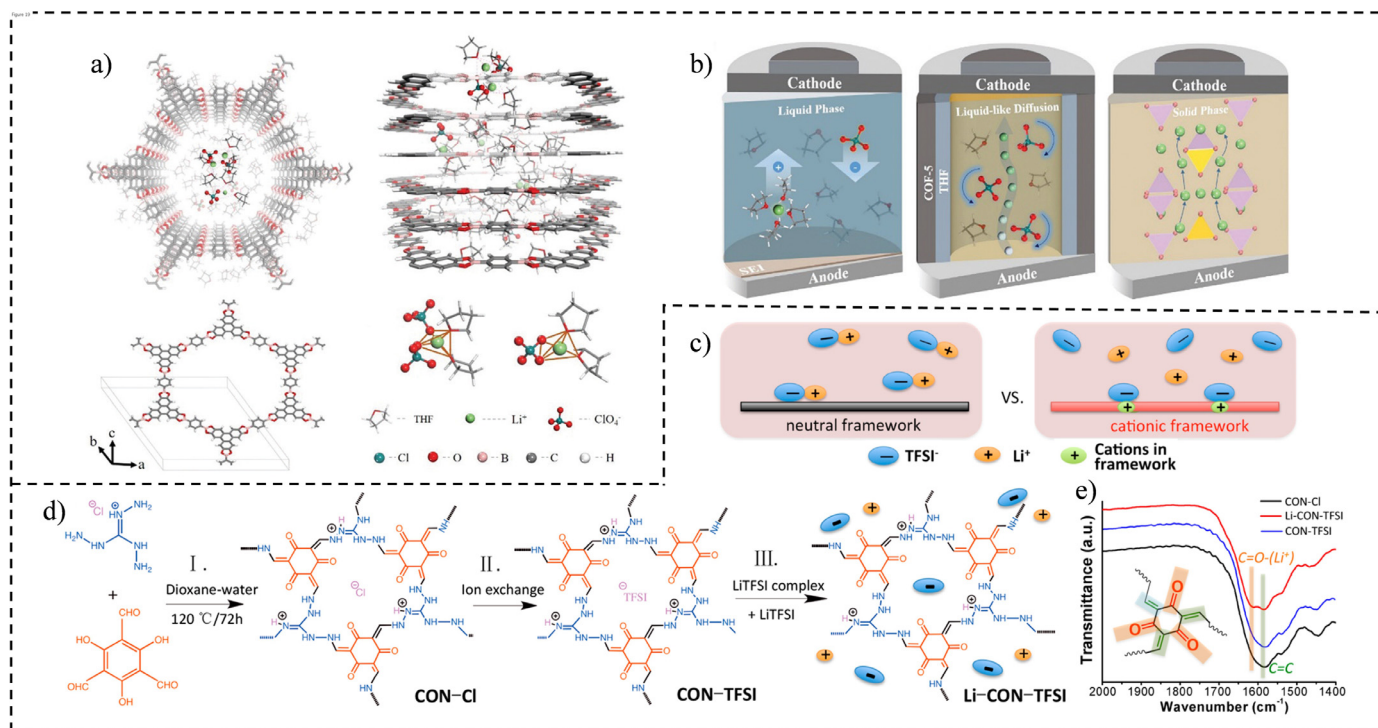


**Fig. 17.** (a) Schematic diagram of 1D Li<sup>+</sup> diffusion in tunnels of 2D-COF filled with Li salt and solvent. (b) Schematic graphs of liquid organic, 2D-COF and solid inorganic electrolyte for LIBs. Reproduced with permission [184]. Copyright 2019, Royal Society of Chemistry. (c) Schematic illustrations of ion association in neutral and cationic COFs, respectively. (d) Synthetic scheme of the Li-CON-TFSI. (e) FTIR spectra of CONs and Li-CON-TFSI. Reproduced with permission [194]. Copyright 2018, American Chemical Society.

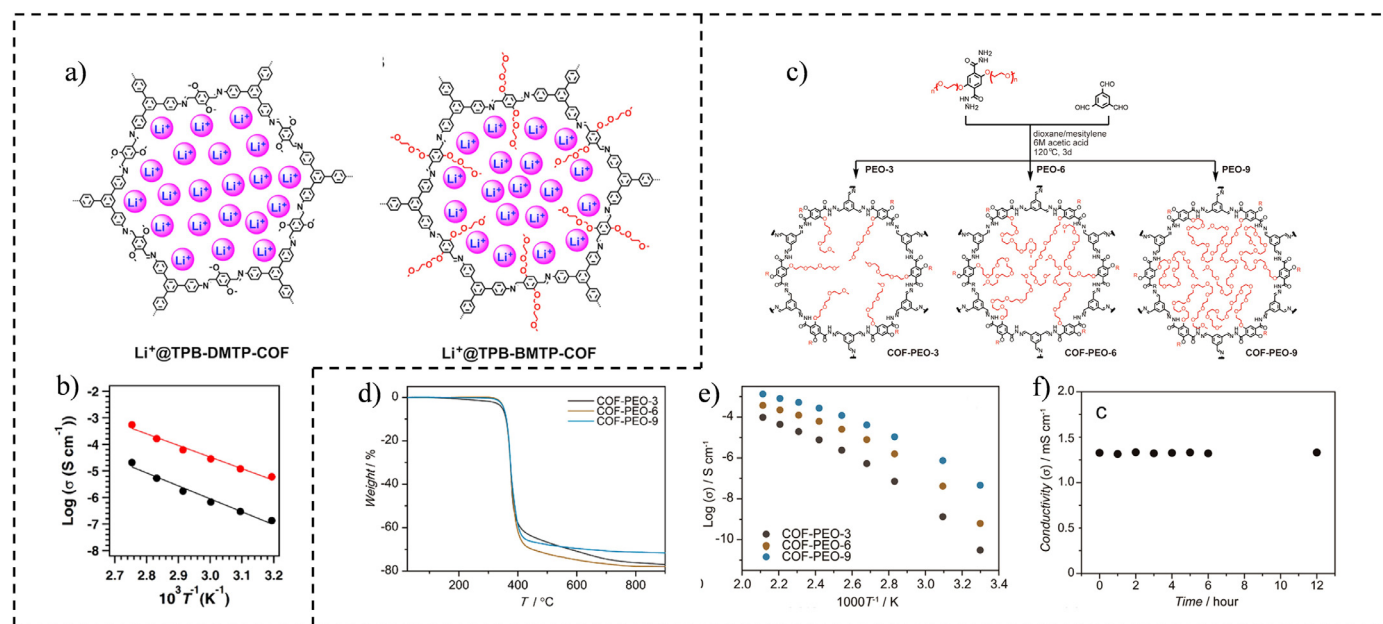


**Fig. 18.** (a) Structure diagram of  $\text{Li}^+$ @TPB-DMTP-COF with bare pore walls and  $\text{Li}^+$ @TPB-BMTP-COF with oligo(ethylene oxide) chains on pore walls. (b) Temperature dependencies of ionic conductivities of  $\text{Li}^+$ @TPB-DMTP-COF (black) and  $\text{Li}^+$ @TPB-BMTP-COF (red). Reproduced with permission [196]. Copyright 2018, American Chemical Society. (c) Synthesis of COF-PEO- $x$  ( $x = 3, 6, 9$ ). (d) TGA profiles measured at  $10^\circ\text{C min}^{-1}$ . (e) Temperature dependencies of ion conductivities of COF-PEO- $x$ -Li ( $x = 3, 6, 9$ ). (f) Time course  $\text{Li}^+$  conductivity of COF-PEO-9-Li at  $200^\circ\text{C}$ . Reproduced with permission [197]. Copyright 2018, American Chemical Society.

group of Li-CON-TFSI may also form the  $\text{Li}^+-\text{O}_{\text{C}=\text{O}}$  coordination bond with  $\text{Li}^+$ , which is beneficial to enhance the conductivity of  $\text{Li}^+$ . FTIR spectra show that there is a clear interaction ( $\text{Li}^+-\text{O}_{\text{C}=\text{O}}$ ) between the carbonyl group and  $\text{Li}^+$  (Fig. 17e). Li et al. [195] introduced defect anchor points on the COF and then performed post-functionalization to introduce cation. Compared with defect-free COFs, the electrolytes based on dCOF-ImTFSI-60 show higher conductivity. However, the introduction of defects on the COF not only cannot guarantee the uniform distribution of defect sites but may also lead to structural instability.

#### 4.2.2. Introducing solvent molecules into COFs

To overcome the shortcomings of the low ionic conductivity of solid-state electrolytes, the introduction of solvent molecules to promote the dissociation of lithium salt ionic bonds has become an attractive option. The strong crystallinity of poly(ethylene oxide) (PEO) at low temperatures seriously hinders the transformation of salt ions. Fortunately, the long-range ordered porous COF materials could accommodate oligomeric PEO to form a solid electrolyte with higher thermal stability, which provides a suitable surrounding for ion diffusion. Xu et al. [196] combined oligo(ethylene oxide) chains with COFs and prepared two types of  $\text{Li}^+$ @TPB-DMTP-COF (short-chain) and  $\text{Li}^+$ @TPB-BMTP-COF (long-chain) materials (Fig. 18a, b). The ionic conductivities of the long-chain COFs measured at 40, 60 and  $80^\circ\text{C}$  were  $6.04 \times 10^{-6}$ ,  $2.85 \times 10^{-5}$  and  $1.66 \times 10^{-4} \text{ S cm}^{-1}$ , respectively, higher than that of short-chain COFs. Compared with the above two COFs, the conductivity of  $\text{Li}^+$ @TPB-TP-COF with bare pore was the smallest. These results indicated that the methoxy chain of COFs contributed to the dissociation of the ionic bond of  $\text{LiClO}_4$  and formed a polyelectrolyte interface after complexation with  $\text{Li}^+$ , which provides a favorable way to promote  $\text{Li}^+$  migration. The dependence relationship between the length of methoxy chains and conductivity was further explored by Zhang et al. [197]. Three PEO chains with different length were integrated with COFs through a simple condensation reaction (Fig. 18c). The ionic conductivities of COF-PEO- $x$ -Li ( $x = 3, 6, 9$ ) at  $200^\circ\text{C}$  increased with the number of PEO units. Significantly, due to the inherently higher thermal stability of the structure, COF-PEO-9-Li-based solid-state elec-

trolytes exhibited excellent long-term stable anode ionic conductivity at  $200^\circ\text{C}$  (Fig. 18d-f).

#### 4.2.3. Introducing anions into COFs

It is well known that the free motion of anions and solvent molecules on the surface/near-surface of the metal electrode is a potential risk because of harmful interface side reactions between them. In order to solve this problem, the lithium salt anion could be fixed on the COFs, or the skeleton of the COFs could be used as the anion to realize the single lithium-ion conduction of the solid electrolyte [198]. A solvent-free single lithium ion-conducted COFs (TpPa-SO<sub>3</sub>Li, Fig. 19a) were synthesized by Jeong et al. [64]. Without adding any lithium salt and solvent, the ionic conductivity and lithium-ion transfer number of lithium sulfonated TpPa-SO<sub>3</sub>Li were  $2.7 \times 10^{-5} \text{ S cm}^{-1}$  and 0.9, respectively, which is attributed to the carefully designed channels and the higher ionic concentration. The DFT calculation results show that the lithium ions migration tends to migrate in the axial direction rather than in the plane (Fig. 19b) due to the shorter transition distance in the axial direction of each step and the promotion of oxygen atoms on adjacent carbonyl groups (migration barrier  $E_m$ , 7.6 kcal mol<sup>-1</sup> and 31.6 kcal mol<sup>-1</sup>). In addition, the assembled Li/Li symmetric batteries showed good cycle stability under a current density of  $10 \mu\text{A cm}^{-2}$ , which indicates that COF has friendly contact stability with Li metal.

Furthermore, Hu et al. [65] developed a series of anionic COFs containing imidazole salts in order to study the influence of the ortho-position substituents of lithium salts on ionic conductivity (Fig. 19c). The ionic conductivities of CF<sub>3</sub>-Li-ImCOF, H-Li-ImCOF and CH<sub>3</sub>-Li-ImCOF measured at room temperature were  $7.2 \times 10^{-3}$ ,  $5.3 \times 10^{-3}$  and  $8.0 \times 10^{-5} \text{ S cm}^{-1}$ , respectively. The -CF<sub>3</sub> group with strong electronegativity delocalizes the negative charge on the N atom, which weakens the interaction of the N-Li bond and increases the bond length, resulting in improved  $\text{Li}^+$  mobility and conductivity. In contrast, the methyl group with electron-donating properties had a weak effect on the distribution of negative charges, resulting in stronger N-Li bond strength and inferior ion mobility. Moreover, faint crystallinity and porosity may also be another reason for the poor conductivity of CH<sub>3</sub>-LiImCOF ions. Interestingly, to prove the importance of the ordered channels of COF for

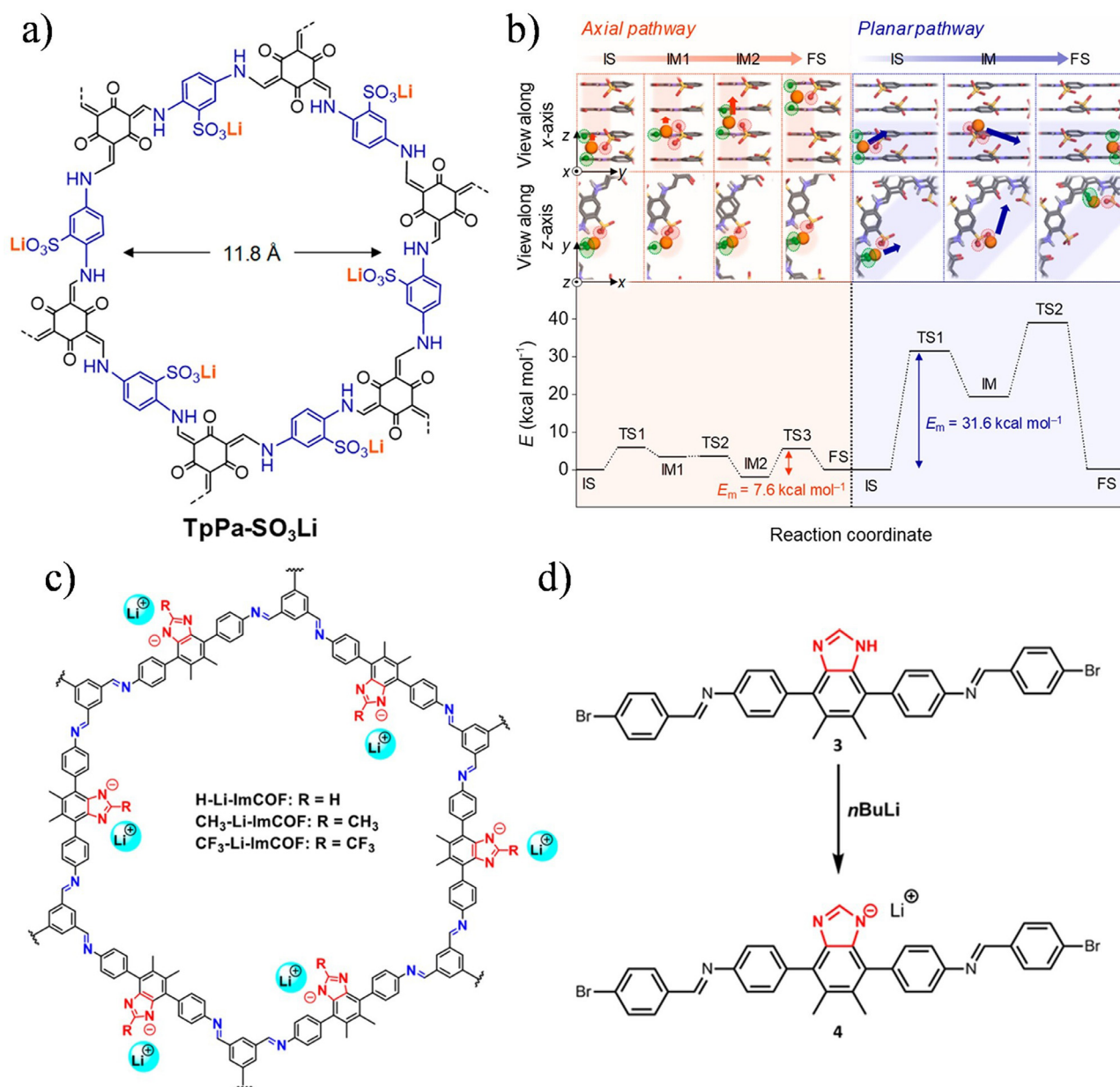


**Fig. 19.** (a) Chemical structure of TpPa-SO<sub>3</sub>Li. (b) Theoretical elucidation of Li<sup>+</sup> diffusion behaviors inside the pore (top) with the corresponding energy graph (bottom). The initial, intermediate, transition, and final states are abbreviated as IS, IM, TS, and FS, respectively. Reproduced with permission [64]. Copyright 2019, American Chemical Society. (c) Structure of Li-ImCOFs. (d) Synthesis of model compound. Reproduced with permission [65]. Copyright 2019, American Chemical Society.

the free transport of ions, a small molecule similar to H-Li-ImCOF was prepared (Fig. 19d). Under the same conditions, the ionic conductivity was only  $7.2 \times 10^{-6} \text{ S cm}^{-1}$ , which further emphasizes the advantages of COF-type structures in solid-state electrolytes.

The performance of solid electrolytes is still not comparable to that of commercial liquid electrolytes, due to slow reaction kinetics, lower ion mobility, and poor contact interface. However, the solid electrolyte is still worthy of further research due to its high safety and reliable electrochemical performance. The emergence of COFs has opened up a new solution for the next generation of solid electrolytes, and these results are of great significance to the solid electrolyte field.

## 5. Conclusions and perspectives

In this review, the structural features of COFs are described in detail. Then the storage principles, optimization methods, and latest research

progress are summarized in energy storage fields, including LIBs/SIBs cathodes, anodes, Li-S batteries, and solid-state electrolytes.

As the cathode/anode materials, COFs with strong designability could furnish a high specific capacity, excellent long-cycle life and various electrode materials worthy of vigorous development. In terms of structural design, electrode materials with higher specific capacity can be made by increasing the proportion of reversible redox functional groups in COFs. Furthermore, continuous conjugated carbon skeleton and introduced heteroatoms have a certain helpful effect on improving the conductivity of materials. In terms of nanostructure design, a series of peeling methods can be used to increase the exposure of active sites to improve the electrochemical performances of batteries. However, poor electronic conductivity is still one of the challenges hindering the development of this material. Therefore, improving the intrinsic conductivity and increasing the relative content of COFs in the electrode is extremely

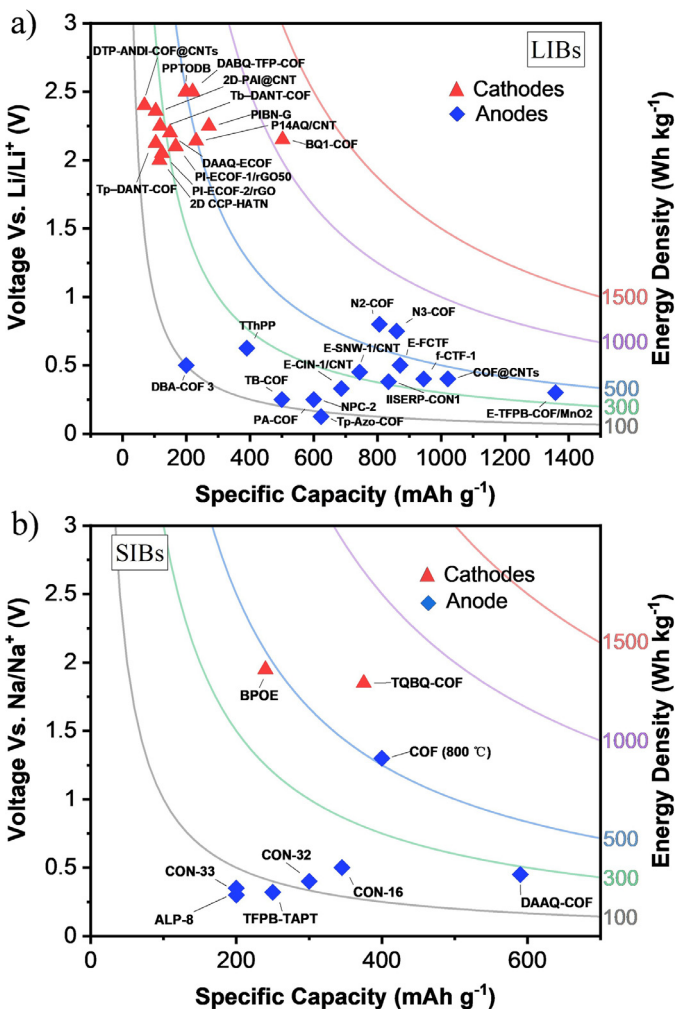


Fig. 20. Energy densities of COFs electrode materials in LIBs (a) and SIBs (b).

urgent for the future development of COF electrode materials. Due to the lower tap density, its volumetric energy density will be significantly affected. The energy density based on the COF electrode materials are summarized in Fig. 20, indicating that the high specific capacity characteristics of the cathodes have not been fully exploited. Besides, the working voltage of the cathode is still lower than that of most inorganic materials, which requires further improvement of the interaction between functional groups or the development of novel active groups with high voltage. In the anodes, there are still many reaction mechanisms that have not been uniformly recognized and explained, which requires a lot of follow-up scientific research to explore the relationship between the structure and performance.

The unique advantages of COFs have played a significant role in Li-S batteries, whether it is utilized as the host material for sulfur cathode or as the separator modification layer. The uniformly distributed heteroatoms (such as N, O) or functional groups on the COF can form secondary bonds with PSs and play a key role in inhibiting the shuttle effect. Therefore, the choice of functional groups is very important. In addition, the method of combining sulfur with COFs through a covalent bond also has an important hindrance to the shuttle of polysulfides. However, gigantic challenges still exist to fit the commercialization standards of Li-S batteries based on COF materials. Prospects worthy of attention are as follows. (1) The content of COF materials exceeds 40% of the entire electrode in general, which darkens the advantages of the high energy density of Li-S Batteries. To improve the overall capacity of the cathodes, the COF materials with energy storage function could be

selected. (2) Compared with graphene, CNTs and other conductive carbon materials, the conductivity of COF materials with large  $\pi$  bonds is still insufficient. It is a relatively feasible solution to design conductive COFs or carbon/COF composites as the host materials. (3) The interaction between COFs with soluble lithium PSs is still weak. Designing more effective functional groups, such as strong electrophilic groups,  $-\text{NO}_2$ ,  $-\text{CF}_3$  and so forth, need to be further developed.

The flourishing application of COFs in the solid-state electrolytes is attributed to its high structural stability, favorable 1D ion transport channel and high designability. The main direction of COFs in the field of the solid-state electrolytes has been laid down through three main strategies, including the introduction of anions, cations and solvent molecules into COFs. There is still a gap between the ionic conductivity of COF-based solid electrolytes ( $10^{-3}$ – $10^{-6}$  S  $\text{cm}^{-1}$ ) and traditional organic liquid electrolytes (about  $10^{-2}$  S  $\text{cm}^{-1}$ ) at room temperature. Although higher ionic conductivity is obtained at high temperatures, it still needs to be improved at room temperature through various methods. Ionic conductivity is one of the core parameters of solid-state electrolytes, but functional groups that could promote ion transport on the COF have yet to be developed.

In short, there is still a long way to promote the application of COFs in the field of energy storage. Through the review and prospect of this work, we hope to provide a few constructive views for the future development of COFs in the EESS. There is reason to believe that the development of COFs will create a new platform for the EESS.

#### Declaration of Competing Interest

There are no conflicts to declare.

#### Acknowledgements

This work was supported by National Key Research and Development Program of China (2017YFE0127600); National Natural Science Foundation of China (51521001, 51972259, and U1804253); Foshan Xianhu Laboratory of the Advanced Energy Science and Technology Guangdong Laboratory (XHT2020-003); Programme of Introducing Talents of Discipline to Universities (B17034); the Natural Science Foundation of Hubei Province (2019CFA001).

#### References

- [1] S. Karak, S. Kandambeth, B.P. Biswal, H.S. Sasmal, S. Kumar, P. Pachfule, R. Banerjee, Constructing ultraporos covalent organic frameworks in seconds via an organic terracotta process, *J. Am. Chem. Soc.* 139 (2017) 1856–1862, doi:10.1021/jacs.6b08815.
- [2] D. Rodriguez-San-Miguel, C. Montoro, F. Zamora, Covalent organic framework nanosheets: preparation, properties and applications, *Chem. Soc. Rev.* 49 (2020) 2291–2302, doi:10.1039/c9cs00890j.
- [3] X. Zhao, P. Pachfule, S. Li, T. Langenhahn, M. Ye, C. Schlesiger, S. Praetz, J. Schmidt, A. Thomas, Macro/Microporous covalent organic frameworks for efficient electrocatalysis, *J. Am. Chem. Soc.* 141 (2019) 6623–6630, doi:10.1021/jacs.9b01226.
- [4] A.K. Mandal, J. Mahmood, J.-B. Baek, Two-dimensional covalent organic frameworks for optoelectronics and energy storage, *ChemNanoMat* 3 (2017) 373–391, doi:10.1002/cnma.201700048.
- [5] M.S. Lohse, T. Bein, Covalent organic frameworks: structures, synthesis, and applications, *Adv. Funct. Mater.* 28 (2018) 1705553, doi:10.1002/adfm.201705553.
- [6] S. Kandambeth, K. Dey, R. Banerjee, Covalent organic frameworks: chemistry beyond the structure, *J. Am. Chem. Soc.* 141 (2019) 1807–1822, doi:10.1021/jacs.8b10334.
- [7] C.S. Diercks, O.M. Yaghi, The atom, the molecule, and the covalent organic framework, *Science* 923 (2017) 355, doi:10.1126/science.aal1585.
- [8] S.Y. Ding, W. Wang, Covalent organic frameworks (COFs): from design to applications, *Chem. Soc. Rev.* 42 (2013) 548–568, doi:10.1039/c2cs35072f.
- [9] N. Huang, P. Wang, D.L. Jiang, Covalent organic frameworks: a materials platform for structural and functional designs, *Nat. Rev. Mater.* 1 (2016) 16068, doi:10.1038/natrevmats.2016.68.
- [10] X.F. Shi, Y.J. Yao, Y.L. Xu, K. Liu, G.S. Zhu, L.F. Chi, G. Lu, Imparting catalytic activity to a covalent organic framework material by nanoparticle encapsulation, *ACS Appl. Mater. Interfaces* 9 (2017) 7481–7488, doi:10.1021/acsami.6b16267.
- [11] S. Lin, C.S. Diercks, Y.B. Zhang, N. Kornienko, E.M. Nichols, Y.B. Zhao, A.R. Paris, D. Kim, P. Yang, O.M. Yaghi, C.J. Chang, Covalent organic frameworks comprising

- cobalt porphyrins for catalytic CO<sub>2</sub> reduction in water, *Science*, 349 (2015) 1208–1213, doi:10.1126/science.aac8343.
- [12] P.F. Wei, M.Z. Qi, Z.P. Wang, S.Y. Ding, W. Yu, Q. Liu, L.K. Wang, H.Z. Wang, W.K. An, W. Wang, Benzoxazole-linked ultrastable covalent organic frameworks for photocatalysis, *J. Am. Chem. Soc.* 140 (2018) 4623–4631, doi:10.1021/jacs.8b00571.
- [13] G.Q. Lin, H.M. Ding, D.Q. Yuan, B.S. Wang, C. Wang, A pyrene-based, fluorescent three-dimensional covalent organic framework, *J. Am. Chem. Soc.* 138 (2016) 3302–3305, doi:10.1021/jacs.6b00652.
- [14] H. Furukawa, O.M. Yaghi, Storage of hydrogen, methane, and carbon dioxide in highly porous covalent organic frameworks for clean energy applications, *J. Am. Chem. Soc.* 131 (2009) 8875–8883, doi:10.1021/ja9015765.
- [15] N. Huang, X. Chen, R. Krishna, D.L. Jiang, Two-dimensional covalent organic frameworks for carbon dioxide capture through channel-wall functionalization, *Angew. Chem. Int. Ed.* 54 (2015) 2986–2990, doi:10.1002/anie.201411262.
- [16] M. Zhang, M. Lu, Z.L. Lang, J. Liu, M. Liu, J.N. Chang, L.Y. Li, L.J. Shang, M. Wang, S.L. Li, Y.Q. Lan, Semiconductor/Covalent-organic-framework z-scheme heterojunctions for artificial photosynthesis, *Angew. Chem. Int. Ed.* 59 (2020) 6500–6506, doi:10.1002/anie.202000929.
- [17] S.Y. Ding, M. Dong, Y.W. Wang, Y.T. Chen, H.Z. Wang, C.Y. Su, W. Wang, Thioether-based fluorescent covalent organic framework for selective detection and facile removal of Mercury(II), *J. Am. Chem. Soc.* 138 (2016) 3031–3037, doi:10.1021/jacs.5b10754.
- [18] X.G. Liu, D.L. Huang, C. Lai, G.M. Zeng, L. Qin, H. Wang, H. Yi, B.S. Li, S.Y. Liu, M.M. Zhang, R. Deng, Y.K. Fu, L. Li, W.J. Xue, S. Chen, Recent advances in covalent organic frameworks (COFs) as a smart sensing material, *Chem. Soc. Rev.* 48 (2019) 5266–5302, doi:10.1039/c9cs00299e.
- [19] P.P. Shao, J. Li, F. Chen, L. Ma, Q.B. Li, M.X. Zhang, J.W. Zhou, A.X. Yin, X. Feng, B. Wang, Flexible films of covalent organic frameworks with ultralow dielectric constants under high humidity, *Angew. Chem. Int. Ed.* 57 (2018) 16501–16505, doi:10.1002/anie.201811250.
- [20] H.S. Sasmal, H.B. Aiyappa, S.N. Bhange, S. Karak, A. Halder, S. Kurunot, R. Banerjee, Superprotonic conductivity in flexible porous covalent organic framework membranes, *Angew. Chem. Int. Ed.* 57 (2018) 10894–10898, doi:10.1002/anie.201804753.
- [21] A.F.M. El-Mahdy, M.G. Mohamed, T.H. Mansoure, H.-H. Yu, T. Chen, S.-W. Kuo, Ultrastable tetraphenyl-p-phenylenediamine-based covalent organic frameworks as platforms for high-performance electrochemical supercapacitors, *Chem. Commun.* 55 (2019) 14890–14893, doi:10.1039/c9cc08107k.
- [22] A.F.M. EL-Mandy, C. Young, J. Kim, J. You, Y. Yamauchi, S.W. Kuo, Hollow microspherical and Microtubular [3+3] carbazole-based covalent organic frameworks and their gas and energy storage applications, *ACS Appl. Mater. Interfaces* 11 (2019) 9343–9354, doi:10.1021/acsami.8b21867.
- [23] S. Liu, L. Yao, Y. Lu, X.L. Hua, J.Q. Liu, Z. Yang, H. Wei, Y.Y. Mai, All-organic covalent organic framework/polyaniline composites as stable electrode for high-performance supercapacitors, *Mater. Lett.* 236 (2019) 354–357, doi:10.1016/j.matlet.2018.10.131.
- [24] Y. Wu, D.W. Yan, Z.Y. Zhang, M.M. Matsushita, K. Awaga, Electron highways into nanochannels of covalent organic frameworks for high electrical conductivity and energy storage, *ACS Appl. Mater. Interfaces* 11 (2019) 7661–7665, doi:10.1021/acsami.8b21696.
- [25] M. Tang, C. Jiang, S. Liu, X. Li, Y. Chen, Y. Wu, J. Ma, C. Wang, Small amount COFs enhancing storage of large anions, *Energy Storage Mater* 27 (2020) 35–42, doi:10.1016/j.ensm.2020.01.015.
- [26] C. Zhang, Y. He, P. Mu, X. Wang, Q. He, Y. Chen, J. Zeng, F. Wang, Y. Xu, J.-X. Jiang, Toward high performance thiophene-containing conjugated microporous polymer anodes for lithium-ion batteries through structure design, *Adv. Funct. Mater.* 28 (2018) 1908445, doi:10.1002/adfm.201705432.
- [27] M. Lee, J. Hong, J. Lopez, Y. Sun, D. Feng, K. Lim, W.C. Chueh, M.F. Toney, Y. Cui, Z. Bao, High-performance sodium-organic battery by realizing four-sodium storage in disodium rhodizonate, *Nat. Energy* 2 (2017) 861–868, doi:10.1038/s41560-017-0014-y.
- [28] J. Luo, B. Hu, C. Debruler, T.L. Liu, A pi-conjugation extended Viologen as a two-electron storage Anolyte for total organic aqueous redox flow batteries, *Angew. Chem. Int. Ed.* 57 (2018) 231–235, doi:10.1002/anie.201710517.
- [29] D. Larcher, J.M. Tarascon, Towards greener and more sustainable batteries for electrical energy storage, *Nat. Chem.* 7 (2015) 19–29, doi:10.1038/nchem.2085.
- [30] T.B. Schon, B.T. McAllister, P.F. Li, D.S. Seferos, The rise of organic electrode materials for energy storage, *Chem. Soc. Rev.* 45 (2016) 6405–6406, doi:10.1039/c6cs90070d.
- [31] D.J. Kim, K.R. Hermann, A. Prokofjevs, M.T. Otle, C. Pezzato, M. Owczarek, J.F. Stoddart, Redox-active macrocycles for organic rechargeable batteries, *J. Am. Chem. Soc.* 139 (2017) 6635–6643, doi:10.1021/jacs.7b01209.
- [32] M.E. Bhosale, S. Chae, J.M. Kim, J.Y. Choi, Organic small molecules and polymers as an electrode material for rechargeable lithium ion batteries, *J. Mater. Chem. A* 6 (2018) 19885–19911, doi:10.1039/c8ta04906h.
- [33] S.F. Wu, W.X. Wang, M.C. Li, L.J. Cao, F.C. Lyu, M.Y. Yang, Z.Y. Wang, Y. Shi, B. Nan, S.C. Yu, Z.F. Sun, Y. Liu, Z.G. Lu, Highly durable organic electrode for sodium-ion batteries via a stabilized alpha-C radical intermediate, *Nat. Commun.* 7 (2016) 13318, doi:10.1038/ncomms13318.
- [34] C. Luo, O. Borodin, X. Ji, S. Hou, K.J. Gaskell, X. Fan, J. Chen, T. Deng, R. Wang, J. Jiang, C. Wang, Azo compounds as a family of organic electrode materials for alkali-ion batteries, *Proc. Natl. Acad. Sci.* 115 (2018) 2004–2009, doi:10.1073/pnas.1717892115.
- [35] M. López-Herrera, E. Castillo-Martínez, J. Carretero-González, J. Carrasco, T. Rojo, M. Armand, Oligomeric-Schiff bases as negative electrodes for sodium ion batteries: unveiling the nature of their active redox centers, *Energy Environ. Sci.* 8 (2015) 3233–3241, doi:10.1039/c5ee01832c.
- [36] C. Wang, C. Jiang, Y. Xu, L. Liang, M. Zhou, J. Jiang, S. Singh, H. Zhao, A. Schober, Y. Lei, A selectively permeable membrane for enhancing cyclability of organic sodium-ion batteries, *Adv. Mater.* 28 (2016) 9182–9187, doi:10.1002/adma.201603240.
- [37] C. Wang, Y. Xu, Y. Fang, M. Zhou, L. Liang, S. Singh, H. Zhao, A. Schober, Y. Lei, Extended pi-conjugated system for fast-charge and -discharge sodium-ion batteries, *J. Am. Chem. Soc.* 137 (2015) 3124–3130, doi:10.1021/jacs.5b00336.
- [38] S. Lee, J. Hong, S.-K. Jung, K. Ku, G. Kwon, W.M. Seong, H. Kim, G. Yoon, I. Kang, K. Hong, H.W. Jang, K. Kang, Charge-transfer complexes for high-power organic rechargeable batteries, *Energy Storage Mater* 20 (2019) 462–469, doi:10.1016/j.ensm.2019.05.001.
- [39] S. Lee, J.E. Kwon, J. Hong, S.Y. Park, K. Kang, The role of substituents in determining the redox potential of organic electrode materials in Li and Na rechargeable batteries: electronic effects vs. substituent-Li/Na ionic interaction, *J. Mater. Chem. A* 7 (2019) 11438–11443, doi:10.1039/c9ta01508f.
- [40] Y. Liang, Y. Jing, S. Gheyani, K.Y. Lee, P. Liu, A. Facchetti, Y. Yao, Universal quinone electrodes for long cycle life aqueous rechargeable batteries, *Nat. Mater.* 16 (2017) 841–848, doi:10.1038/nmat4919.
- [41] S.-H. Kim, H.H. Lee, J.-M. Kim, S.Y. Hong, S.-Y. Lee, Heteromat-framed metal-organic coordination polymer anodes for high-performance lithium-ion batteries, *Energy Storage Mater* 19 (2019) 130–136, doi:10.1016/j.ensm.2019.02.010.
- [42] M. Kolek, F. Otteny, P. Schmidt, C. Mück-Lichtenfeld, C. Einholz, J. Becking, E. Schleicher, M. Winter, P. Bieker, B. Esser, Ultra-high cycling stability of poly(vinylphenothiazine) as a battery cathode material resulting from  $\pi$ - $\pi$  interactions, *Energy Environ. Sci.* 10 (2017) 2334–2341, doi:10.1039/c7ee01473b.
- [43] Y. Lu, Q. Zhang, L. Li, Z.Q. Niu, J. Chen, Design strategies toward enhancing the performance of organic electrode materials in metal-ion batteries, *Chem-Us* 4 (2018) 2786–2813, doi:10.1016/j.chempr.2018.09.005.
- [44] Q. Zhao, J.B. Wang, C.C. Chen, T. Ma, J. Chen, Nanostructured organic electrode materials grown on graphene with covalent-bond interaction for high-rate and ultra-long-life lithium-ion batteries, *Nano Res* 10 (2017) 4245–4255, doi:10.1007/s12274-017-1580-9.
- [45] Z. Zhao-Karger, P. Gao, T. Ebert, S. Klyatskaya, Z. Chen, M. Ruben, M. Fichtner, New organic electrode materials for ultrafast electrochemical energy storage, *Adv. Mater.* 31 (2019) 1806599, doi:10.1002/adma.201806599.
- [46] Y. Liang, Z. Tao, J. Chen, Organic electrode materials for rechargeable lithium batteries, *Adv. Energy Mater.* 2 (2012) 742–769, doi:10.1002/aenm.201100795.
- [47] Z. Luo, L. Liu, Q. Zhao, F. Li, J. Chen, An insoluble benzoquinone-based organic cathode for use in rechargeable lithium-ion batteries, *Angew. Chem. Int. Ed.* 56 (2017) 12561–12565, doi:10.1002/anie.201706604.
- [48] K.A. See, S. Hug, K. Schwinghammer, M.A. Lumley, Y. Zheng, J.M. Nolt, G.D. Stucky, F. Wudl, B.V. Lotsch, R. Seshadri, Lithium charge storage mechanisms of cross-linked triazine networks and their porous carbon derivatives, *Chem. Mater.* 27 (2015) 3821–3829, doi:10.1021/acs.chemmater.5b00772.
- [49] M.S. Kim, W.J. Lee, S.M. Paek, J.K. Park, Covalent organic nanosheets as effective sodium-ion storage materials, *ACS Appl. Mater. Interfaces* 10 (2018) 32102–32111, doi:10.1021/acsami.8b09546.
- [50] Y.M. Zhang, Z.Q. Gao, High performance anode material for sodium-ion batteries derived from covalent-organic frameworks, *Electrochim. Acta* 301 (2019) 23–28, doi:10.1016/j.electacta.2019.01.147.
- [51] L. Bai, Q. Gao, Y. Zhao, Two fully conjugated covalent organic frameworks as anode materials for lithium ion batteries, *J. Mater. Chem. A* 4 (2016) 14106–14110, doi:10.1039/c6ta06449c.
- [52] H. Yang, S. Zhang, L. Han, Z. Zhang, Z. Xue, J. Gao, Y. Li, C. Huang, Y. Yi, H. Liu, Y. Li, High conductive two-dimensional covalent organic framework for lithium storage with large capacity, *ACS Appl. Mater. Interfaces* 8 (2016) 5366–5375, doi:10.1021/acsami.5b12370.
- [53] D.H. Tang, W.T. Zhang, Z.A. Qiao, Y.L. Liu, D.H. Wang, Polyanthraquinone/CNT nanocomposites as cathodes for rechargeable lithium ion batteries, *Mater. Lett.* 214 (2018) 107–110, doi:10.1016/j.matlet.2017.11.119.
- [54] D.H. Tang, Z.Q. Yao, D.H. Wu, Y.H. Zhang, Z. Zhou, X.H. Bu, Structure-modulated crystalline covalent organic frameworks as high-rate cathodes for Li-ion batteries, *J. Mater. Chem. A* 4 (2016) 18621–18627, doi:10.1039/c6ta07606h.
- [55] Y. Lu, J. Chen, Prospects of organic electrode materials for practical lithium batteries, *Nat. Rev. Chem.* 4 (2020) 127–142, doi:10.1038/s41570-020-0160-9.
- [56] H. Tang, Z. Peng, L. Wu, F. Xiong, C. Pei, Q. An, L. Mai, Vanadium-based cathode materials for rechargeable multivalent batteries: challenges and opportunities, *Electrochem. Energy Rev.* 1 (2018) 169–199, doi:10.1007/s41918-018-0007-y.
- [57] Q. Jiang, Y.S. Li, X.X. Zhao, P.X. Xiong, X. Yu, Y.H. Xu, L. Chen, Inverse-vulcanization of vinyl functionalized covalent organic frameworks as efficient cathode materials for Li-S batteries, *J. Mater. Chem. A* 6 (2018) 17977–17981, doi:10.1039/c8ta07008c.
- [58] X. Song, M. Zhang, M. Yao, C. Hao, J. Qiu, New insights into the anchoring mechanism of polysulfides inside nanoporous covalent organic frameworks for lithium-sulfur batteries, *ACS Appl. Mater. Interfaces* 10 (2018) 43896–43903, doi:10.1021/acsami.8b16172.
- [59] H. Wei, S. Chai, N. Hu, Z. Yang, L. Wei, L. Wang, The microwave-assisted solvothermal synthesis of a crystalline two-dimensional covalent organic framework with high CO<sub>2</sub> capacity, *Chem. Commun.* 51 (2015) 12178–12181, doi:10.1039/c5cc04680g.
- [60] X. Zhang, Z. Wang, L. Yao, Y. Mai, J. Liu, X. Hua, H. Wei, Synthesis of core-shell covalent organic frameworks/multi-walled carbon nanotubes nanocomposite and application in lithium-sulfur batteries, *Mater. Lett.* 213 (2018) 143–147, doi:10.1016/j.matlet.2017.11.002.

- [61] D.D. Chen, S. Huang, L. Zhong, S.J. Wang, M. Xiao, D.M. Han, Y.Z. Meng, Situ preparation of thin and rigid COF film on Li anode as artificial solid electrolyte interphase layer resisting Li Dendrite Puncture, *Adv. Funct. Mater.* 30 (2020) 1907717, doi:10.1002/adfm.201907717.
- [62] Z.Y. Cheng, M.L. Xie, Y.Y. Mao, J.X. Ou, S.J. Zhang, Z. Zhao, J.L. Li, F. Fu, J.H. Wu, Y.B. Shen, D.R. Lu, H.W. Chen, Building Lithiophilic ion-conduction highways on garnet-type solid-state Li<sup>+</sup> conductors, *Adv. Energy Mater.* 10 (2020) 1904230, doi:10.1002/aenm.201904230.
- [63] D.R. Dong, H. Zhang, B. Zhou, Y.F. Sun, H.L. Zhang, M. Cao, J.B. Li, H. Zhou, H. Qian, Z.Y. Lin, H.W. Chen, Porous covalent organic frameworks for high transference number polymer-based electrolytes, *Chem. Commun.* 55 (2019) 1458–1461, doi:10.1039/c8cc08725c.
- [64] K. Jeong, S. Park, G.Y. Jung, S.H. Kim, Y.H. Lee, S.K. Kwak, S.Y. Lee, Solvent-free, single lithium-ion conducting covalent organic frameworks, *J. Am. Chem. Soc.* 141 (2019) 5880–5885, doi:10.1021/jacs.9b00543.
- [65] Y.M. Hu, N. Dunlap, S. Wan, S.L. Lu, S.F. Huang, I. Sellinger, M. Ortiz, Y.H. Jin, S.H. Lee, W. Zhang, Crystalline lithium imidazolate covalent organic frameworks with high Li-ion conductivity, *J. Am. Chem. Soc.* 141 (2019) 7518–7525, doi:10.1021/jacs.9b02448.
- [66] H.C. Ma, C.C. Zhao, G.J. Chen, Y.B. Dong, Photothermal conversion triggered thermal asymmetric catalysis within metal nanoparticles loaded homochiral covalent organic framework, *Nat. Commun.* 10 (2019) 3368, doi:10.1038/s41467-019-11355-x.
- [67] X.T. Li, J. Zou, T.H. Wang, H.C. Ma, G.J. Chen, Y.B. Dong, Construction of covalent organic frameworks via three-component one-pot Strecker and Povarov reactions, *J. Am. Chem. Soc.* 142 (2020) 6521–6526, doi:10.1021/jacs.0c00969.
- [68] Y. Li, W. Chen, G. Xing, D. Jiang, L. Chen, New synthetic strategies toward covalent organic frameworks, *Chem. Soc. Rev.* 49 (2020) 2852–2868, doi:10.1039/d0cs00199f.
- [69] H. Ding, A. Mal, C. Wang, Tailored covalent organic frameworks by post-synthetic modification, *Mater. Chem. Front.* 4 (2020) 113–127, doi:10.1039/c9qm00555b.
- [70] K. Sakaushi, M. Antonietti, Carbon- and Nitrogen-based organic frameworks, *Acc. Chem. Res.* 48 (2015) 1591–1600, doi:10.1021/acs.accounts.5b00010.
- [71] A.P. Cote, A.I. Benin, N.W. Ockwig, M. O'Keeffe, A.J. Matzger, O.M. Yaghi, Porous, crystalline, covalent organic frameworks, *Science* 310 (2005) 1166–1170, doi:10.1126/science.1120411.
- [72] S. Dalapati, E.Q. Jin, M. Addicoat, T. Heine, D.L. Jiang, Highly emissive covalent organic frameworks, *J. Am. Chem. Soc.* 138 (2016) 5797–5800, doi:10.1021/jacs.6b02700.
- [73] Q.R. Fang, J.H. Wang, S. Gu, R.B. Kaspar, Z.B. Zhuang, J. Zheng, H.X. Guo, S.L. Qiu, Y.S. Yan, 3D porous crystalline polyimide covalent organic frameworks for drug delivery, *J. Am. Chem. Soc.* 137 (2015) 8352–8355, doi:10.1021/jacs.5b04147.
- [74] P. Kuhn, M. Antonietti, A. Thomas, Porous, covalent triazine-based frameworks prepared by ionothermal synthesis, *Angew. Chem. Int. Ed.* 47 (2008) 3450–3453, doi:10.1002/anie.200705710.
- [75] M.R. Rao, Y. Fang, S. De Feyter, D.F. Perepichka, Conjugated covalent organic frameworks via Michael addition–elimination, *J. Am. Chem. Soc.* 139 (2017) 2421–2427, doi:10.1021/jacs.6b12005.
- [76] F.J. Uribe-Romo, J.R. Hunt, H. Furukawa, C. Klock, M. O'Keeffe, O.M. Yaghi, A crystalline imine-linked 3-D porous covalent organic framework, *J. Am. Chem. Soc.* 131 (2009) 4570–+, doi:10.1021/ja8096256.
- [77] S. Cao, B. Li, R. Zhu, H. Pang, Design and synthesis of covalent organic frameworks towards energy and environment fields, *Chem. Eng. J.* 355 (2019) 602–623, doi:10.1016/j.cej.2018.08.184.
- [78] L. Kong, M. Liu, H. Huang, Y. Xu, X. Bu, Metal/Covalent-Organic Framework Based Cathodes for Metal-Ion Batteries, *Adv. Energy Mater.* (2021) 2100172, doi:10.1002/aenm.202100172.
- [79] Y. Yin, F. Xiong, C. Pei, Y. Xu, Q. An, S. Tan, Z. Zhuang, J. Sheng, Q. Li, L. Mai, Robust three-dimensional graphene skeleton encapsulated Na<sub>3</sub>V<sub>2</sub>O<sub>7</sub>(PO<sub>4</sub>)<sub>2</sub>F nanoparticles as a high-rate and long-life cathode of sodium-ion batteries, *Nano Energy* 41 (2017) 452–459, doi:10.1016/j.nanoen.2017.09.056.
- [80] S. Tan, Y. Pan, Q. Wei, Y. Jiang, F. Xiong, X. Yao, Z. Cai, Q. An, L. Zhou, L. Mai, Polyol solvation effect on tuning the universal growth of binary metal oxide Nanodots@Graphene oxide heterostructures for electrochemical applications, *Chem. Eur. J.* 25 (2019) 14604–14612, doi:10.1002/chem.201902697.
- [81] Z.W. Seh, Y.M. Sun, Q.F. Zhang, Y. Cui, Designing high-energy lithium-sulfur batteries, *Chem. Soc. Rev.* 45 (2016) 5605–5634, doi:10.1039/c5cs00410a.
- [82] B. Zhang, X. Qin, G.R. Li, X.P. Gao, Enhancement of long stability of sulfur cathode by encapsulating sulfur into micropores of carbon spheres, *Energy Environ. Sci.* 3 (2010) 1531–1537, doi:10.1039/c002639e.
- [83] F. Liu, T. Wang, X. Liu, L.-Z. Fan, Challenges and Recent Progress on Key Materials for Rechargeable Magnesium Batteries, *Adv. Energy Mater.* (2020) 2000787, doi:10.1002/aenm.202000787.
- [84] S.S. Tan, Y.L. Jiang, Q.L. Wei, Q.M. Huang, Y.H. Dai, F.Y. Xiong, Q.D. Li, Q.Y. An, X. Xu, Z.Z. Zhu, X.D. Bai, L.Q. Mai, Multidimensional synergistic nanoarchitecture exhibiting highly stable and ultrafast sodium-ion storage, *Adv. Mater.* 30 (2018) 1707122, doi:10.1002/adma.201707122.
- [85] J. Xie, P.Y. Gu, Q.C. Zhang, Nanostructured conjugated polymers: toward high-performance organic electrodes for rechargeable batteries, *ACS Energy Lett* 2 (2017) 1985–1996, doi:10.1021/acsenenergyl.7b00494.
- [86] Q. Zhao, Y. Lu, J. Chen, Advanced Organic Electrode Materials for Rechargeable Sodium-Ion Batteries, *Adv. Energy Mater.* 7 (2017) 1601792, doi:10.1002/aenm.201601792.
- [87] C. Han, H. Li, R. Shi, T. Zhang, J. Tong, J. Li, B. Li, Organic quinones towards advanced electrochemical energy storage: recent advances and challenges, *J. Mater. Chem. A* 7 (2019) 23378–23415, doi:10.1039/c9ta05252f.
- [88] X. Yin, S. Sarkar, S. Shi, Q.A. Huang, H. Zhao, L. Yan, Y. Zhao, J. Zhang, Recent progress in advanced organic electrode materials for sodium-ion batteries: synthesis, mechanisms, challenges and perspectives, *Adv. Funct. Mater.* 30 (2020) 1908445, doi:10.1002/adfm.201908445.
- [89] E. Castillo-Martinez, J. Carretero-Gonzalez, M. Armand, Polymeric Schiff bases as low-voltage redox centers for sodium-ion batteries, *Angew. Chem. Int. Ed.* 53 (2014) 5341–5345, doi:10.1002/anie.201402402.
- [90] T.B. Schon, B.T. McAllister, P.F. Li, D.S. Seferos, The rise of organic electrode materials for energy storage, *Chem. Soc. Rev.* 45 (2016) 6345–6404, doi:10.1039/c6cs00173d.
- [91] S. Chandra, T. Kundu, S. Kandambeth, R. Babarao, Y. Marathe, S.M. Kunjir, R. Banerjee, Phosphoric acid loaded azo (-N horizontal lineN-) based covalent organic framework for proton conduction, *J. Am. Chem. Soc.* 136 (2014) 6570–6573, doi:10.1021/ja502212v.
- [92] J. Xie, Z. Wang, Z. Xu, Q. Zhang, H.D. Abruna, W.R. Dichtel, Toward a High-Performance All-Plastic Full Battery with a Single Organic Polymer as Both Cathode and Anode, *Adv. Energy Mater.* (2018) 1703509, doi:10.1002/aenm.201703509.
- [93] Z. Luo, L. Liu, J. Ning, K. Lei, Y. Lu, F. Li, J. Chen, A microporous covalent-organic framework with abundant accessible carbonyl groups for Lithium-Ion batteries, *Angew. Chem. Int. Ed.* 57 (2018) 9443–9446, doi:10.1002/anie.201805540.
- [94] C.J. Yao, Z. Wu, J. Xie, F. Yu, W. Guo, Z.J. Xu, D.S. Li, S. Zhang, Q. Zhang, Two-Dimensional (2D) covalent organic framework as efficient cathode for binder-free lithium-ion battery, *ChemSusChem* 13 (2020) 2457–2463, doi:10.1002/cssc.201903007.
- [95] F. Xu, S. Jin, H. Zhong, D. Wu, X. Yang, X. Chen, H. Wei, R. Fu, D. Jiang, Electrochemically active, crystalline, mesoporous covalent organic frameworks on carbon nanotubes for synergistic lithium-ion battery energy storage, *Sci. Rep.* 5 (2015) 8225, doi:10.1038/srep08225.
- [96] X. Yu, C. Li, Y. Ma, D. Li, H. Li, X. Guan, Y. Yan, V. Valtchev, S. Qiu, Q. Fang, Crystalline, porous, covalent polyoxometalate-organic frameworks for lithium-ion batteries, *Microporous Mesoporous Mater* 299 (2020) 110105, doi:10.1016/j.micromeso.2020.110105.
- [97] E.R. Wolfson, N. Xiao, L. Schkeryantz, W.K. Haug, Y. Wu, P.L. McGrier, A dehydrobenzoannulene-based two-dimensional covalent organic framework as an anode material for lithium-ion batteries, *Mol. Syst. Des. Eng.* 5 (2020) 97–101, doi:10.1039/c9me00104b.
- [98] K.S. Weeraratne, A.A. Alzharani, H.M. El-Kaderi, Redox-active porous organic polymers as novel electrode materials for green rechargeable sodium-ion batteries, *ACS Appl. Mater. Interfaces* 11 (2019) 23520–23526, doi:10.1021/acsmi.9b05956.
- [99] B.C. Patra, S.K. Das, A. Ghosh, A. Raj K, P. Moitra, M. Addicoat, S. Mitra, A. Bhaumik, S. Bhattacharya, A. Pradhan, Covalent organic framework based microspheres as an anode material for rechargeable sodium batteries, *J. Mater. Chem. A* 6 (2018) 16655–16663, doi:10.1039/c8ta04611e.
- [100] K. Sakaushi, E. Hosono, G. Nickerl, T. Gemming, H. Zhou, S. Kaskel, J. Eckert, Aromatic porous-honeycomb electrodes for a sodium-organic energy storage device, *Nat. Commun.* 4 (2013) 1485, doi:10.1038/ncomms2481.
- [101] H. Chen, Y. Zhang, C. Xu, M. Cao, H. Dou, X. Zhang, Two pi-conjugated covalent organic frameworks with long-term cyclability at high current density for lithium ion battery, *Chem. Eur. J.* 25 (2019) 15472–15476, doi:10.1002/chem.201903733.
- [102] S. Xu, G. Wang, B.P. Biswal, M. Addicoat, S. Paasch, W. Sheng, X. Zhuang, E. Brunner, T. Heine, R. Berger, X. Feng, A Nitrogen-Rich 2D sp<sup>2</sup> -carbon-linked conjugated polymer framework as a high-performance cathode for lithium-ion batteries, *Angew. Chem. Int. Ed.* 58 (2019) 849–853, doi:10.1002/anie.201812685.
- [103] J. Hong, M. Lee, B. Lee, D.-H. Seo, C.B. Park, K. Kang, Biologically inspired pteridine redox centres for rechargeable batteries, *Nat. Commun.* 5 (2014) 5335, doi:10.1038/ncomms6335.
- [104] Y.Q. Chen, S. Manzhos, Lithium and sodium storage on tetracyanoethylene (TCNE) and TCNE-(doped)-graphene complexes: a computational study, *Mater. Chem. Phys.* 156 (2015) 180–187, doi:10.1016/j.matchemphys.2015.02.045.
- [105] Y. Chen, S. Manzhos, A comparative computational study of lithium and sodium insertion into van der Waals and covalent tetracyanoethylene (TCNE)-based crystals as promising materials for organic lithium and sodium ion batteries, *PCCP* 18 (2016) 8874–8880, doi:10.1039/c5cp07474f.
- [106] X.Y. Han, G.Y. Qing, J.T. Sun, T.L. Sun, How Many Lithium Ions Can Be Inserted onto Fused C<sub>6</sub> Aromatic Ring Systems? *Angew. Chem. Int. Ed.* 51 (2012) 5147–5151, doi:10.1002/anie.201109187.
- [107] M. Wu, Y. Zhao, B. Sun, Z. Sun, C. Li, Y. Han, L. Xu, Z. Ge, Y. Ren, M. Zhang, Q. Zhang, Y. Lu, W. Wang, Y. Ma, Y. Chen, A 2D covalent organic framework as a high-performance cathode material for lithium-ion batteries, *Nano Energy* 70 (2020) 104498, doi:10.1016/j.nanoen.2020.104498.
- [108] R. Shi, L. Liu, Y. Lu, C. Wang, Y. Li, L. Li, Z. Yan, J. Chen, Nitrogen-rich covalent organic frameworks with multiple carbonyls for high-performance sodium batteries, *Nat. Commun.* 11 (2020) 178, doi:10.1038/s41467-019-13739-5.
- [109] Z. Wang, Y. Li, P. Liu, Q. Qi, F. Zhang, G. Lu, X. Zhao, X. Huang, Few layer covalent organic frameworks with graphene sheets as cathode materials for lithium-ion batteries, *Nanoscale* 11 (2019) 5330–5335, doi:10.1039/c9nr00088g.
- [110] S. Wang, Q. Wang, P. Shao, Y. Han, X. Gao, L. Ma, S. Yuan, X. Ma, J. Zhou, X. Feng, B. Wang, Exfoliation of covalent organic frameworks into few-layer redox-active nanosheets as cathode materials for lithium-ion batteries, *J. Am. Chem. Soc.* 139 (2017) 4258–4261, doi:10.1021/jacs.7b02648.
- [111] E. Castillo-Martinez, J. Xie, Q. Zhang, Recent Progress in Multivalent Metal (Mg, Zn, Ca, and Al) and Metal-Ion Rechargeable Batteries with Organic Materials as Promising Electrodes, *Small* 15 (2019) 1805061, doi:10.1002/smll.201805061.
- [112] C. Luo, G.L. Xu, X. Ji, S. Hou, L. Chen, F. Wang, J. Jiang, Z. Chen, Y. Ren, K. Amine, C. Wang, Reversible redox chemistry of Azo compounds for sodium-ion batteries, *Angew. Chem. Int. Ed.* 57 (2018) 2879–2883, doi:10.1002/anie.201713417.

- [113] K.C. Kim, T.Y. Liu, S.W. Lee, S.S. Jang, First-principles density functional theory modeling of Li binding: thermodynamics and redox properties of quinone derivatives for lithium-ion batteries, *J. Am. Chem. Soc.* 138 (2016) 2374–2382, doi:10.1021/jacs.5b13279.
- [114] G. Wang, N. Chandrasekhar, B.P. Biswal, D. Becker, S. Paasch, E. Brunner, M. Addicoat, M.H. Yu, R. Berger, X.L. Feng, A Crystalline, 2D Polyarylimide cathode for Ultrastable and ultrafast Li storage, *Adv. Mater.* 31 (2019) 1901478, doi:10.1002/adma.201901478.
- [115] C.R. Mulzer, L.X. Shen, R.P. Bisbey, J.R. McKone, N. Zhang, H.D. Abruna, W.R. Dichtel, Superior charge storage and power density of a conducting polymer-modified covalent organic framework, *ACS Cent. Sci.* 2 (2016) 667–673, doi:10.1021/acscentsci.6b00220.
- [116] E. Vitaku, C.N. Gannett, K.L. Carpenter, L. Shen, H.D. Abruna, W.R. Dichtel, Phenazine-based covalent organic framework cathode materials with high energy and power densities, *J. Am. Chem. Soc.* 142 (2020) 16–20, doi:10.1021/jacs.9b08147.
- [117] X. Li, H. Wang, H. Chen, Q. Zheng, Q. Zhang, H. Mao, Y. Liu, S. Cai, B. Sun, C. Dun, M.P. Gordon, H. Zheng, J.A. Reimer, J.J. Urban, J. Ciston, T. Tan, E.M. Chan, J. Zhang, Y. Liu, Dynamic covalent synthesis of crystalline porous graphitic frameworks, *Chem-US 6* (2020) 933–944, doi:10.1016/j.chempr.2020.01.011.
- [118] G. Wang, N. Chandrasekhar, B.P. Biswal, D. Becker, S. Paasch, E. Brunner, M. Addicoat, M. Yu, R. Berger, X. Feng, A Crystalline, 2D Polyarylimide Cathode for Ultrastable and ultrafast Li storage, *Adv. Mater.* (2019) 31 e1901478, doi:10.1002/adma.201901478.
- [119] V. Singh, J. Kim, B. Kang, J. Moon, S. Kim, W.Y. Kim, H.R. Byon, Thiazole-linked covalent organic framework promoting fast two-electron transfer for lithium-organic batteries, *Adv. Energy Mater.* (2021) 2003735, doi:10.1002/aenm.202003735.
- [120] C. Wu, M. Hu, X. Yan, G. Shan, J. Liu, J. Yang, Azo-linked covalent triazine-based framework as organic cathodes for ultrastable capacitor-type lithium-ion batteries, *Energy Storage Mater* 36 (2021) 347–354, doi:10.1016/j.ensm.2021.01.016.
- [121] J. Wang, C.S. Chen, Y. Zhang, Hexaazatrinaphthylene-based porous organic polymers as organic cathode materials for lithium-ion batteries, *ACS Sustainable Chem. Eng.* 6 (2017) 1772–1779, doi:10.1021/acssuschemeng.7b03165.
- [122] R. Sun, S. Hou, C. Luo, X. Ji, L. Wang, L. Mai, C. Wang, A covalent organic framework for fast-charge and durable rechargeable Mg storage, *Nano Lett* 20 (2020) 3880–3888, doi:10.1021/acs.nanolett.0c01040.
- [123] G. Zhao, Y. Zhang, Z. Gao, H. Li, S. Liu, S. Cai, X. Yang, H. Guo, X. Sun, Dual active site of the Azo and carbonyl-modified covalent organic framework for high-performance Li storage, *ACS Energy Lett* 5 (2020) 1022–1031, doi:10.1021/acsenerylett.0c00069.
- [124] Z. Lei, Q. Yang, Y. Xu, S. Guo, W. Sun, H. Liu, L.P. Lv, Y. Zhang, Y. Wang, Boosting lithium storage in covalent organic framework via activation of 14-electron redox chemistry, *Nat. Commun.* 9 (2018) 576, doi:10.1038/s41467-018-02889-7.
- [125] Z. Lei, X. Chen, W. Sun, Y. Zhang, Y. Wang, Exfoliated triazine-based covalent organic nanosheets with Multielectron redox for high-performance lithium organic batteries, *Adv. Energy Mater.* 9 (2019) 1801010, doi:10.1002/aenm.201801010.
- [126] H. Zhang, W. Sun, X. Chen, Y. Wang, Few-layered fluorinated triazine-based covalent organic nanosheets for high-performance alkali organic batteries, *ACS Nano* 13 (2019) 14252–14261, doi:10.1021/acsnano.9b07360.
- [127] X.D. Chen, Y.S. Li, L. Wang, Y. Xu, A.M. Nie, Q.Q.O. Li, F. Wu, W.W. Sun, X. Zhang, R. Vajtai, P.M. Ajayan, L. Chen, Y. Wang, High-lithium-affinity chemically exfoliated 2D covalent organic frameworks, *Adv. Mater.* 31 (2019) 1901640, doi:10.1002/adma.201901640.
- [128] Y. Zhu, X. Chen, Y. Cao, W. Peng, Y. Li, G. Zhang, F. Zhang, X. Fan, Reversible intercalation and exfoliation of layered covalent triazine frameworks for enhanced lithium ion storage, *Chem. Commun.* 55 (2019) 1434–1437, doi:10.1039/c8cc10262g.
- [129] S. Haldar, K. Roy, S. Nandi, D. Chakraborty, D. Puthusseri, Y. Gawli, S. Ogale, R. Vaidhyanathan, High and reversible lithium ion storage in self-exfoliated Triazole-Triformyl phloroglucinol-based covalent organic nanosheets, *Adv. Energy Mater.* 8 (2018) 1702170, doi:10.1002/aenm.201702170.
- [130] S. Gu, S. Wu, L. Cao, M. Li, N. Qin, J. Zhu, Z. Wang, Y. Li, Z. Li, J. Chen, Z. Lu, Tunable redox chemistry and stability of radical intermediates in 2D covalent organic frameworks for high performance sodium ion batteries, *J. Am. Chem. Soc.* 141 (2019) 9623–9628, doi:10.1021/jacs.9b03467.
- [131] X. Yao, Y. Ke, W. Ren, X. Wang, F. Xiong, W. Yang, M. Qin, Q. Li, L. Mai, Defect-rich soft carbon porous nanosheets for fast and high-capacity sodium-ion storage, *Adv. Energy Mater.* 9 (2018) 1803260, doi:10.1002/aenm.201803260.
- [132] J.Z. Chen, J.L. Xu, S. Zhou, N. Zhao, C.P. Wong, Nitrogen-doped hierarchically porous carbon foam: A free-standing electrode and mechanical support for high-performance supercapacitors, *Nano Energy* 25 (2016) 193–202, doi:10.1016/j.nanoen.2016.04.037.
- [133] X.J. Zhang, G. Zhu, M. Wang, J.B. Li, T. Lu, L.K. Pan, Covalent-organic-frameworks derived N-doped porous carbon materials as anode for superior long-life cycling lithium and sodium ion batteries, *Carbon* (2017) 686–694 116, doi:10.1016/j.carbon.2017.02.057.
- [134] B. Ni, Y. Li, T. Chen, T. Lu, L. Pan, Covalent organic frameworks converted N, B co-doped carbon spheres with excellent lithium ion storage performance at high current density, *J. Colloid Interface Sci.* 542 (2019) 213–221, doi:10.1016/j.jcis.2019.02.009.
- [135] G. Kim, J. Yang, N. Nakashima, T. Shiraki, Highly microporous nitrogen-doped carbon synthesized from azine-linked covalent organic framework and its supercapacitor function, *Chem. Eur. J.* 23 (2017) 17504–17510, doi:10.1002/chem.201702805.
- [136] M.K. Shehab, K.S. Weeraratne, T. Huang, K.U. Lao, H.M. El-Kaderi, Exceptional sodium-ion storage by an Aza-covalent organic framework for high energy and power density sodium-ion batteries, *ACS Appl. Mater. Interfaces* (2021) 10.1021/acsaami.1020c20915, doi:10.1021/acsaami.1020c20915.
- [137] S. Haldar, D. Kaleeswaran, D. Rase, K. Roy, S. Ogale, R. Vaidhyanathan, Tuning the electronic energy level of covalent organic frameworks for crafting high-rate Na-ion battery anode, *Nanoscale Horiz* 5 (2020) 1264–1273, doi:10.1039/d0nh00187b.
- [138] R. van der Jagt, A. Vasileiadis, H. Veldhuizen, P. Shao, X. Feng, S. Ganapathy, N.C. Habisreutinger, M.A. van der Veen, C. Wang, M. Wagemaker, S. van der Zwaag, A. Nagai, Synthesis and structure-property relationships of polyimide covalent organic frameworks for carbon dioxide capture and (Aqueous) sodium-ion batteries, *Chem. Mater.* 33 (2021) 818–833, doi:10.1021/acs.chemmater.0c03218.
- [139] C. Jiang, M. Tang, S. Zhu, J. Zhang, Y. Wu, Y. Chen, C. Xia, C. Wang, W. Hu, Constructing universal ionic sieves via alignment of two-dimensional Covalent Organic Frameworks (COFs), *Angew. Chem. Int. Ed.* 57 (2018) 16072–16076, doi:10.1002/anie.201809907.
- [140] J.Y. Wang, W.W. Qin, X.X. Zhu, Y.Q. Teng, Covalent organic frameworks (COF)/CNT nanocomposite for high performance and wide operating temperature lithium-sulfur batteries, *Energy* 199 (2020) 117372, doi:10.1016/j.energy.2020.117372.
- [141] Y. Wu, Z. Zhang, S. Bandow, K. Awaga, A novel strategy to functionalize covalent organic frameworks for high-energy rechargeable lithium organic batteries via graft polymerization in nano-channels, *Bull. Chem. Soc. Jpn.* 90 (2017) 1382–1387, doi:10.1246/bcsj.20170247.
- [142] H.J. Peng, J.Q. Huang, X.B. Cheng, Q. Zhang, Review on high-loading and high-energy lithium-sulfur batteries, *Adv. Energy Mater.* 7 (2017) 1700260, doi:10.1002/aenm.201700260.
- [143] J.J. Song, X. Guo, J.Q. Zhang, Y. Chen, C.Y. Zhang, L.Q. Luo, F.Y. Wang, G.X. Wang, Rational design of free-standing 3D porous MXene/rGO hybrid aerogels as polysulfide reservoirs for high-energy lithium-sulfur batteries, *J. Mater. Chem. A* 7 (2019) 6507–6513, doi:10.1039/c9ta00212j.
- [144] C. Lin, L. Qu, J. Li, Z. Cai, H. Liu, P. He, X. Xu, L. Mai, Porous nitrogen-doped carbon/MnO coaxial nanotubes as an efficient sulfur host for lithium sulfur batteries, *Nano Res* 12 (2018) 205–210, doi:10.1007/s12274-018-2203-9.
- [145] Y.Q. Chen, H.Z. Zhang, W.B. Xu, X.F. Yang, Y. Yu, X.F. Li, H.M. Zhang, Polysulfide stabilization: a pivotal strategy to achieve high energy density Li-S batteries with long cycle life, *Adv. Funct. Mater.* 28 (2018) 1704987, doi:10.1002/adfm.201704987.
- [146] W. Kou, X.C. Li, Y. Liu, X.P. Zhang, S.R. Yang, X.B. Jiang, G.H. He, Y. Dai, W.J. Zhen, G.H. Yu, Triple-Layered Carbon-SiO<sub>2</sub> composite membrane for high energy density and long cycling Li-S batteries, *ACS Nano* 13 (2019) 5900–5909, doi:10.1021/acsnano.9b01703.
- [147] Y.J. Li, W.Y. Wang, X.X. Liu, E.Y. Mao, M.T. Wang, G.C. Li, L. Fu, Z. Li, A.Y.S. Eng, Z.W. Seh, Y.M. Sun, Engineering stable electrode-separator interfaces with ultrathin conductive polymer layer for high-energy-density Li-S batteries, *Energy Storage Mater* 23 (2019) 261–268, doi:10.1016/j.ensm.2019.05.005.
- [148] F. Pei, L.L. Lin, A. Fu, S.G. Mo, D.H. Ou, X.L. Fang, N.F. Zheng, A two-dimensional porous carbon-modified separator for high-energy-density Li-S batteries, *Joule* 2 (2018) 323–336, doi:10.1016/j.joule.2017.12.003.
- [149] J.T. Lee, Y.Y. Zhao, S. Thieme, H. Kim, M. Oschatz, L. Borchardt, A. Magasinski, W.I. Cho, S. Kaskel, G. Yushin, Sulfur-Infiltrated Micro- and mesoporous silicon carbide-derived carbon cathode for high-performance lithium sulfur batteries, *Adv. Mater.* 25 (2013) 4573–4579, doi:10.1002/adma.201301579.
- [150] Z.H. Sun, J.Q. Zhang, L.C. Yin, G.J. Hu, R.P. Fang, H.M. Cheng, F. Li, Conductive porous vanadium nitride/graphene composite as chemical anchor of polysulfides for lithium-sulfur batteries, *Nat. Commun.* 8 (2017) 14627, doi:10.1038/ncomms14627.
- [151] D. Bresser, S. Passerini, B. Scrosati, Recent progress and remaining challenges in sulfur-based lithium secondary batteries - a review, *Chem. Commun.* 49 (2013) 10545–10562, doi:10.1039/c3cc46131a.
- [152] S.Q. Chen, B. Sun, X.Q. Xie, A.K. Mondal, X.D. Huang, G.X. Wang, Multi-chambered micro/mesoporous carbon nanocubes as new polysulfides reservoirs for lithium-sulfur batteries with long cycle life, *Nano Energy* 16 (2015) 268–280, doi:10.1016/j.nanoen.2015.05.034.
- [153] Y.Z. Song, W.L. Cai, L. Kong, J.S. Cai, Q. Zhang, J.Y. Sun, Rationalizing electrocatalysis of Li-S chemistry by mediator design: progress and prospects, *Adv. Energy Mater.* 10 (2020) 1901075, doi:10.1002/aenm.201901075.
- [154] B. Li, S.M. Li, J.H. Liu, B. Wang, S.B. Yang, Vertically aligned sulfur-graphene Nanowalls on substrates for ultrafast lithium-sulfur batteries, *Nano Lett* 15 (2015) 3073–3079, doi:10.1021/acs.nanolett.5b00064.
- [155] Y. Zhao, W.L. Wu, J.X. Li, Z.C. Xu, L.H. Guan, Encapsulating MWNTs into hollow porous carbon nanotubes: a tube-in-tube carbon nanostructure for high-performance Lithium-Sulfur batteries, *Adv. Mater.* 26 (2014) 5113–5118, doi:10.1002/adma.201401191.
- [156] S. Moon, Y.H. Jung, W.K. Jung, D.S. Jung, J.W. Choi, D.K. Kim, Encapsulated monoclinic sulfur for stable cycling of Li-S rechargeable batteries, *Adv. Mater.* 25 (2013) 6547–6553, doi:10.1002/adma.201303166.
- [157] Y.J. Hong, J.K. Lee, Y.C. Kang, Yolk-shell carbon microspheres with controlled yolk and void volumes and shell thickness and their application as a cathode material for Li-S batteries, *J. Mater. Chem. A* 5 (2017) 988–995, doi:10.1039/c6ta08328e.
- [158] F. Li, M.R. Kaiser, J.M. Ma, Z.P. Guo, H.K. Liu, J.Z. Wang, Free-standing sulfur-polypyrrole cathode in conjunction with polypyrrole-coated separator for flexible Li-S batteries, *Energy Storage Mater* 13 (2018) 312–322, doi:10.1016/j.ensm.2018.02.007.
- [159] Z.S. Wang, J.D. Shen, S.M. Ji, X.J. Xu, S.Y. Zuo, Z.B. Liu, D.C. Zhang, R.Z. Hu, L.Z. Ouyang, J. Liu, M. Zhu, N. Codoped B, Graphitic nanotubes loaded with Co nanoparticles as superior sulfur host for advanced Li-S batteries, *Small* 16 (2020) 1906634, doi:10.1002/smll.201906634.

- [160] M.J. Yang, X.H. Hu, Z.S. Fang, L. Sun, Z.K. Yuan, S.Y. Wang, W. Hong, X.D. Chen, D.S. Yu, Bifunctional MOF-Derived Carbon photonic crystal architectures for advanced Zn-Air and Li-S batteries: highly exposed graphitic nitrogen matters, *Adv. Funct. Mater.* 27 (2017) 1701971, doi:10.1002/adfm.201701971.
- [161] X.Y. Tao, J.G. Wang, C. Liu, H.T. Wang, H.B. Yao, G.Y. Zheng, Z.W. Seh, Q.X. Cai, W.Y. Li, G.M. Zhou, C.X. Zu, Y. Cui, Balancing surface adsorption and diffusion of lithium-polysulfides on nonconductive oxides for lithium-sulfur battery design, *Nat. Commun.* 7 (2016) 11203, doi:10.1038/ncomms11203.
- [162] H. Liao, H. Ding, B. Li, X. Ai, C. Wang, Covalent-organic frameworks: potential host materials for sulfur impregnation in lithium-sulfur batteries, *J. Mater. Chem. A* 2 (2014) 8854–8858, doi:10.1039/c4ta00523f.
- [163] X. Yang, B. Dong, H. Zhang, R. Ge, Y. Gao, H. Zhang, Sulfur impregnated in a mesoporous covalent organic framework for high performance lithium-sulfur batteries, *RSC Adv* 5 (2015) 86137–86143, doi:10.1039/c5ra16235a.
- [164] H.P. Liao, H.M. Wang, H.M. Ding, X.S. Meng, H. Xu, B.S. Wang, X.P. Ai, C. Wang, A 2D porous porphyrin-based covalent organic framework for sulfur storage in lithium sulfur batteries, *J. Mater. Chem. A* 4 (2016) 7416–7421, doi:10.1039/c6ta00483k.
- [165] Z.B. Xiao, L.Y. Li, Y.J. Tang, Z.B. Cheng, H. Pan, D.X. Tian, R.H. Wang, Covalent organic frameworks with lithiophilic and sulphophilic dual linkages for cooperative affinity to polysulfides in lithium-sulfur batteries, *Energy Storage Mater* 12 (2018) 252–259, doi:10.1016/j.ensm.2018.01.018.
- [166] X.H. Hu, J.H. Jian, Z.S. Fang, L.F. Zhong, Z.K. Yuan, M.J. Yang, S.J. Ren, Q. Zhang, X.D. Chen, D.S. Yu, Hierarchical assemblies of conjugated ultrathin COF nanosheets for high-sulfur-loading and long-lifespan lithium-sulfur batteries: fully-exposed porphyrin matters, *Energy Storage Mater* 22 (2019) 40–47, doi:10.1016/j.ensm.2018.12.021.
- [167] Z.A. Ghazi, L.Y. Zhu, H. Wang, A. Naeem, A.M. Khattak, B. Liang, N.A. Khan, Z.X. Wei, L.S. Li, Z.Y. Tang, Efficient polysulfide chemisorption in covalent organic frameworks for high-performance lithium-sulfur batteries, *Adv. Energy Mater.* 6 (2016) 1601250, doi:10.1002/aenm.201601250.
- [168] F. Xu, S. Yang, X. Chen, Q. Liu, H. Li, H. Wang, B. Wei, D. Jiang, Energy-storage covalent organic frameworks: improving performance via engineering polysulfide chains on walls, *Chem. Sci.* 10 (2019) 6001–6006, doi:10.1039/c8sc04518f.
- [169] S.H. Je, H.J. Kim, J. Kim, J.W. Choi, A. Coskun, Perfluoroaryl-Elemental Sulfur SNAr chemistry in covalent triazine frameworks with high sulfur contents for Lithium-Sulfur batteries, *Adv. Funct. Mater.* 27 (2017) 1703947, doi:10.1002/adfm.201703947.
- [170] D.G. Wang, N. Li, Y. Hu, S. Wan, M. Song, G. Yu, Y. Jin, W. Wei, K. Han, G.C. Kuang, W. Zhang, Highly Fluoro-substituted covalent organic framework and its application in lithium-sulfur batteries, *ACS Appl. Mater. Interfaces* 10 (2018) 42233–42240, doi:10.1021/acsami.8b14213.
- [171] S. Royuela, J. Almaraz, M.J. Mancheno, J.C. Perez-Flores, E.G. Michel, M.M. Ramos, F. Zamora, P. Ocon, J.L. Segura, Synergistic effect of covalent bonding and physical encapsulation of sulfur in the pores of a microporous COF to improve cycling performance in Li-S batteries, *Chem. Eur. J.* 25 (2019) 12394–12404, doi:10.1002/chem.201902052.
- [172] J. Kim, A. Elabd, S.-Y. Chung, A. Coskun, J.W. Choi, Covalent triazine frameworks incorporating charged polypyrrole channels for high-performance Lithium-Sulfur batteries, *Chem. Mater.* 32 (2020) 4185–4193, doi:10.1021/acs.chemmater.0c00246.
- [173] X. Zhang, L. Yao, S. Liu, Q. Zhang, Y.Y. Mai, N.T. Hu, H. Wei, High-performance lithium sulfur batteries based on nitrogen-doped graphitic carbon derived from covalent organic frameworks, *Mater. Today Energy* 7 (2018) 141–148, doi:10.1016/j.mtener.2018.01.003.
- [174] X.D. Chen, Y.J. Xu, F.H. Du, Y. Wang, Covalent organic framework derived boron/Oxygen codoped porous carbon on CNTs as an efficient sulfur host for lithium-sulfur batteries, *Small Methods* 3 (2019) 1900338, doi:10.1002/smt.201900338.
- [175] Z. Yang, C. Peng, R. Meng, L. Zu, Y. Feng, B. Chen, Y. Mi, C. Zhang, J. Yang, Hybrid anatase/rutile nanodots-embedded covalent organic frameworks with complementary polysulfide adsorption for high-performance lithium-sulfur batteries, *ACS Cent. Sci.* 5 (2019) 1876–1883, doi:10.1021/acscentsci.9b00846.
- [176] Y. Meng, G. Lin, H. Ding, H. Liao, C. Wang, Impregnation of sulfur into a 2D pyrene-based covalent organic framework for high-rate lithium-sulfur batteries, *J. Mater. Chem. A* 6 (2018) 17186–17191, doi:10.1039/c8ta05508d.
- [177] Q. Xu, K. Zhang, J. Qian, Y. Guo, X. Song, H. Pan, D. Wang, X. Li, Boosting Lithium-Sulfur battery performance by integrating a redox-active covalent organic framework in the separator, *ACS Appl. Energy Mater.* 2 (2019) 5793–5798, doi:10.1021/acsaem.9b00920.
- [178] J. Wang, W. Qin, X. Zhu, Y. Teng, Covalent organic frameworks (COF)/CNT nanocomposite for high performance and wide operating temperature lithium-sulfur batteries, *Energy* 199 (2020) 117372, doi:10.1016/j.energy.2020.117372.
- [179] Y. Cao, C. Liu, M. Wang, H. Yang, S. Liu, H. Wang, Z. Yang, F. Pan, Z. Jiang, J. Sun, Lithiation of covalent organic framework nanosheets facilitating lithium-ion transport in lithium-sulfur batteries, *Energy Storage Mater* 29 (2020) 207–215, doi:10.1016/j.ensm.2020.04.029.
- [180] J. Wang, L. Si, Q. Wei, X. Hong, S. Cai, Y. Cai, Covalent organic frameworks as the coating layer of ceramic separator for high-efficiency Lithium-Sulfur batteries, *ACS Appl. Nano Mater.* 1 (2017) 132–138, doi:10.1021/acsnano.7b00057.
- [181] Y. Yang, X.-J. Hong, C.-L. Song, G.-H. Li, Y.-X. Zheng, D.-D. Zhou, M. Zhang, Y.-P. Cai, H. Wang, Lithium bis(trifluoromethanesulfonyl)imide assisted dual-functional separator coating materials based on covalent organic frameworks for high-performance lithium-selenium sulfide batteries, *J. Mater. Chem. A* 7 (2019) 16323–16329, doi:10.1039/c9ta04614c.
- [182] J. Janek, W.G. Zeier, A solid future for battery development, *Nat. Energy* 1 (2016) 16141, doi:10.1038/Nenergy.2016.141.
- [183] A. Manthiram, X.W. Yu, S.F. Wang, Lithium battery chemistries enabled by solid-state electrolytes, *Nat. Rev. Mater.* 2 (2017) 16103, doi:10.1038/natrevmats.2016.103.
- [184] K. Zhang, B. Zhang, M. Weng, J. Zheng, S. Li, F. Pan, Lithium ion diffusion mechanism in covalent organic framework based solid state electrolyte, *PCCP* 21 (2019) 9883–9888, doi:10.1039/c9cp02117e.
- [185] F. Han, A.S. Westover, J. Yue, X. Fan, F. Wang, M. Chi, D.N. Leonard, N.J. Dudney, H. Wang, C. Wang, High electronic conductivity as the origin of lithium dendrite formation within solid electrolytes, *Nat. Energy* 4 (2019) 187–196, doi:10.1038/s41560-018-0312-z.
- [186] H. Liu, X.-B. Cheng, J.-Q. Huang, H. Yuan, Y. Lu, C. Yan, G.-L. Zhu, R. Xu, C.-Z. Zhao, L.-P. Hou, C. He, S. Kaskel, Q. Zhang, Controlling dendrite growth in solid-state electrolytes, *ACS Energy Lett* 5 (2020) 833–843, doi:10.1021/acsenergylett.9b02660.
- [187] Q. Zhao, S. Stalin, C.-Z. Zhao, L.A. Archer, Designing solid-state electrolytes for safe, energy-dense batteries, *Nat. Rev. Mater.* 5 (2020) 229–252, doi:10.1038/s41578-019-0165-5.
- [188] L. Zhang, Q. Zhang, H. Ren, H. Yan, J. Zhang, H. Zhang, J. Gu, Calculation of band gap in long alkyl-substituted heterocyclic-thiophene-conjugated polymers with electron donor-acceptor fragment, *Sol. Energy Mater. Sol. Cells* 92 (2008) 581–587, doi:10.1016/j.solmat.2007.12.010.
- [189] G. Bian, J. Yin, J. Zhu, Recent advances on conductive 2D covalent organic frameworks, *Small* (2021) e2006043, doi:10.1002/sml.202006043.
- [190] Y. Li, J. Zou, H.-L. Yip, C.-Z. Li, Y. Zhang, C.-C. Chueh, J. Intemann, Y. Xu, P.-W. Liang, Y. Chen, A.K.Y. Jen, Side-chain effect on cyclopentadithiophene/fluorobenzothiadiazole-based low band gap polymers and their applications for polymer solar cells, *Macromolecules* 46 (2013) 5497–5503, doi:10.1021/ma4009302.
- [191] H. Ari, Z. Büyükmumcu, Comparison of DFT functionals for prediction of band gap of conjugated polymers and effect of HF exchange term percentage and basis set on the performance, *Comput. Mater. Sci* 138 (2017) 70–76, doi:10.1016/j.commatsci.2017.06.012.
- [192] H.V. Babu, M.G.M. Bai, M. Rajeswara Rao, Functional  $\pi$ -conjugated two-dimensional covalent organic frameworks, *ACS Appl. Mater. Interfaces* 11 (2019) 11029–11060, doi:10.1021/acsami.8b19087.
- [193] Z.-C. Guo, Z.-Q. Shi, X.-Y. Wang, Z.-F. Li, G. Li, Proton conductive covalent organic frameworks, *Coord. Chem. Rev.* (2020) 422, doi:10.1016/j.ccr.2020.213465.
- [194] H. Chen, H. Tu, C. Hu, Y. Liu, D. Dong, Y. Sun, Y. Dai, S. Wang, H. Qian, Z. Lin, L. Chen, Cationic covalent organic framework nanosheets for fast Li-Ion conduction, *J. Am. Chem. Soc.* 140 (2018) 896–899, doi:10.1021/jacs.7b12292.
- [195] Z. Li, Z.W. Liu, Z.Y. Li, T.X. Wang, F.L. Zhao, X.S. Ding, W. Feng, B.H. Han, Defective 2D covalent organic frameworks for postfunctionalization, *Adv. Funct. Mater.* 30 (2020) 1909267, doi:10.1002/adfm.201909267.
- [196] Q. Xu, S. Tao, Q. Jiang, D. Jiang, Ion conduction in polyelectrolyte covalent organic frameworks, *J. Am. Chem. Soc.* 140 (2018) 7429–7432, doi:10.1021/jacs.8b03814.
- [197] G. Zhang, Y.L. Hong, Y. Nishiyama, S. Bai, S. Kitagawa, S. Horike, Accumulation of Glassy Poly(ethylene oxide) anchored in a covalent organic framework as a solid-state Li(+) electrolyte, *J. Am. Chem. Soc.* 141 (2019) 1227–1234, doi:10.1021/jacs.8b07670.
- [198] Z. Guo, Y. Zhang, Y. Dong, J. Li, S. Li, P. Shao, X. Feng, B. Wang, Fast ion transport pathway provided by polyethylene glycol confined in covalent organic frameworks, *J. Am. Chem. Soc.* 141 (2019) 1923–1927, doi:10.1021/jacs.8b13551.